Vol. 14 N0. 2 December 2017

P-ISSN 0216-6739; E-ISSN 2549-516X
No. 774/AU3/P2MI-LIPI/08/2017

International Journal of Remote Sensing and Earth Sciences

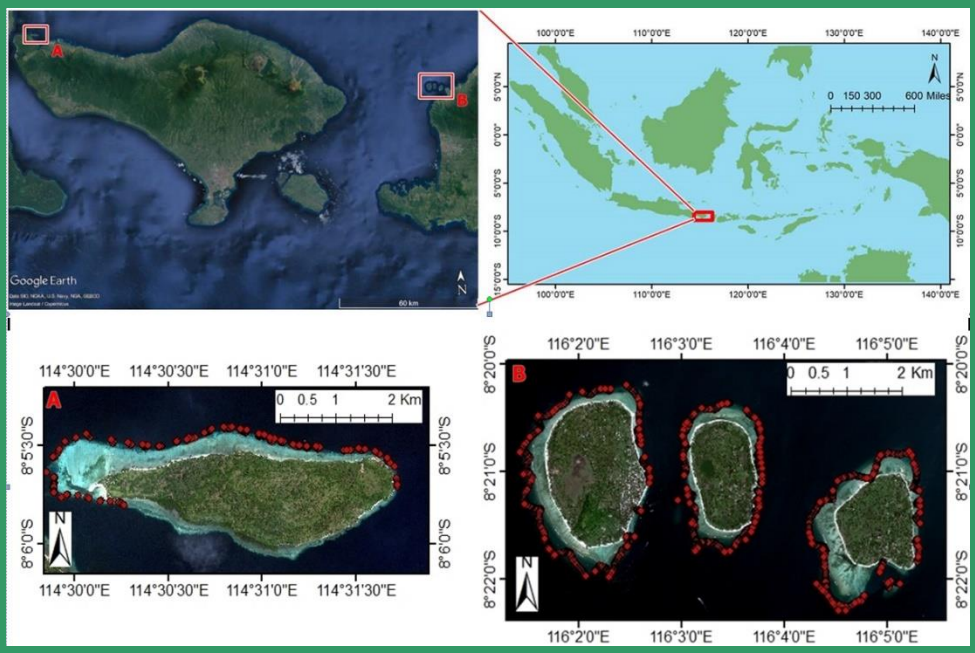

Published by
Indonesian National Institute of Aeronautics and Space
(LAPAN)

Vol. 14 N0. 2 December 2017

P-ISSN 0216-6739; E-ISSN 2549-516X
No. 774/AU3/P2MI-LIPI/08/2017

International Journal of Remote Sensing and Earth Sciences

Published by
Indonesian National Institute of Aeronautics and Space
(LAPAN)

Editorial Committee Preface

Dear IJReSES Readers,

We sincerely thank you for reading the International Journal of Remote Sensing and Earth Sciences Vol. 14 No 2, December 2017. In general, this journal is expected to enrich the serial publications on earth sciences. In particular this journal is aimed to present improvement in remote sensing studies and its applications on earth sciences. This journal also serves as the enrichment on earth sciences publication, not only in Indonesia and Asia but also worldwide.

This journal consists of papers discussing the particular interest in remote sensing field. Those papers are having remote sensing data for image processing, geosciences, oceanography, environment, disaster, mining activities, etc. A variety of topics are discussed in this fourteenth edition. Briefly, the topics discussed in this edition are the studies of remote sensing data processing issues such as the peat thickness classes estimated from land cover, spatial projection of land use and its connection with urban ecology spatial planning, compression on remote sensing data, and preliminary study of LSU-02 photo data application to support 3D modeling. Meanwhile the topics on remote sensing applications and validation are also discussed such as determination of the best methodology for bathymetry mapping, carbon stock estimation of mangrove vegetation, detecting the area damage due to coal mining activities, and information criterion-based mangrove land classification.

The publication of IJReSES is intended to supply the demands regarding the information on the Remote Sensing and Earth Sciences. This journal is also intended to motivate Indonesian as well as Asian scientists to submit their research results. Thus, by their submitted research results, it will contribute to the development and strengthening in remote sensing field particularly in Asia. To that end, we invite scientists to play their parts in this journal by submitting their scientific research papers. We look forward to receiving your research works for the next edition of this journal.

Editor-in-Chief,

Dr M. Rokhis Khomarudin

IJReSES Secretariat
National Institute of Aeronautics and Space of Indonesia (LAPAN)
Jl. Pemuda Persil No. 1, Rawamangun, Jakarta 13220, INDONESIA
Phone. (021) 4892802 ext. 144 – 145 (Hunting) Fax. (021) 47882726
Pukasi.lapan@gmail.com; publikasi@lapan.go.id

Published by:
National Institute of Aeronautics and Space of Indonesia
(LAPAN)

INTERNATIONAL JOURNAL OF
REMOTE SENSING AND EARTH SCIENCES
Vol. 14 No. 2 December 2017
P-ISSN 0216-6739; E- ISSN 2549-516X
No. 774/AU3/P2MI-LIPI/08/2017

Contents

Published by:
National Institute of Aeronautics and Space of Indonesia (LAPAN)

International Journal of
Remote Sensing and Earth Sciences
P-ISSN 0216 – 6739; E- ISSN 2549-516X Vol. 14 No.1, June 2017
No. 774/AU3/P2MI-LIPI/08/2017

ABSTRACT

HARMFUL ALGAL BLOOM 2012 EVENT VERIFICATION IN LAMPUNG BAY USING RED TIDE DETECTION ON SPOT 4 IMAGE / Emiyati1, Ety Parwati, and Syarif Budhiman
IJRESES, 14 (1) 2017 : 1- 8

In mid-December 2012, harmful algal bloom phenomenon occurred in Lampung Bay. Harmful Algal Bloom (HAB) is blooming of algae in aquatic ecosystems. It has negative impact on living organism, due to its toxic. This study was applied Red Tide (RT) detection algorithm on SPOT 4 images and verified the distribution of HAB 2012 event in Lampung Bay. The HAB event in 2012 in Lampung Bay can be detected by using RT algorithm on SPOT 4 images quantitatively and qualitatively. According to field measurement, the phytoplankton blooming which happen at Lampung Bay in 2012 were Cochlodinium sp. Image analysis showed that Cochlodinium sp has specific pattern of RT with values, digitally, were 13 to 41 and threshold value of red band SPOT 4 image was 57. The total area of RT distribution, which are found in Lampung Bay, was 11,545.3 Ha. Based on the RT classification of RT images and field data measurement, the RT which is caused many fishes died on the western coastal of Lampung Bay spread out from Bandar Lampung City to Batumenyan village. By using confusion matrix, the accuracy of this this method was 74.05 %. This method was expected to be used as early warning system for HAB monitoring in Lampung Bay and perhaps in another coastal region of Indonesia.

Keywords: *harmful algal bloom, Lampung Bay, SPOT 4 image, red tide algorithm*

A PARTIAL ACQUISITION TECHNIQUE OF SAR SYSTEM USING COMPRESSIVE SAMPLING METHOD / Rahmat Arief
IJRESES, 14 (1) 2017 : 9-18

In line with the development of Synthetic Aperture Radar (SAR) technology, there is a serious problem when the SAR signal is acquired using high rate analog digital converter (ADC), that require large volumes data storage. The other problem on compressive sensing method, which frequently occurs, is a large measurement matrix that may cause intensive calculation. In this paper, a new approach was proposed, particularly on the partial acquisition technique of SAR system using compressive sampling method in both the azimuth and range direction. The main objectives of the study are to reduce the radar raw data by decreasing the sampling rate of ADC and to reduce the computational load by decreasing the dimension of the measurement matrix. The simulation results found that the reconstruction of SAR image using partial acquisition model has better resolution compared to the conventional method (Range Doppler Algorithm/RDA). On a target of a ship, that represents a low-level sparsity, a good reconstruction image could be achieved from a fewer number measurement. The study concludes that the method may speed up the computation time by a factor 4.49 times faster than with a full acquisition matrix.

Keywords: *partial acquisition technique, synthetic aperture radar, compressive sampling*

International Journal of
Remote Sensing and Earth Sciences
P-ISSN 0216 – 6739; E- ISSN 2549-516X Vol. 14 No.1, June 2017
No. 774/AU3/P2MI-LIPI/08/2017

ABSTRACT

VALIDATION OF COCHLODINIUM POLYKRIKOIDES RED TIDE DETECTION USING SEAWIFS-DERIVED CHLOROPHYLL-A DATA WITH NFRDI RED TIDE MAP IN SOUTH EAST KOREAN WATERS / Gathot Winarso and Joji Ishizaka
IJRESES, 14 (1) 2017 : 19-26

Annual summer red tides of Cochlodinium polykrikoides have happenned at southern coastal of the South Korea, accounted economic losses of 76.4 billion won in 1995 on fisheries and other economic substantial losses. Therefore, it is important to eliminate the damage and losses by monitoring the bloom and to forecast their development and movement. On previous study, ocean color satellite, SeaWiFS, standard chlorophyll-a data was used to detect the red tide, using threshold value of chlorophyll-a concentration ≥ 5 mg/m3, resulted a good correlation using visual comparison. However, statistic based accuracy analysis has not be done yet. In this study, the accuracy of detection method was analyzed using spatial statistic. Spatial statistical match up analysis resulted 68% of red tide area was not presented in satellite data due to masking. Within red tide area where data existed, 36% was in high chlorophyll-a area and 64% was in low chlorophyll-a area. Within the high chlorophyll-a area 13% and 87% was in and out of the red tide area. It was found that the accuracy of this detection is low. However if the accuracy was yearly splitted, its found that 75% accuracy on 2002 where visually red tide detected spead out to the off-shore area. The fail and false detection are not due to the failure of the detection method but caused by limitation of the technology due to the natural condition i.e. type of red tide spreading, cloud cover and other flags such as turbid water, stray light etc.

Keywords: *cochlodinium polykrikoides, chlorophyll-a, SeaWiFS, red tide*

A COMPARISON OF OBJECT-BASED AND PIXEL-BASED APPROACHES FOR LAND USE/LAND COVER CLASSIFICATION USING LAPAN-A2 MICROSATELLITE DATA / Jalu Tejo Nugroho1, Zylshal, Nurwita Mustika Sari, and Dony Kushardono
IJRESES, 14 (1) 2017: 27-36

In recent years, small satellite industry has been a rapid trend and become important especially when associated with operational cost, technology adaptation and the missions. One mission of LAPAN-A2, the 2nd generation of microsatellite that developed by Indonesian National Institute of Aeronautics and Space (LAPAN), is Earth observation using digital camera that provides imagery with 3.5 m spatial resolution. The aim of this research is to compare between object-based and pixel-based classification of land use/land cover (LU/LC) in order to determine the appropriate classification method in LAPAN-A2 data processing (case study Semarang, Central Java).The LU/LC were classified into eleven classes, as follows: sea, river, fish pond, tree, grass, road, building 1, building 2, building 3, building 4 and rice field. The accuracy of classification outputs were assessed using confusion matrix. The object-based and pixel-based classification methods result for overall accuracy are 31.63% and 61.61%, respectively. According to accuracy result, it was thought that blurring effect on LAPAN-A2 data may be the main cause of accuracy decrease. Furthermore, the result is suggested to use pixel-based classification to be applied in LAPAN-A2 data processing.

Keywords: *LAPAN-A2 microsatellite, LU/LC, object-based, pixel-based*

International Journal of
Remote Sensing and Earth Sciences
P-ISSN 0216 – 6739; E- ISSN 2549-516X Vol. 14 No.1, June 2017
No. 774/AU3/P2MI-LIPI/08/2017

ABSTRACT

VERIFICATION OF PISCES DISSOLVED OXYGEN MODEL USING IN SITU MEASUREMENT IN BIAK, ROTE, AND TANIMBAR SEAS, INDONESIA / Armyanda Tussadiah, Joko Subandriyo, Sari Novita, Widodo S. Pranowo
IJRESES, 14 (1) 2017: 37-46

Dissolved oxygen (DO) is one of the most chemical primary data in supported life for marine organisms. Ministry of Marine Affairs and Fisheries Republic of Indonesia through Infrastructure Development for Space Oceanography (INDESO) Project provides dissolved oxygen data services in Indonesian Seas for 7 days backward and 10 days ahead (9,25 km x 9.25 km, 1 daily). The data based on Biogeochemical model (PISCES) coupled with hydrodynamic model (NEMO), with input data from satellite acquisition. This study investigated the performance and accuracy of dissolved oxygen from PISCES model, by comparing with the measurement in situ data in Indonesian Seas specifically in three outermost islands of Indonesia (Biak Island, Rote Island, and Tanimbar Island). Results of standard deviation values between in situ DO and model are around two (St.dev ± 2). Based on the calculation of linear regression between in situ DO with the standard deviation obtained a high determinant coefficient, greater than 0.9 (R2 ≥ 0.9). Furthermore, RMSE calculation showed a minor error, less than 0.05. These results showed that the equation of the linear regression might be used as a correction equation to gain the verified dissolved oxygen.

Keywords: verification, PISCES model, dissolved oxygen, in situ measurement, indonesia, linear regression

IN-SITU MEASUREMENT OF DIFFUSE ATTENUATION COEFFICIENT AND ITS RELATIONSHIP WITH WATER CONSTITUENT AND DEPTH ESTIMATION OF SHALLOW WATERS BY REMOTE SENSING TECHNIQUE / Budhi Agung Prasetyo, Vincentius Paulus Siregar, Syamsul Bahri Agus, Wikanti Asriningrum
IJRESES, 14 (1) 2017: 47-60

Diffuse attenuation coefficient, Kd(λ), has an empirical relationship with water depth, thus potentially to be used to estimate the depth of the water based on the light penetration in the water column. The aim of this research is to assess the relationship of diffuse attenuation coefficient with the water constituent and its relationship to estimate the depth of shallow waters of Air Island, Panggang Island and Karang Lebar lagoons and to compare the result of depth estimation from Kd model and derived from Landsat 8 imagery. The measurement of Kd(λ) was carried out using hyperspectral spectroradiometer TriOS-RAMSES with range 320 – 950 nm. The relationship between measurement Kd(λ) on study site with the water constituent was the occurrence of absorption by chlorophyll-a concentration at the blue and green spectral wavelength. Depth estimation using band ratio from Kd(λ) occurred at 442,96 nm and 654,59 nm, which had better relationship with the depth from in-situ measurement compared to the estimation based on Landsat 8 band ratio. Depth estimated based on Kd(λ) ratio and in-situ measurement are not significantly different statistically. Depth estimated based on Kd(λ) ratio and in-situ measurement are not significantly different statistically. However, depth estimation based on Kd(λ) ratio was inconsistent due to the bottom albedo reflection because the Kd(λ) measurement was carried out in shallow waters. Estimation of water depth based on Kd(λ) ratio had better results compared to the Landsat 8 band ratio.

Keywords: *in-situ measurement, diffuse attenuation coefficient, relationship with water constituent, depth estimation, shallow water, remote sensing*

International Journal of
Remote Sensing and Earth Sciences
P-ISSN 0216 – 6739; E- ISSN 2549-516X Vol. 14 No.1, June 2017
No. 774/AU3/P2MI-LIPI/08/2017

ABSTRACT

TIME SERIES ANALYSIS OF TOTAL SUSPENDED SOLID (TSS) USING LANDSAT DATA IN BERAU COASTAL AREA, INDONESIA / Ety Parwati1 and Anang Dwi Purwanto
IJRESES, 14 (1) 2017: 61-70

Water quality information is usually used for the first examination of the pollution. One of the parameters of water quality is Total Suspended Solid (TSS), which describes the amount of matter of particles suspended in the water. TSS information is also used as initial information about waters condition of a region. TSS could be derive from Landsat data with several combinations of spectral channels to evaluate the condition of the observation area for both the waters and the surrounding land. The study aimed to evaluate Berau waters condition in Kalimantan, Indonesia, by utilizing TSS dynamics extracted from Landsat data. Validated TSS extraction algorithm was obtained by choosing the best correlation between field data and image data. Sixty pairs of points had been used to build validated TSS algorithms for the Berau Coastal area. The algorithm was TSS = 3.3238 * exp (34 099 * Red Band Reflectance). The data used for this study were Landsat 5 TM, Landsat 7 ETM and Landsat 8 data acquisition in 1994, 1996, 1998, 2002, 2004, 2006, 2008 and 2013. For detailed evaluation, 20 regions were created along the watershed up to the coast. The results showed the fluctuation of TSS values in each selected region. TSS value increased if there was a change of any kind of land cover/land used into bareland, ponds, settlements or shrubs. Conversely, TSS value decreased if there was a wide increase of mangrove area or its position was very closed to the ocean.

Keywords: *TSS, Landsat 5 TM, Landsat 7 ETM +, Landsat 8, watershed, mangrove*

SIMULATION OF DIRECT GEOREFERENCING FOR GEOMETRIC SYSTEMATIC CORRECTION ON LSA PUSHBROOM IMAGER / Muchammad Soleh1, Wismu Sunarmodo, and Ahmad Maryanto
IJRESES, 14 (1) 2017: 71-82

LAPAN has developed remote sensing data collection by using a pushbroom linescan imager camera sensor mounted on LSA (Lapan Surveillance Aircraft). The position accuracy and orientation system for LSA applications are required for Direct Georeferencing and depend on the accuracy of off-the-shelf integrated GPS/inertial system, which used on the camera sensor. This research aims to give the accuracy requirement of Inertial Measurement Unit (IMU) sensor and GPS to improve the accuracy of the measurement results using direct georeferencing technique. Simulations were performed to produce geodetic coordinates of longitude, latitude and altitude for each image pixel in the imager pushbroom one array detector, which has been geometrically corrected. The simulation results achieved measurement accuracies for mapping applications with Ground Sample Distance (GSD) or spatial resolution of 0,6 m of the IMU parameter (pitch, roll and yaw) errors about 0.1; 0.1; and 0.1 degree respectively, and the error of GPS parameters (longitude and latitude) about 0.00002 and 0.2 degree. The results are expected to be a reference for a systematic geometric correction to image data pushbroom linescan imager that would be obtained by using LSA spacecraft.

Keywords: *direct georeferencing, pushbroom imager, systematic geometric correction, LSA*

International Journal of
Remote Sensing and Earth Sciences
P-ISSN 0216 – 6739; E- ISSN 2549-516X Vol. 14 No.2, December 2017
No. 774/AU3/P2MI-LIPI/08/2017

ABSTRACT

CAN THE PEAT THICKNESS CLASSES BE ESTIMATED FROM LAND COVER TYPE APPROACH?/Bambang Trisakti Bambang, Atriyon Julzarika, Udhi C. Nugroho, Dipo Yudhatama, and Yudi Lasmana
IJRESES, 14 (2) 2017: 83-94

Indonesia has been known as a home of the tropical peatlands. The peatlands are mainly in Sumatera, Kalimantan and Papua Islands. Spatial information on peatland depth is needed for the planning of agricultural land extensification. The research objective was to develop a preliminary estimation model of peat thickness classes based on land cover approach and analyse its applicability using Landsat 8 image. Ground data, including land cover, location and thickness of peat, were obtained from various surveys and peatlands potential map (Geology Map and Wetlands Peat Map). The land cover types were derived from Landsat 8 image. All data were used to build an initial model for estimating peat thickness classes in Merauke Regency. A table of relationships among land cover types, peat potential areas and peat thickness classes were made using ground survey data and peatlands potential maps of that were best suited to ground survey data. Furthermore, the table was used to determine peat thickness classes using land cover information produced from Landsat 8 image. The results showed that the estimated peat thickness classes in Merauke Regency consist of two classes, i.e., very shallow peatlands and shallow peatlands. Shallow peatlands were distributed at the upper part of Merauke Regency with mainly covered by forest. In comparison with Indonesia Peatlands Map, the number of classes was the two classes. The spatial distribution of shallow peatlands was relatively similar for its precision and accuracy, but the estimated area of shallow peatlands was greater than the area of shallow peatlands from Indonesia Peatlands Map. This research answered the question that peat thickness classes could be estimated by the land cover approach qualitatively. The precise estimation of peat thickness could not be done due to the limitation of insitu data.

Keywords: *Peat thickness, Landsat 8 image, land cover, Merauke Regency, shallow peatlands*

SPATIAL PROJECTION OF LAND USE AND ITS CONNECTION WITH URBAN ECOLOGY SPATIAL PLANNING IN THE COASTAL CITY, CASE STUDY IN MAKASSAR CITY, INDONESIA/Syahrial Nur Amri, Luky Adrianto, Dietriech Geoffrey Bengen, and Rahmat Kurnia
IJRESES, 14 (2) 2017: 95-110

The arrangement of coastal ecological space in the coastal city area aims to ensure the sustainability of the system, the availability of local natural resources, environmental health and the presence of the coastal ecosystems. The lack of discipline in the supervision and implementation of spatial regulations resulted in inconsistencies between urban spatial planning and land use facts. This study aims to see the inconsistency between spatial planning of the city with the real conditions in the field so it can be used as an evaluation material to optimize the planning of the urban space in the future. This study used satellite image interpretation, spatial analysis, and projection analysis using markov cellular automata, as well as consistency evaluation for spatial planning policy. The results show that there has been a significant increase of open spaces during 2001-2015 and physical development was relatively spreading irregularly and indicated the urban sprawl phenomenon. There has been an open area deficits for the green open space in 2015-2031, such as integrated maritime, ports, and warehousing zones. Several islands in Makassar City are predicted to have their built-up areas decreased, especially in Lanjukang Island, Langkai Island, Kodingareng Lompo Island, Bone Tambung Island, Kodingareng Keke Island and Samalona Island. Meanwhile, the increase of the built up area is predicted to occur in Lumu Island, Barrang Caddi Island, Barrang Lompo Island, Lae-lae Island, and Kayangan Island. The land cover is caused by the human activities. Many land conversions do not comply with the provision of percentage of green open space allocation in the integrated strategic areas, established in the spatial plan. Thus, have the potential of conflict in the spatial plan of marine and small islands in Makassar City.

Keywords: *spatial projection, land use, spatial planning, remote sensing, coastal city*

International Journal of
Remote Sensing and Earth Sciences
P-ISSN 0216 – 6739; E- ISSN 2549-516X Vol. 14 No.2, December 2017
No. 774/AU3/P2MI-LIPI/08/2017

ABSTRACT

THE EFFECT OF JPEG2000 COMPRESSION ON REMOTE SENSING DATA OF DIFFERENT SPATIAL RESOLUTIONS/ Anis Kamilah Hayati and Haris Suka Dyatmika
IJRESES, 14 (2) 2017: 111-118

The huge size of remote sensing data implies the information technology infrastructure to store, manage, deliver and process the data itself. To compensate these disadvantages, compressing technique is a possible solution. JPEG2000 compression provide lossless and lossy compression with scalability for lossy compression. As the ratio of lossy compression getshigher, the size of the file reduced but the information loss increased. This paper tries to investigate the JPEG2000 compression effect on remote sensing data of different spatial resolution. Three set of data (Landsat 8, SPOT 6 and Pleiades) processed with five different level of JPEG2000 compression. Each set of data then cropped at a certain area and analyzed using unsupervised classification. To estimate the accuracy, this paper utilized the Mean Square Error (MSE) and the Kappa coefficient agreement. The study shows that compressed scenes using lossless compression have no difference with uncompressed scenes. Furthermore, compressed scenes using lossy compression with the compression ratioless than 1:10 have no significant difference with uncompressed data with Kappa coefficient higher than 0.8.

Keywords: *compression, effect, spatial resolution, remote sensing, JPEG2000*

PRELIMINARY STUDY OF LSU-02 PHOTO DATA APPLICATION TO SUPPORT 3D MODELING OF TSUNAMI DISASTER EVACUATION MAP/Linda Yunita, Nurwita Mustika Sari, and Dony Kushardono
IJRESES, 14 (2) 2017: 119-126

The southern coast of Pacitan Regency is one of the vulnerable areas to the tsunami. Therefore, the map of the vulnerable and safe area from the tsunami disaster is required. Currently, there are many mapping technologies with UAVs used for spatial analysis. One of the UAV technologies which used in this research is LAPAN Surveillance UAV 02 (LSU-02). This study aims to map the evacuation plan area from LSU-02 aerial imagery. Tsunami evacuation area was identified by processing the aerial photo data into orthomosaic and Digital Elevation Model (DEM). The result shows that there are four points identified as the tsunami evacuation plan area. These points are located higher than the surrounding area and are easily accessible.

Keywords: *Aerial remote sensing, photo data of LSU-02, 3D modelling, tsunami*

International Journal of
Remote Sensing and Earth Sciences
P-ISSN 0216 – 6739; E- ISSN 2549-516X Vol. 14 No.2, December 2017
No. 774/AU3/P2MI-LIPI/08/2017

ABSTRACT

DETERMINATION OF THE BEST METHODOLOGY FOR BATHYMETRY MAPPING USING SPOT 6 IMAGERY: A STUDY OF 12 EMPIRICAL ALGORITHMS/Masita Dwi Mandini Manessa, Muhammad Haidar, Maryani Hastuti, and Diah Kirana
IJRESES, 14 (2) 2017: 127-136

For the past four decades, many researchers have published a novel empirical methodology for bathymetry extraction using remote sensing data. However, a comparative analysis of each method has not yet been done. Which is important to determine the best method that gives a good accuracy prediction. This study focuses on empirical bathymetry extraction methodology for multispectral data with three visible band, specifically SPOT 6 Image. Twelve algorithms have been chosen intentionally, namely, 1) Ratio transform (RT); 2) Multiple linear regression (MLR); 3) Multiple nonlinear regression (RF); 4) Second-order polynomial of ratio transform (SPR); 5) Principle component (PC); 6) Multiple linear regression using relaxing uniformity assumption on water and atmosphere (KNW); 7) Semiparametric regression using depth-independent variables (SMP); 8) Semiparametric regression using spatial coordinates (STR); 9) Semiparametric regression using depth-independent variables and spatial coordinates (TNP), 10) bagging fitting ensemble (BAG); 11) least squares boosting fitting ensemble (LSB); and 12) support vector regression (SVR). This study assesses the performance of 12 empirical models for bathymetry calculations in two different areas: Gili Mantra Islands, West Nusa Tenggara and Menjangan Island, Bali. The estimated depth from each method was compared with echosounder data; RF, STR, and TNP results demonstrate higher accuracy ranges from 0.02 to 0.63 m more than other nine methods. The TNP algorithm, producing the most accurate results (Gili Mantra Island RMSE = 1.01 m and R^2=0.82, Menjangan Island RMSE = 1.09 m and R^2=0.45), proved to be the preferred algorithm for bathymetry mapping.

Keywords: *bathymetry; SPOT 6; empirical methodology; multispectral image*

CARBON STOCK ESTIMATION OF MANGROVE VEGETATION USING REMOTE SENSING IN PERANCAK ESTUARY, JEMBRANA DISTRICT, BALI/Amandangi Wahyuning Hastuti, Komang Iwan Suniada, and Fikrul Islamy
IJRESES, 14 (2) 2017: 137-150

Mangrove vegetation is one of the forest ecosystems that offers a potential of substantial greenhouse gases (GHG) emission mitigation, due to its ability to sink the amount of CO_2 in the atmosphere through the photosynthesis process. Mangroves have been providing multiple benefits either as the source of food, the habitat of wildlife, the coastline protectors as well as the CO_2 absorber, higher than other forest types. To explore the role of mangrove vegetation in sequestering the carbon stock, the study on the use of remotely sensed data in estimating carbon stock was applied. This paper describes an examination of the use of remote sensing data particularly Landsat-data with the main objective to estimate carbon stock of mangrove vegetation in Perancak Estuary, Jembrana, Bali. The carbon stock was estimated by analyzing the relationship between NDVI, Above Ground Biomass (AGB) and Below Ground Biomass (BGB). The total carbon stock was obtained by multiplying the total biomass with the carbon organic value of 0.47. The study results show that the total accumulated biomass obtained from remote sensing data in Perancak Estuary in 2015 is about 47.20±25.03 ton ha^{-1} with total carbon stock of about 22.18±11.76 tonC $ha^{-1}$and CO_2 sequestration 81.41±43.18 tonC ha^{-1}.

Keywords: *Perancak Estuary, carbon stock estimation, mangrove, CO_2 sequestration, NDVI*

International Journal of
Remote Sensing and Earth Sciences
P-ISSN 0216 – 6739; E- ISSN 2549-516X Vol. 14 No.2, December 2017
No. 774/AU3/P2MI-LIPI/08/2017

ABSTRACT

DETECTING THE AREA DAMAGE DUE TO COAL MINING ACTIVITIES USING LANDSAT MULTITEMPORAL (CASE STUDY: KUTAI KARTANEGARA, EAST KALIMANTAN) /Suwarsono, Nanik Suryo Haryani, Indah Prasasti, Hana Listi Fitriana M. Priyatna, and M. Rokhis Khomarudin
IJRESES, 14 (2) 2017: 151-158

Coal is one of the most mining commodities to date, especially to supply both national and international energy needs. Coal mining activities that are not well managed will have an impact on the occurrence of environmental damage. This research tried to utilize the multitemporal Landsat data to analyze the land damage caused by coal mining activities. The research took place at several coal mine sites in East Kalimantan Province. The method developed in this research is the method of change detection. The study tried to know the land damage caused by mining activities using NDVI (Normalized Difference Vegetation Index), NDSI (Normalized Difference Soil Index), NDWI (Normalized Difference Water Index) and GEMI (Global Environment Monitoring Index) parameter based change detection method. The results showed that coal mine area along with the damage that occurred in it can be detected from multitemporal Landsat data using NDSI value-based change detection method. The area damage due to coal mining activities can be classified into high, moderate, and low classes based on the mean and standard deviation of NDSI changes (ΔNDSI). The results of this study are expected to be used to support government efforts and mining managers in post-mining land reclamation activities.

Keywords: *damage area, coal mining, landsat multitemporal*

AKAIKE INFORMATION CRITERION BASED MANGROVE LAND CLASSIFICATION USING WORLDVIEW-2 SATELLITE IMAGES IN NUSA LEMBONGAN ISLAND/Aulia Ilham and Marza Ihsan Marzuki
IJRESES, 14 (2) 2017: 159-166

Machine learning is an empirical approach for regressions, clustering and/or classifying (supervised or unsupervised) on a non-linear system. This method is mainly used to analyze a complex system for wide data observation. In remote sensing, machine learning method could be used for image data classification with software tools independence. This research aims to classify the distribution, type, and area of mangroves using Akaike Information Criterion approach for case study in Nusa Lembongan Island. This study is important because mangrove forests have an important role ecologically, economically, and socially. For example is as a green belt for protection of coastline from storm and tsunami wave. Using satellite images Worldview-2 with data resolution of 0.46 meters, this method could identify automatically land class, sea class/water, and mangroves class. Three types of mangrove have been identified namely: *Rhizophora apiculata*, *Sonnetaria alba*, and other mangrove species. The result showed that the accuracy of classification was about 68.32%.

Keywords: *clustering, machine learning, remote sensing data*

CAN THE PEAT THICKNESS CLASSES BE ESTIMATED FROM LAND COVER TYPE APPROACH?

Bambang Trisakti[1]*, Atriyon Julzarika[1], Udhi C. Nugroho[1], Dipo Yudhatama[1], and Yudi Lasmana[2]
[1] Remote Sensing Applications Center, Pusfatja, LAPAN
[2]Balai Litbang Teknologi Rawa, Puslitbang Air, Ministry of Public Works and Public Housing
* e-mail: bambang.trisakti@lapan.go.id, atriyon.julzarika@lapan.go.id
Received: 6 June 2017; Revised: 9 November 2017; Approved: 10 November 2017

Abstract. Indonesia has been known as a home of the tropical peatlands. The peatlands are mainly in Sumatera, Kalimantan and Papua Islands. Spatial information on peatland depth is needed for the planning of agricultural land extensification. The research objective was to develop a preliminary estimation model of peat thickness classes based on land cover approach and analyse its applicability using Landsat 8 image. Ground data, including land cover, location and thickness of peat, were obtained from various surveys and peatlands potential map (Geology Map and Wetlands Peat Map). The land cover types were derived from Landsat 8 image. All data were used to build an initial model for estimating peat thickness classes in Merauke Regency. A table of relationships among land cover types, peat potential areas and peat thickness classes were made using ground survey data and peatlands potential maps of that were best suited to ground survey data. Furthermore, the table was used to determine peat thickness classes using land cover information produced from Landsat 8 image. The results showed that the estimated peat thickness classes in Merauke Regency consist of two classes, i.e., very shallow peatlands and shallow peatlands. Shallow peatlands were distributed at the upper part of Merauke Regency with mainly covered by forest. In comparison with Indonesia Peatlands Map, the number of classes was the two classes. The spatial distribution of shallow peatlands was relatively similar for its precision and accuracy, but the estimated area of shallow peatlands was greater than the area of shallow peatlands from Indonesia Peatlands Map. This research answered the question that peat thickness classes could be estimated by the land cover approach qualitatively. The precise estimation of peat thickness could not be done due to the limitation of insitu data.

Keywords: *Peat thickness, Landsat 8 image, land cover, Merauke Regency, shallow peatlands*

1 INTRODUCTION

Agricultural extensification is an expansion of agricultural areas by opening new land for agriculture. One of the potential land to be developed for agricultural cultivation is wetland. The area of wetland in Indonesia reached ± 33.4 million ha (Jumakir and Endrizal 2016), while the potential area for agricultural cultivation reached ± 10.2 million hectares. Papua Province has ± 2.8 million ha of potential wetland area for agriculture use, it is second ranks in Indonesia after Sumatera ± 3.9 million ha (Alihamsyah 2004). Therefore, this area is very potential for agricultural extensification for supporting of food sovereignty programs in Indonesia.

The type of soil in wetland may be alluvial or peat. The alluvial soil is a precipitate formed from a mixture of materials such as mud, humus, and sand

with different mixing ratios, while Peat is the result of weathering of organic materials such as leaves, branches, and shrubs in a state of saturated water for a very long time. A soil is called peat soil if the peat thickness is more than 50 cm, thus, peatland is wetland with peat thickness greater than 50 cm (Driessen 1978). Indonesia has the largest peatlands among tropical countries, which is about 21 million ha, spread mainly in Sumatera, Kalimantan and Papua (BB Litbang SDLP 2008). Most of the peatlands are still forest cover and are habitat for various species of fauna and rare plants. More importantly, peatlands store carbon (C) in large quantities. Peat also has a high water holding power so that it serves as a buffer hydrology surrounding areas. Peatlands conversion will disrupt all the functions of the peatlands ecosystem (Agus and Subiksa 2008).

Based on Law no. 80, 1999 on General Guidelines for Planning and Management of Peatlands Development Zone in Central Kalimantan, peatlands with thickness less than three meters can be used for forestry, agriculture, fishery, and plantation cultivation, while peatlands with thickness more than three meters are used for conservation. Although the law is specifically designed to address the problem of peatlands in Central Kalimantan, but the law generally can be applied in peatlands in other areas (Tjahjono 2006). Therefore information on peat thickness is needed to determine the policy of peatlands utilization for agricultural activities.

The utilization of remote sensing data for the identification, mapping and utilization of peatlands has been done in several studies. (Setiawan *et al.* 2016) identified 23 types of significant patterns of Enhance Vegetation Index (EVI) from MODIS imagery that were characterized by land cover type and peat depth. The EVI patterns indicated different types of ecosystems and/or different response of ecosystems to the changing environment in the Sumatera. Peat depth modelled was developed as a function topography (Rudiyanto *et al.* 2015), and also as a function topography and spatial position (Rudiyanto *et al.* 2016) for Sumatera and Kalimantan Islands. The spatial models were calibrated with the ground observations, and the models of the peat depth prediction were 0.67 to 0.92 of coefficient determination. (Jainicke *et al.* 2008) used DEM SRTM and Landsat ETM + imagery to delineate boundary of peat domes (i.e. peat accumulation that results in a form structure like a dome) in seven locations in Indonesia. (Wahyunto *et al.* 2004) estimated carbon stock using a product of peat area, depth/thickness of peat, carbon content and bulk density, after they delineated the peat distributions into land mapping units or polygons.

The uses of radar data were also conducted to identify and map the peat thickness. (Prihastomo 2016) was using ground penetrating radar (GPR) method to estimate peat thickness in Riau Siak Region, and obtained result that the estimated peatlands thickness in study area was ranged about 0.5-4.5 m. (Kripsiana 2015) utilized Light Detection and Ranging (LiDAR) to build digital terrain model (DTM), further the DTM was used for peat mapping for Kampar Riau region. At the national scale, peat thickness mapping has also been conducted based on a combination of satellite data and ground survey data.

Beginning with the question whether the peat thickness could be classified using optical remote sensing data, the research objective is to analyse and develop a preliminary estimation model of peat thickness classes based on land

cover approach and analyse its applicability using Landsat 8 image. The preliminary estimation model of peat thickness classes was developed using ground survey data, peatlands map, and Landsat 8 image.

2 MATERIALS AND METHODOLOGY

The study area was located in Merauke Regency, as shown in Figure 2-1. Merauke Regency was adjacent to Mappi and Boven Digoel regencies in the north, with Arafuru Sea in the south, and Papua New Guinea in the East. The spatial data used in this research consisted Landsat 8 satellite mosaic imagery period 2015-2016 to produce land cover information of Merauke Regency, Geology Map of 1995 from Geology Research and Development Center, and Peatlands Map of 2000-2001 from Wetlands International Indonesia Wetlands (2006). Ground survey was conducted on 30 October-4 November 2016 by joint survey team consisting of Remote Sensing Applications Center (Pusfatja) team and Balai Rawa Team to get information of land cover and peat thickness. This research also utilized ground measurement data from survey team of KESDM on March 18th – May 2nd 2008, (Subarnas 2008), Geodesy Geomatics survey team in 2009-2010 (survey related to exploration geoelectric and Geology parameters in South Papua) and survey team from Papua Provincial Mining Department. The survey data from the geodesy survey team and the Papua Provincial Mining Department survey team were obtained from discussions with them.

The flowchart of this research is shown in Figure 2-2. The survey data provided information about location coordinates, land cover conditions and peat thickness in several locations of study area. Location coordinates and peat thickness were used to evaluate the more suitable maps to determine peatlands boundaries in Merauke Regency. The evaluated maps were the Geology Map and Peatlands Map of Wetlands. After determining the more suitable map, the information on the map was used to determine peat potential area (peat areas and peatlands boundaries).

The relationship between land cover on peat potential areas and peat thickness classes was analysed based on ground survey measurements, both conducted by joint survey team, as well as ground survey from other teams. Furthermore, a relationship table between land cover and peat thickness class was developed. The peat thickness classes referred to the definition of Climate Change forests and Peatlands in Indonesia (CCFPI) and several publications (Agus and Subiksa 2008; Syahruddin and Nuraini 1997).

Figure 2-1: Study area in Merauke Regency

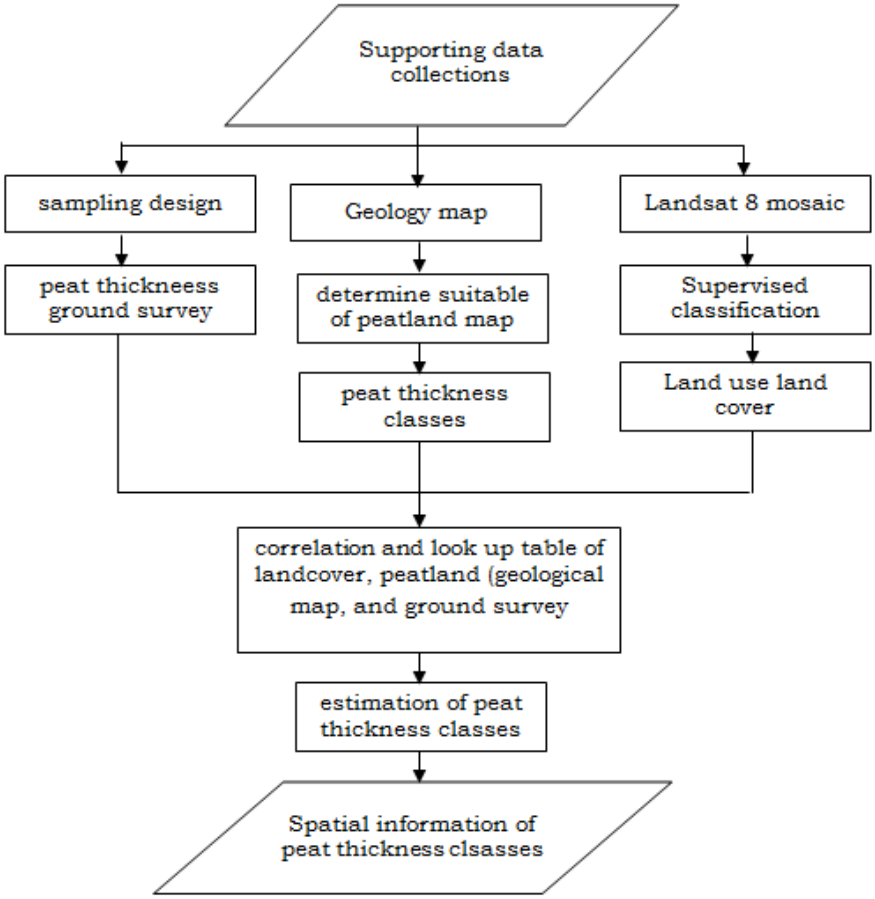

Figure 2-2: Flowchart of preliminary estimation (peat thickness classes)

The relationship table between land cover and peat thickness classes then were used to estimate peat thickness class based on land cover information of Merauke Regency. Land cover information was made using Landsat 8 2015-2016 mosaic imagery using visual interpretation and on screen digitation method. Land cover classes consisted forest, plantation, shrub, cultivated land, rice field, savannah pasture, settlement, swamp, mangrove, water body and open land. The Land cover information was overlaid with peatlands boundary from the map, so the distribution land cover on peatlands area was obtained. The next step was to predict peat thickness class on each land cover type using the relationship table between land cover and peat thickness classes, and then verify the results with ground survey data.

3 RESULTS AND DISCUSSION

The joint ground survey was conducted by Pusfatja and Balai Rawa teams to observe land cover conditions and measure peat thickness at 64 location points in the southern part of Merauke Regency, as shown in Figure 3-1. Peat thickness measurements were carried out by drilling at four representative location points. Based on the observation of the land cover condition, most of the survey location points (77%) were performed at very shallow peatlands (peat thickness less than 50 cm) with various land cover, i.e. swamp, rice field, plantation, forest and shrub. While the other survey location points were performed at a non

peatlands area (23%) having land cover of open land, settlement and water body. In this survey, it was not found a location with peat thickness greater than 50 cm.

Furthermore, based on data from other survey teams obtained from literature and discussions with those survey team members (Ministry of Energy and Mineral Resources survey team, Geodesy Survey team and Papua Provincial Mining Department survey team), additional information was obtained regarding the condition of peatlands in Papua, as follows: KESDM team conducted a survey in period March-May 2008 in several locations of Merauke Regency (Anasai, Kumbe, Domande, Wapeko, Rawa Biru and Sota villages). The team did not found indication of peat deposits except in Anasai and Kumbe villages. The team found swamps deposits with Lithology of black clay covered by a layer of humus with a thickness about 10-15 cm (very shallow peatlands).

a. The Geodesy Geomatics team found that the area around the river basin was very shallow peatlands with a thickness about 0-50 cm.
b. Mining Department survey team found that the area observed was very shallow peatlands (0-50 cm) in general, but shallow peatlands (50-100 cm) was found in forest areas around Muting district and at the upper area of Merauke Regency.

The peatlands locations and peat thickness classes obtained from the ground survey were inconsistent with information released by Peat Map of Wetlands, particularly on peat thickness classes. The Wetlands map had three classes of peat thickness for Merauke Regency, they are very shallow peatlands (0-50 cm), shallow peatlands (50-100 cm) and medium peatlands (100-200 cm).

The Geology Map did not provide information on peat thickness but provided information on the type of lithology that had the potential peat. The peatlands location obtained from the ground survey in accordance with the potential of peat from the Geology map. Based on the above considerations, the peatlands boundaries were determined using Geology Map.

Figure 3-2 shows the spatial information of lithology in Merauke Regency from Geology Map. There were 5 classes of lithology, where 2 of them are potentially peat area. Those were young swamp deposits and old swamp deposits. Based on the definition in the Geology Map, young swamp deposits were very fine-grained clay deposits composed of clays, mud, silt, and fine sand containing carbonan, whereas old swamp deposits are fine clay deposits composed of mud and fine carbonan sand, and peat. Then peat potential areas were determined by classified whole study area into 3 classes (Figure 3-3), those were:

a. Non peatlands
b. Peatlands potential (young swamp deposits)
c. Peatlands potential (old swamp deposits)

Peat-containing soils were naturally present in the uppermost layer, under the peat layer there were alluvial layers in varying thickness. Based on Climate Change Forest and Peatlands in Indonesia (CCFPI) and several publications (Agus and Subiksa 2008; Syahruddin and Nuraini 1997), peat thickness was divided into 6 classes as following:

a. Non peatlands

b. Very shallow peatlands (peat thickness less than 50 cm),
c. Shallow peatlands (peat thickness between 50-100 cm),
d. Medium peatlands (peat thickness between 100-200 cm),
e. Deep peatlands (peat thickness between 200-300 cm),
f. Very deep peatlands (peat thickness greater than 300 cm.

According to the survey data from several teams in Merauke Regency, it was found that most of the land covers in Merauke Regency were on very shallow peatlands area (peat thickness 0-50 cm). Shallow peat (peat thickness between 50-100 cm) was found in forest located in the upper part of Merauke Regency (around Muting district). While non peatlands was generally found in settlement, open land and water body. Based on these facts, a table that showed relationships among land cover, peat potential area and peat thickness classes was made, as shown in Table 3-1.

Survey location points in the southern part of Merauke Regency

Peat thickness of less than 50 cm on swamp area

Figure 3-1: Survey location and an example of peatlands in Merauke Regency

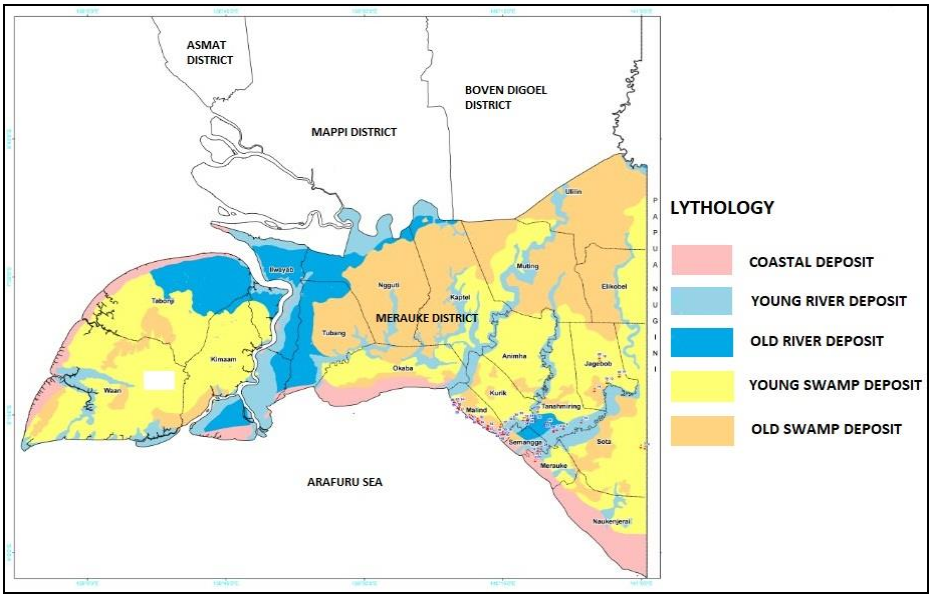

Figure 3-2: Spatial information of lithology in Merauke Regency from geology map

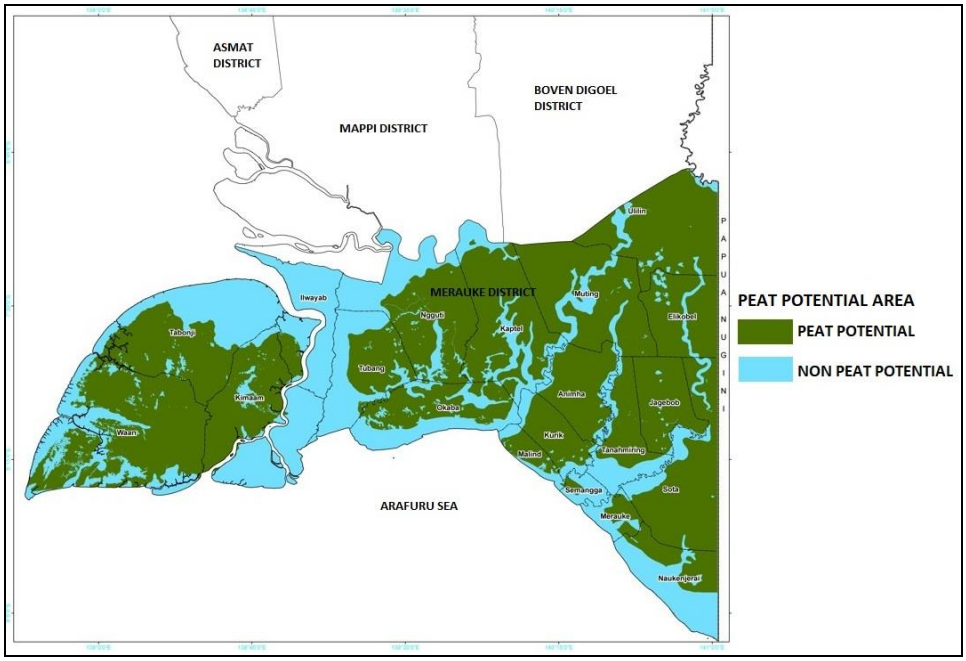

Figure 3-3: Peat potential area in Merauke Regency based on geology map

The rules of this relationship were as follow:

a. Non Peatlands class appeared when the land cover types were open land, settlement and water body, or when all types of land cover classes meet non peatlands area.
b. Shallow peatlands class appeared when forest meets peat potential area of old swamp deposits.
c. Very shallow peatlands class appeared when other land covers meet peat potential areas, young swamp deposits or old swamp deposits.

Land cover of Merauke Regency was made using six scene imageries from Landsat 8 in the period 2015-2016. Land cover information was made using visual interpretation methods and digitized on the screen. The first result of land cover information was then verified using the ground cover observation data. The accuracy of land cover information (especially for peatlands estimation) based on Landsat 8 image for the study area was more than 80 %.

Misinterpretation was often found when distinguishing several land cover types, such as shrub, cultivated land, open land, rice field and swamp. The data and knowledge about land cover condition in Merauke Regency obtained from ground survey were then used to improve the land cover classification, so that the interpretation error became minimized and the accuracy improved. Figure 3-6 showed the final result of land cover information in Merauke Regency, and land cover was divided into 11 classes.

After all data were collected, ie: spatial information on potential peat areas (Figure 3-3), spatial land cover information (Figure 3-4), and table of land cover relationships, peat potential areas and peat thickness classes (Table 3-1), then the data were overlaid and peat thickness classes were estimated using the rules in Table 3-1. The spatial information of estimated peat thickness was shown in Figure 3-5. The area of Merauke Regency was divided into three peat thickness classes, as follows:

a. Non peatlands class, it is shown in cyan color,
b. Very shallow peatlands class (peat thickness between 0-50 cm), this class (Light green) was distributed in almost all districts in Merauke Regency,
c. Shallow peatlands class (peat thickness between 50-100 cm), this class was spread at upper part of Merauke regency, especially in Muting, Kimaam, Eligobel, Ulilin, Ngguti and Kaptel districts.

Table 3-1: Correlation and look up table of land cover, peat potential area and peat thickness classes

No	Land cover	Peat potential area based on Geology Map	Peat thickness classes
1.	Forest	Non peatlands area	Non peatlands
		Young swamp deposits	Very shallow peatlands
		Old swamp deposits	Shallow peatlands
2.	Plantations	Non peatlands area	Non peatlands
		Young swamp deposits	Very shallow peatlands
		Old swamp deposits	Very shallow peatlands
3.	Shrub	Non peatlands area	Non peatlands
		Young swamp deposits	Very shallow peatlands
		Old swamp deposits	Very shallow peatlands
4.	Cultivated land	Non peatlands area	Non peatlands
		Young swamp deposits	Very shallow peatlands
		Old swamp deposits	Very shallow peatlands
5.	Open land	Non peatlands area	Non peatlands
		Young swamp deposits	Non peatlands
		Old swamp deposits	Non peatlands
6.	Settlement	Non peatlands area	Non peatlands
		Young swamp deposits	Non peatlands
		Old swamp deposits	Non peatlands
7.	Swamp	Non peatlands area	Non peatlands
		Young swamp deposits	Very shallow peatlands
		Old swamp deposits	Very shallow peatlands
8.	Mangrove	Non peatlands area	Non peatlands
		Young swamp deposits	Very shallow peatlands

No	Land cover	Peat potential area based on Geology Map	Peat thickness classes
		Old swamp deposits	Very shallow peatlands
9.	Water body	Non peatlands area	Non peatlands
		Young swamp deposits	Non peatlands
		Old swamp deposits	Non peatlands
10.	Rice field	Non peatlands area	Non peatlands
		Young swamp deposits	Very shallow peatlands
		Old swamp deposits	Very shallow peatlands
11.	Savanna pasture	Non peatlands area	Non peatlands
		Young swamp deposits	Very shallow peatlands
		Old swamp deposits	Very shallow peatlands

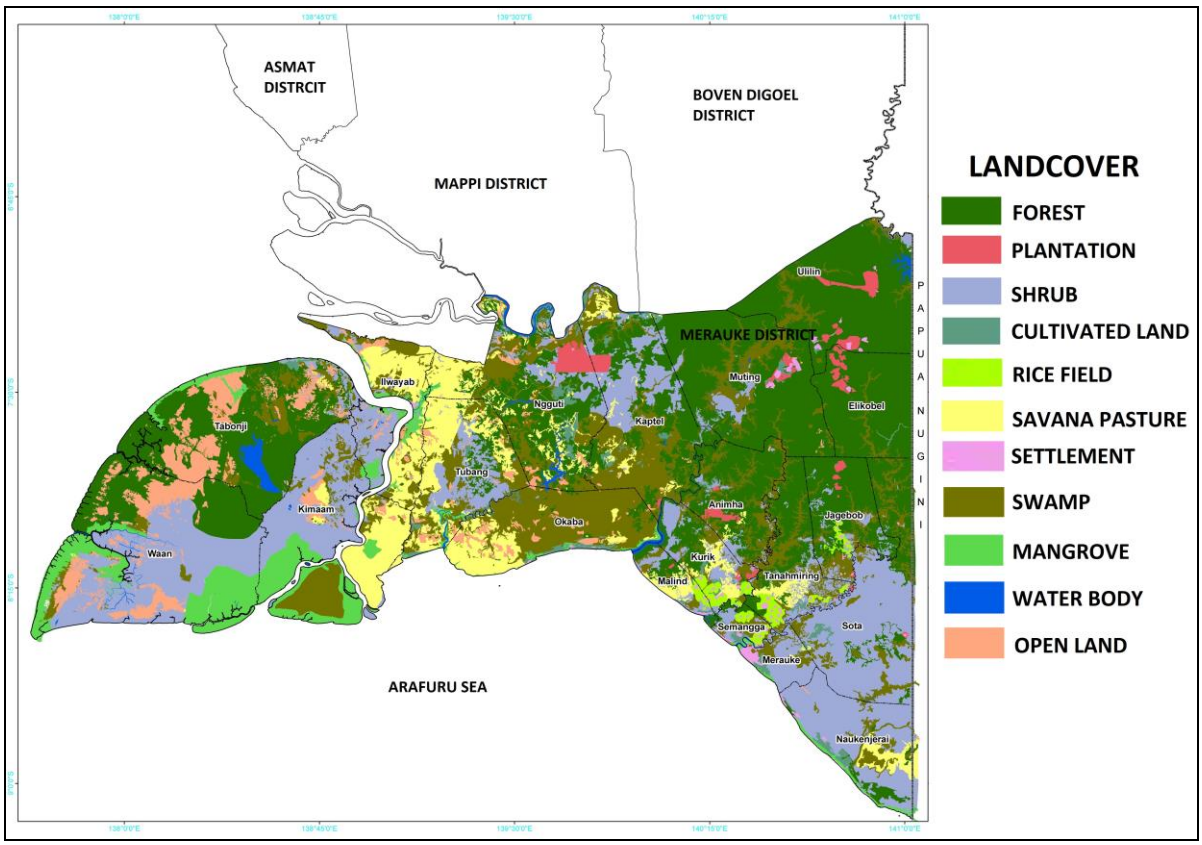

Figure 3-4: Spatial information of land cover in Merauke Regency in period 2015-2016

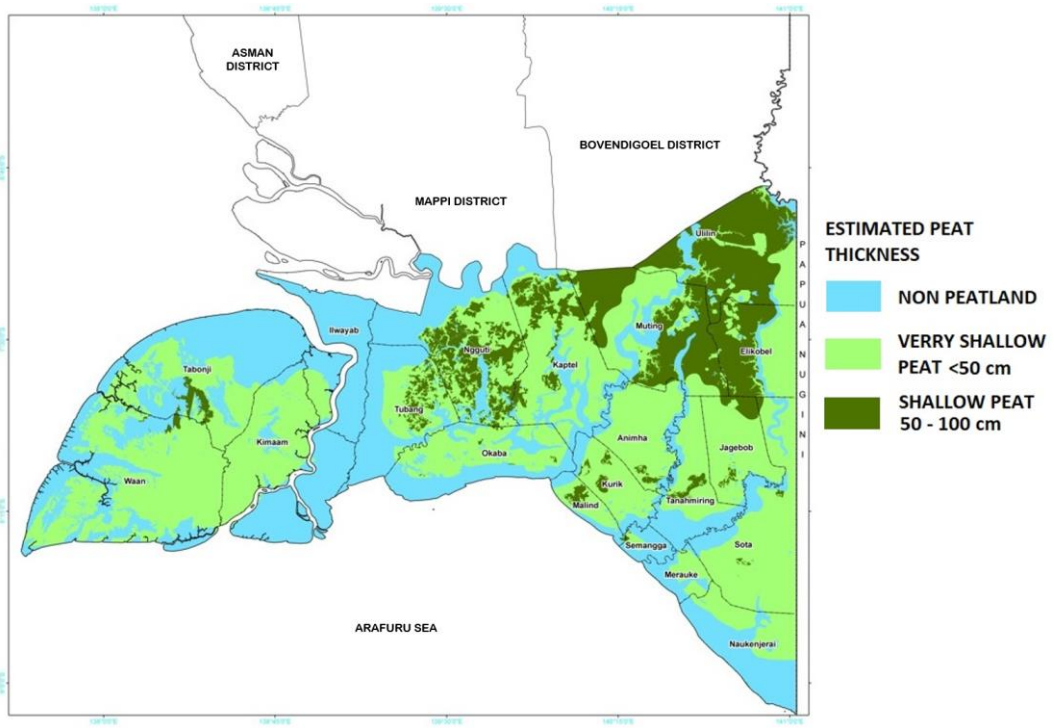

Figure 3-5: Spatial information of estimated peat thickness classes in Merauke Regency

Estimated peat thickness classes in Merauke Regency obtained from this research was evaluated by comparing the result with Indonesia Peatlands Map with scale 1: 250.000 issued by the Ministry of Agriculture (Kementan 2011) for the December 2011 edition. This map were made using ground survey data and land mapping with various scales of 1: 250.000, 1: 100.000 and 1: 50.000. Indonesia peatlands map divided peat thickness classes in Merauke Regency (Figure 3-6) into 2 classes: D0 class (peat thickness less than 50 cm), and D1 class (peat thickness between 50-100 cm). Even the map stated D0 class as one of peat thickness classes, but D0 class was not spatially displayed in the map, because it is though due to peat thickness less than 50 cm can be classified as non-peatlands (Driessen 1978).

The comparison of the estimated peat thickness classes produced in this activity with Indonesia Peatlands Map showed that the number of peat thickness classes in Merauke Regency was almost the same, where there were two peat thickness classes, i.e. very shallow peatlands (peat thickness less than 50 cm) and shallow peatlands (peat thickness between 50-100 cm). According to the area and location of peatlands in Merauke Regency, the comparison was only be done in shallow peatlands. The area of shallow peatlands in Indonesian Peatlands Map was smaller than the estimated shallow peatlands, and the location of the shallow peatlands in the Indonesian Peatlands Map was relatively similar or adjacent to the location of estimated shallow peatlands obtained from this activity. Further analysis showed that the shallow peatlands obtained from Indonesia Peatlands Map was located in forest and swamp area. According to geostatistical test, the confidence level 3σ or more than 90 %, most of shallow peatlands was located in forest and swamp area.

In fact, information of peat thickness had been issued in some maps, such as Indonesia Peatlands Map from Ministry of Agriculture or Map of Peatlands

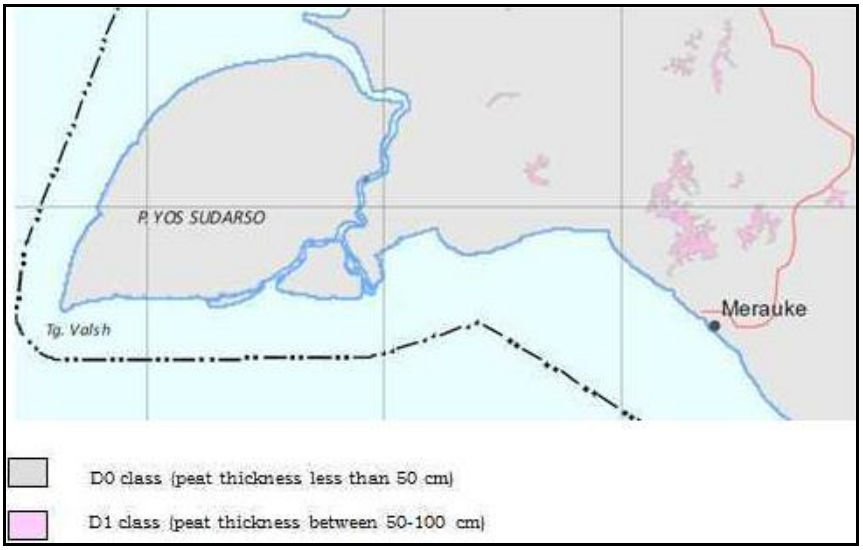

Figure 3-6: Peat thickness classes in Merauke Regency from Indonesia peatlands map

Distribution Area and Carbon Content in Kalimantan from Wetlands International. But their results are quite different, so it makes difficult for user to determine which information is correct and can be used as a reference. Therefore, the ground survey data becomes a very important reference data to evaluate the accuracy of the produced information. According to Adjustment (Geodesy-Statistic), Remote Sensing data is only focus in precision, not focus in accuracy. Accuracy will be have high true value and least bias value if it compares the ground data using least square adjustment methods. The advantages of this model are having higher level of precision, effective in cost mapping, efficient and time use especially in preliminary surveys. The weakness of the resulted model is the level of object detail and it has not been tested into other areas.

This model is only used for preliminary survey of geology, mining, and others engineering.

Ground surveys are still required for ground checking as these models have not yet produced higher accuracy. Improving the accuracy model needs to change the algorithm by least square adjustment approach. Least square adjustment is one of the geodesy statistical (geostatistical) method to get high true value, least bias value, and minimum error. It also required multi-sensor data for more precise mapping.

4 CONCLUSION

The results have shown that preliminary estimation model of peat thickness classes could be developed using land cover condition approach on Landsat 8 image. The preliminary estimation of peat thickness classes was verified against the Indonesian peat map. The peat potential area was determined using Geology Map because it was relatively similar with ground survey data. The preliminary estimation of peat thickness model was conducted using a table of relationships among land cover, peat potential areas and peat thickness classes constructed using ground survey data and Geology Map. Very shallow peatlands class (thickness less than 50 cm) was spread in almost all districts in Merauke Regency, whereas shallow peat thickness class (thickness between 50 - 100 cm) was found at the upper part of Merauke Regency.

The verified result shows that the shallow peatlands area of the estimated shallow peatlands was relatively similar with the Indonesia peatlands Map, and the location of shallow peatlands of Indonesian Peatlands Map was relatively similar or adjacent to the location of estimated shallow peatlands.

The advantages of this model is to have a higher level of precision, effective in cost mapping, efficient and time use especially in preliminary surveys. The weakness of the resulted model is the level of object detail (LoD) not fully satisfying and it has not been tested and proven for other areas. To improve the model accuracy, the algorithm needs to be changed by least square adjustment approach. It also required multi-sensor data for more precise mapping.

ACKNOWLEDGEMENTS

This research was funded and facilitated by Remote Sensing Applications Center LAPAN. The authors would like to thank Balai Rawa of Ministry of Public Works and Public Housing for providing facilities during the implementation of this research, as well as Remote Sensing Technology and Data Center of LAPAN for providing Landsat 8 data.

REFERENCES

Agus F., Subiksa IGM, (2008), Lahan Gambut: Potensi untuk Pertanian dan Aspek Lingkungan. Balai Penelitian Tanah dan World Agroforestry Centre (ICRAF) Bogor (in Indonesian).

Alihamsyah T., (2004), Potensi dan Pendayagunaan Lahan Rawa untuk Peningkatan Produksi Padi, Ekonomi Padi dan Beras Indonesia. Badan Litbang Pertanian, Jakarta (in Indonesian).

Driessen PM, (1978), Peat Soils. in: IRRI. Soil and Rice. IRRI, Los Banos, Philippines, 763-779.

Jaenicke J., Rieley JO, Mott C., *et al.*, (2008), Determination of the Amount of Carbon Stored in Indonesian Peatlands. Geoderma 147:151–158. doi:10.1016/j.geoderma.2008.08.008.

Jumakir, Endrizal, (2017), Optimizing Land with Surjan System Through Crop Diversification in Lowland Swamp Jambi Province. Jurnal Penelitian Pertanian Terapan Vol. 17 (1):26-32 (in Indonesian).

Kripsiana AA, (2015), Pembuatan Peta Kedalaman Lahan Gambut Berbasis MTD Hasil Pemetaan Lidar. Undergraduated Thesis, Universitas Gadjah Mada Yogyakarta (in Indonesian).

Prihastomo L., (2016), Ketebalan Gambut Menggunakan Metode Ground Penetrating Radar (GPR) di Daerah Siak Riau. Undergraduated Thesis, Universitas Pembangunan Nasional "Veteran" Yogyakarta (in Indonesian).

Rudiyanto, Minasny B., Setiawan BI, *et al.*, (2016), Digital Mapping for Cost-Effective and Accurate Prediction of the Depth and Carbon Stocks in Indonesian Peatlands. Geoderma 272 (2016) 20–31.

Rudiyanto, Setiawana BI, Ariefa C., *et al.*, (2015), Estimating Distribution of Carbon Stock in Tropical Peatland using a Combination of an Empirical Peat Depth Model and GIS. Procedia Environmental Sciences 24 (2015) 152 – 157.

Setiawan Y., Pawitan H., Prasetyo LB, *et al.*, (2016), Characterizing Spatial Distribution and Environments of Sumatran Peat Swamp Area using 250 m Multi-Temporal MODIS Data. Procedia Environmental Sciences 33 (2016) 117 – 127.

Subarnas A., (2008), Inventarisasi Endapan Gambut Daerah Kabupaten Merauke, Provinsi Papua, Http://Psdg.Bgl.Esdm. Go. Id/ (in Indonesian).

Syahruddin AK, Nuraini, (1997), Identifikasi Gambut di Lapangan, Lokakarya Fungsional Non Peneliti 1997 (in Indonesian).

Tjahjono EJA, (2006), Kajian Potensi Endapan Gambut Indonesia Berdasarkan Aspek Lingkungan. Proceeding Pemaparan Hasil-Hasil Kegiatan Lapangan Dan Non Lapangan Tahun 2006, Pusat Sumber Daya Geologi (in Indonesian).

Wahyunto S., Ritung, Subagjo H., (2004), Maps of Area of Peatland Distribution and Carbon Content in Sumatera, 1990–2002. Bogor, Indonesia: Wetlands International - Indonesia Programme & Wildlife Habitat Canada (WHC).

Wetlands, (2006), Peta-Peta Sebaran Lahan Gambut, Luas dan Kandungan Karbon di Papua. Wetlands International-Indonesia Programme (in Indonesian).

SPATIAL PROJECTION OF LAND USE AND ITS CONNECTION WITH URBAN ECOLOGY SPATIAL PLANNING IN THE COASTAL CITY, CASE STUDY IN MAKASSAR CITY, INDONESIA

Syahrial Nur Amri[1]*, Luky Adrianto[2], Dietriech Geoffrey Bengen[2], Rahmat Kurnia[2]
[1)]Researcher in Marine and Fisheries Ministry of Indonesia
[2)]Lecturer in Bogor Agriculture University (IPB) Indonesia
*e-mail: sn_amri@yahoo.co.id
Received: 21 June 2017; Revised: 15 November 2017; Approved: 24 November 2017

Abstract. The arrangement of coastal ecological space in the coastal city area aims to ensure the sustainability of the system, the availability of local natural resources, environmental health and the presence of the coastal ecosystems. The lack of discipline in the supervision and implementation of spatial regulations resulted in inconsistencies between urban spatial planning and land use facts. This study aims to see the inconsistency between spatial planning of the city with the real conditions in the field so it can be used as an evaluation material to optimize the planning of the urban space in the future. This study used satellite image interpretation, spatial analysis, and projection analysis using markov cellular automata, as well as consistency evaluation for spatial planning policy. The results show that there has been a significant increase of open spaces during 2001-2015 and physical development was relatively spreading irregularly and indicated the urban sprawl phenomenon. There has been an open area deficits for the green open space in 2015-2031, such as integrated maritime, ports, and warehousing zones. Several islands in Makassar City are predicted to have their built-up areas decreased, especially in Lanjukang Island, Langkai Island, Kodingareng Lompo Island, Bone Tambung Island, Kodingareng Keke Island and Samalona Island. Meanwhile, the increase of the built up area is predicted to occur in Lumu Island, Barrang Caddi Island, Barrang Lompo Island, Lae-lae Island, and Kayangan Island. The land cover is caused by the human activities. Many land conversions do not comply with the provision of percentage of green open space allocation in the integrated strategic areas, established in the spatial plan. Thus, have the potential of conflict in the spatial plan of marine and small islands in Makassar City.

Keywords: *spatial projection, land use, spatial planning, remote sensing, coastal city*

1 INTRODUCTION

As an archipelagic country, Indonesia has many urban areas located in the coastal areas. Indonesia has 150 cities which are situated in coastal areas. The number is increasing due to the trend of urbanization rate in the urban region (Rahmat *et al.* 2016). The rapid development of the coastal cities is an indicator of how attractive the region to the most people (Bambang 2012). However, the socio-economic growth in this region is not accompanied by good city planning (Baja 2012). Urban spatial planning in many coastal areas adopted the spatial planning base on land city. In fact, the characteristics of coastal areas are very different from areas that do not

have the sea. Coastal boundaries between ecosystems where the conditions are affected by changes occurring at the sea and on the land (Article 1 of Law No. 27 of 2007 on the management of the sea, coastal, and small islands). High biodiversity levels, accessibility, and marine as the common properties cause the coastal areas to be vulnerable to damage and destruction. In addition, the consistency between policy and its implementation on the field is often low, so the concept of sustainability is very difficult to achieve.

To achieve the sustainability of coastal city system, it is important to understand the concept of sustainable spatial planning. By definition, sustainable development is a development to fulfill the needs of present human life without ignoring the necessities of human life in the future (Brundlandt 2001 in Suweda 2011). In principle, coastal spatial planning plays important role in defining development and goals needed to improve the welfare of communities with the need to protect, preserve and improve the quality of the environment and coastal ecosystems.

The initial step to achieve that is identifying the LUCC through image interpretation and spatial analysis. Land use/cover change (LUCC), as an important factor in global change, is a topic that has recently received considerable attention in the prospective modeling domain (Jean *et al.* 2014). Monitoring these changes and planning urban development can be successfully achieved using multi-temporal remotely sensed data, spatial metrics, and modeling (Yikalo and Pedro 2010). There are many approaches and software packages for modeling LUCC, many of them are empirical approaches based on past LUCC such as CLUE, DINAMICA, terrestrial ecosystems and marine CA_MARKOV and Land Change Modeler (both available in IDRISI) (Jean *et al.* 2014).

Makassar City as a coastal city in the last 15 years has been transformed into a metropolitan city parallel to other big cities in Indonesia. Common problems in coastal cities in Indonesia are also occurring in Makassar, such as floods, rob, traffic jams, and social problems. All these things happen because of inconsistent implementation of the spatial plan. Therefore, a study is needed to see how far the inconsistencies are, so that in the evaluation phase, a better management concept can be determined.

This study aims to describe the dynamics of the land use change in relation to the consistency of the implementation of urban spatial planning policy in the coastal area, so that it can be used as an evaluation material for better urban spatial planning.

2 MATERIALS AND METHODOLOGY

2.1 Location and Data

This research was done in Makassar City, located in the coastal area (Figure 2-1).

Multitemporal Landsat satellite imagery (1994, 2001, and 2015) was used in this study. These data were Landsat 5 (1994) path and row114/064, Landsat 7 (2001) path and row114/064, and Landsat 8 OLI TIRS (2015) path and row114/064.

2.2 Limitations of Analysis

Land use change analysis works on vector database, whereas for Projection simulation works based on raster database. Therefore, it is necessary to convert vector data to raster data. The size of the raster data used is 30x30 meters size adjusted to the raster size of the

Landsat satellite imagery used (Peruge *et al.* 2012).

Spatial data of the land use is obtained through multi-temporal landsat satellite image analysis and interpretation. Because using images with low spatial resolution, the determination of the type of land cover or land use is not very accurate. Land use interpreted by Landsat satellite imagery cannot be divided into clearer built up land types, so the zone division is only described in macro.

The study of land use change is focused on the change from the open area to the built up area, especially on agricultural and aquaculture land which is converted to industrial and settlement areas. In this study, open space area is categorized into: green open space (mangroves and terrestrial vegetation), non-vegetated open space, agriculture and aquaculture land, and water bodies (rivers and swamps). While the built up land is consists of: settlements, industrial and ware housing areas, and infrastructure (Purwanto *et al.* 2016; Amri 2017).

2.3 Land Use or Land Cover Analysis by Satellite Imagery Interpretation

Remote sensing and GIS techniques are the powerful tool to investigate, predict and forecast environmental change in a reliable, repetitive, non-invasive, rapid and cost effective way with considerable decision making strategies (Amiri *et al.* 2014). The advent of satellite data in the last few decades opened up a new dimension for the generation of land cover information. While the extraction of such information is possible using the 'traditional' approaches of surveying or digitizing, land cover information extraction that is based on image classification has attracted the attention of many remote sensing researchers (Lu and Weng 2007). But, the latter is now considered the standard approach (Farzaneh 2007).

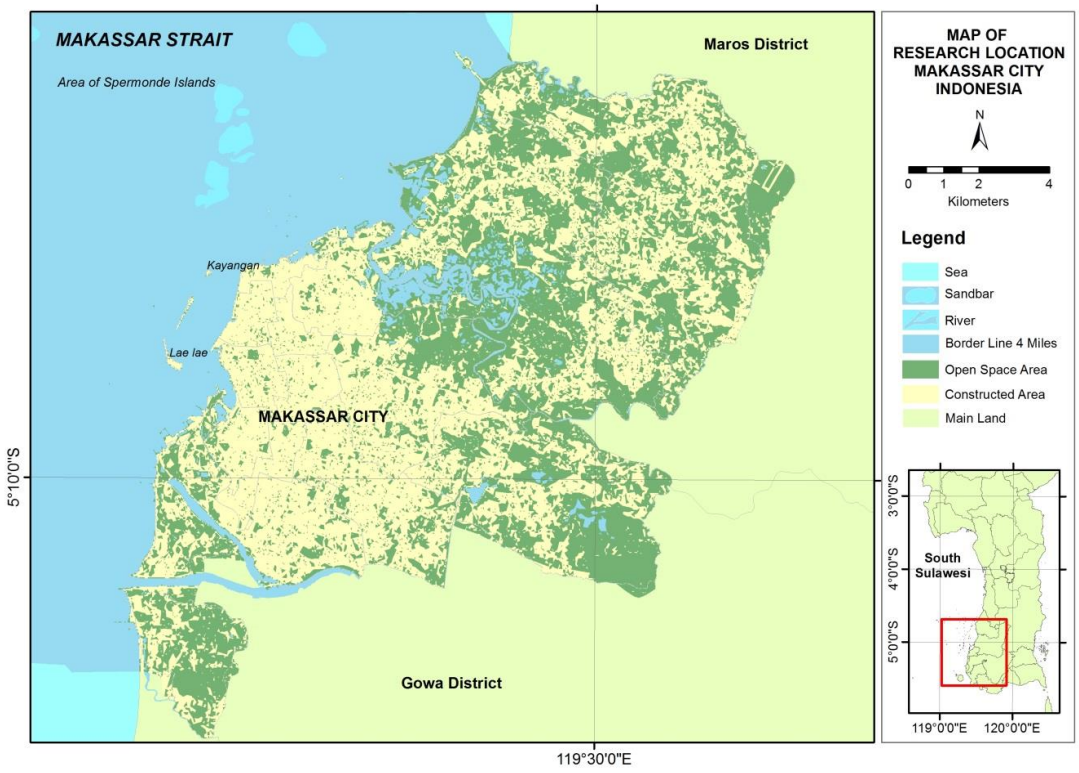

Figure 2-1: Map of research location in Makassar City

The method of LULC change detection and analysis was performed using a series of processes including data acquisition, data pre-processing, supervised classification and post classification (Boori *et al.* 2016a; Romero *et al.* 2013). Image preprocessing is the initials processing of the raw data and normally involves processes like geometric correction, image enhancement and topographical correction (Choudhary *et al.* 2017). Geometric correction was performed using UTM-WGS84 projection (Kaliraj *et al.* 2017; Choudhary *et al.* 2017).

Recently, several image classification techniques and algorithms have been developed extensively for the landuse and land cover analysis throughout the world (Kaliraj *et al.* 2017). These techniques are include vector machine (SVM), artificial neural network (ANN), Maximum Likelihood Classifier (MLC), fuzzy analysis, as well as segmentation and clustering (Kaliraj *et al.* 2017). Among them, the Maximum Likelihood Classifier (MLC) technique depends on a combination of ground samples and personal experience with the study area and is strictly used the field observed training samples of real ground surface (Purwanto *et al.* 2016; Amri 2017; Jayanth *et al.* 2015).

To verify the land cover data into land use data is done through ground truth, thematic map review, and guides from the high resolution satellite imagery (SPOT 5) to check the land use in 2001.

2.4 Spatial Projection Analysis

The model of land-use simulation (projection) in 2031 is done through the Cellular Automata - Markov Chain analysis (Trisasongko *et al.* 2009; Peruge *et al.* 2012). A Cellular Automata – Markov model is capable of simulating temporal and spatial dynamics of LCLU change by integrating remote sensing and GIS based data with biophysical and socio-economic data (Myint and Wang 2006; Courage *et al.* 2009; Tong *et al.* 2012). The Markov-CA model is also called combined Cellular Automata/ Markov Chain/ Multi-Criteria/ Multi-Objective Land Allocation land cover prediction method, which adds an element of spatial contiguity, specific decision from multi-criteria evaluation and also the knowledge of dynamic distribution from MC analysis (Sang *et al.* 2011).

The Markov Chain module produces a transitional or probability matrix which is the transition matrix of change from the previous year to the projection year (t_1-t_0). The Markov equation is constructed using the distribution of land use at the beginning and end of the observation period presented in a vector (single column matrix), and a transition matrix (Figure 2-2).

0	0	1	0	0
0	1	1	1	0
1	1	1	1	1
0	1	1	1	0
0	0	1	0	0

Figure 2-2: The pixel values at the filter 5x5

The contribution of the matrix in the simulation process is to provide information about the variation of land use change from a type of land use in the center pixel of the filter matrix 5x5. The filter matrix 5x5 is the translation of the neighborhood concept, meaning that land use change in the central pixel is affected by the land use at the surrounding of 24

pixels. The 30x30 meter pixel size indicates an effect radius of 60-90 meters.

Moving filter means that the neighboring analysis is performed on every window with 5 pixels horizontal and 5 pixels vertical. 5x5 value is used to normalize the land suitability (Munibah 2008; Peruge *et al.* 2012).

The next step is to run the Cellular Automata module to obtain a land use prediction in 2031. The data entered as input is the transition matrix and land use in 2015 as the base year of land use (t_0).

Predicted land use change obtained from the simulation results, need to be tested for accuracy. This accuracy test also acts as a validation of the simulation results. Validation was done by comparing the 2015 simulated land use with observed land use (satellite image analysis) of 2015, based on the value of Kappa (Jensen 1996):

$$K = \frac{N * \sum_{i=1}^{z} X_{ii} - \sum_{i=1}^{z} (X_{i+} * X_{+i})}{N^2 - \sum_{i=1}^{z} (X_{i+} * X_{+i})} \quad (2\text{-}1)$$

Where:

K = Kappa Value

X_{ii} = area of land use type to-i simulation results that corresponds to the area of the land use type to-i observation results (diagonal)

X_{i+} = area of land use type to-i simulation results

X_{+i} = area of land use type to-i observation results

N = total area of all types of land use

Z = number of land use types

The calculation result of Kappa value (K) shows the level of conformity between the land uses of simulation result with the land use of observation result. K value >0.75 or 75% means that the simulation or projection analysis can be proceed.

2.5 Spatial Consistency Evaluation

Spatial planning policy of Makassar City refers to the Spatial Plan of Makassar City (RTRW) for 2010-2030. Spatial Projection result in 2031 of Makassar City will be compared with RTRW (*Rencana Tata Ruang Wilayah*) of Makassar City then look for any spatial Incompatibility. This information then used to assess the level of sustainable utilization and management of land resources in Makassar City. Using the linkages matrix of the spatial utilization and the zonation plan of the coastal area and the small islands of Makassar City, it is possible to identify the potential conflicts in the future.

3 RESULTS AND DISCUSSION

3.1 Land Use

Land use is closely linked to human activities that involve utilization and management (Dwiyanti 2013). The high rate of population growth with all its social and economic activities has resulted in increased land demand. This then increased the complex functions of space in coastal city, whether as industrial centers, government, trade and services, settlement areas, natural resource production spaces and ecological spaces.

The spatial analysis shows that there has been a significant increase of open space during 21 years (1994-2015) (Table 3-1).

During the observation period, physical development was relatively spreading irregularly and indicated the urban sprawl phenomenon (Figure 3-1), a peripheral growth phenomenon that extends beyond its location and is not adjacent to the metropolitan area development center (Barnes *et al.* 2001). Urban sprawl is a complex phenomenon, which not only has environmental

impacts, but also social impacts (Barnes *et al.* 2001).

Table 3-1: The LUCC of Makassar City in 1994 to 2015 and spatial projection in 2031

Year	Built-Up Area (ha)	Open Area (ha)	Water Body (ha)
1994	3.791	11.570	98,260
2001	6.478	8.738	98,190
2015	9.839	6.396	97.740
2031	11.600	5.654	97,290

3.2 Spatial Projection of Land Use in 2031

Validation is needed to find out how accurately the data projection can be acknowledged and be guaranteed to continue the projection analysis (Munibah 2008). Validation results show an 85.4% value, which means that between the land uses of simulation result and the land use of observed result show the value of the area and distribution that almost matched.

The Markov Chain module produces a transitional or probability matrix which is the transition matrix of change from the previous year to the projection year (t_1-t_0) (Munibah 2008). The Markov equation is constructed using the distribution of land use at the beginning and the end of observation period presented in a vector (single column matrix), and a transition matrix (Table 3-2).

The spatial projection results in 2031 indicate significant increase of built-up areas in suburbs areas, namely Biringkanaya and Tamalanrea Sub-district (Figure 3-2). This condition is caused by several things, among others, the expansion of Makassar industrial area (Tamalanrea and Biringkanaya), the highway of Sutami (Tamalanrea and Biringkanaya), the international airport of Sultan Hasanuddin (Biringkanaya), and the new road access of Mamminasata (Biringkanaya).

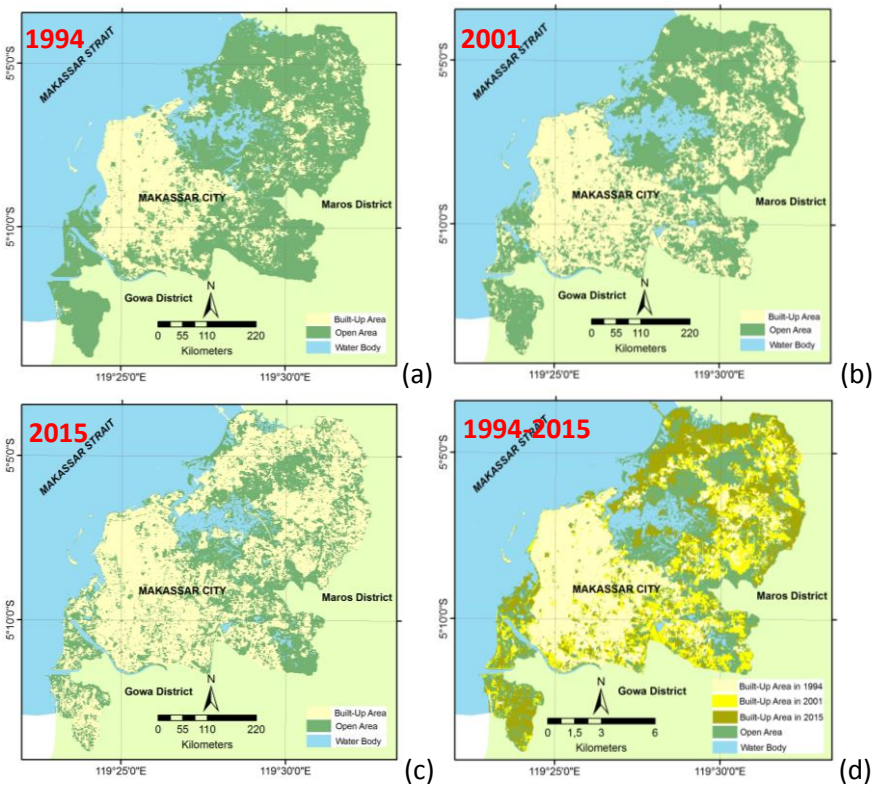

Figure 3-1: The land use of Makassar City in 1994 (a), 2001 (b), 2015 (c), and the trend of the land use in 1994 to 2015 (d)

Table 3-2: Probability matrix and land transition matrix

	Cl. 1	Cl. 2	Cl. 3		Cl. 1	Cl. 2	Cl. 3
Class 1	0.8046	0.1069	0.0884	Class 1	51834	6888	5697
Class 2	0.0394	0.4596	0.5010	Class 2	3358	39170	42691
Class 3	0.0052	0.2255	0.7693	Class 3	540	23523	80242

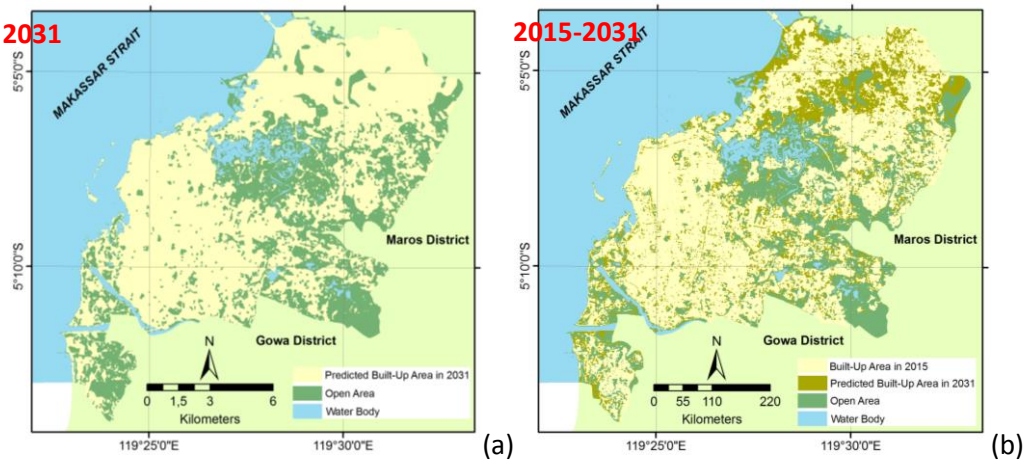

Figure 3-2: The result of spatial projection of land use of Makassar City in 2031 (a) and the trend of the land use in 2015 to 2031 (b)

Table 3-3: Comparison of population and built-up area in 2015 and projection in 2031 in Makassar City

Year	Land Use Area (hectares)				Population	Economic Growth (Million)
	Open Space		Built-up Area			
	Extensive (ha)	%	Extensive (ha)	%		
2015	7.682,40	44,99	9.392,49	55,01	1.547.941	88.740.213,15
2031	5.611,75	32,73	11.531,36	67,27	2.060.309	1.159.463.308

Source: Analysis Result (Amri 2017)

Based on the projection analysis, the built-up area in the mainland area of Makassar City in 2031 is predicted to increase to 11,531.36 hectares or 67.27%, while the remaining area is only 5,611.75 hectares or 32.73%. The number of built-up areas increased significantly compared to the conditions of land use in 2015. The increase is aligned with the projected population growth in 2031 of 2,060,309 people (Table 3-3).

Biringkanaya Sub-district adjacent to Maros District experienced the greatest land conversion, where the prediction of land use change in 2031 left 766.72 hectares or 22.95% of the total area in Biringkanaya Sub-District, and 39.58% for Tamalanrea Sub-District (Table 3-4). The area is far in comparison to the built-up area in 2015, where Biringkanaya Sub-District still leaves an open area of 50.66% and 56.82% for Tamalanrea Sub-District.

Meanwhile, for the archipelago areas within the administrative boundaries of Makassar City, there are 11 small islands namely, Lanjukang Island, Langkai Island, Lumu-lumu Island, Kodingareng Lompo Island, Kodingareng Keke Island, Bone Tambung Island, Barrang Lompo Island, Barrang Caddi Island, Samalona Island, Lae-lae Island, and Kayangan Island (Figure 3-3). The islands are all inhabited with the highest density present in Lumu-lumu Island with the density of 262 people per hectare and spread evenly across the island. The highest population is found in Kodingareng Keke Island (4,170 people), Barrang Lompo Island (3,563 people), Barrang Island Caddi (1,263 people), and Lae-lae Island (1,500 people). In 2015, the total area of the built-up area in the archipelago region in Makassar City is amounted to 55.7 hectares and open area of 66.83 hectares (Table 3-5). Based on the comparison of the island, the highest proportion of built-up areas is in Lumu-lumu Island which is 92.62% and the lowest is Lanjukang Island with only 10% of the built-up area.

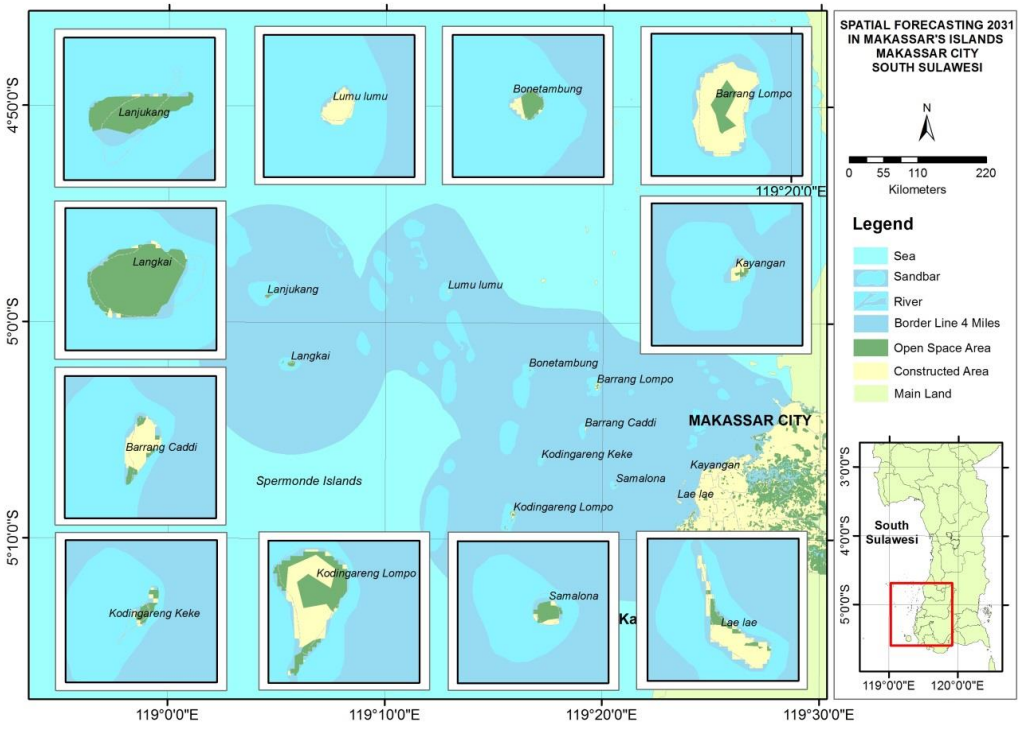

Figure 3-3: Spatial projection in the Makassar's islands in 2031.

Table 3-4: Number of population predictions in two peri-urban sub-districts and built-up area in 2031 in Makassar City

Projection Year	Population		Built-up Area (Hectares)		Open Space (Hectares)	
	Sub-District		Sub-District		Sub-District	
	Tamalan-rea	Biring-kanaya	Tamalan-rea	Biring-kanaya	Tamalan-rea	Biring-kanaya
2015	109.471	190.829	1.731,68	1.649,09	2.278,93	1.693,34
2031	148.997	338.883	2.429,35	2.574,27	1.591,66	766,72

Source: Analysis Results (Amri 2017)

Table 3-5: The condition of the land use in 2015 and spatial projection in 2031 in the archipelagic area of Makassar City

Islands	2015				2031			
	Built-up Area (Hectares)	%	Open Space (Hectares)	%	Built-up Area (Hectares)	%	Open Space (Hectares)	%
Lanjukang	1,54	10,00	13,82	90,00	0,27	1,90	13,97	98,10
Langkai	4,34	14,14	26,36	85,86	0,96	3,35	27,76	96,65
Lumulumu	3,60	92,62	0,29	7,38	3,78	100,00	0,00	0,00
Kodingareng Lompo		53,61	12,35	46,39	12,53	50,31	12,37	49,69
Bone Tambung	1,44	43,83	1,84	56,17	0,79	26,94	2,15	73,06
Kodingareng Keke	0,75	37,08	1,26	62,92	0,33	17,59	1,54	82,41
Barrang Caddi	4,60	72,70	1,73	27,30	5,25	83,33	1,05	16,67
Barrang Lompo	15,46	73,75	5,50	26,25	17,16	83,20	3,47	16,80
Samalona	0,85	34,69	1,61	65,31	0,78	29,37	1,88	70,63
Lae-lae	7,83	81,79	1,74	18,21	11,11	86,91	1,67	13,09
Kayangan	1,02	75,54	0,33	24,46	1,49	66,63	0,75	33,37

Source: Analysis Result (Amri 2017)

Table 3-6: The condition of the land use in the archipelagic area of Makassar City

Islands	Built-up Area		Open Space	
	Difference	Status	Difference	Status
Lanjukang	-1,265	Decrease	0,146	Increase
Langkai	-3,378	Decrease	1,404	Increase
Lumulumu	0,179	Increase	-0,287	Decrease
Kodingareng Lompo	-1,752	Decrease	0,020	Increase
Bone Tambung	-0,643	Decrease	0,308	Increase
Kodingareng Keke	-0,416	Decrease	0,276	Increase
Barrang Caddi	0,655	Increase	-0,675	Decrease
Barrang Lompo	1,701	Increase	-2,036	Decrease
Samalona	-0,072	Decrease	0,273	Increase
Laelae	3,279	Increase	-0,070	Decrease
Kayangan	0,470	Increase	0,417	Increase

Source: Analysis Result (Amri 2017)

The decrease and increase mean that several islands in Makassar City are predicted to decrease of the built-up areas and increased of the open areas, especially in Lanjukang Island, Langkai Island, Kodingareng Lompo Island, Bone Tambung Island, Kodingareng Keke Island and Samalona Island (Table 3-6). The condition is caused by the government policy that makes the islands as conservation and tourism area. Meanwhile, the increase of the built up area is predicted to occur in Lumu Island, Barrang Caddi Island, Barrang Lompo Island, Lae-lae Island, and Kayangan Island. The condition is caused by the increased number of populations, thus correspond to the land conversion.

Especially for Kayangan Island, both constructed and open areas are relatively increased. It is because Kayangan Island which is a government asset of Makassar City is managed by the private sector as tourist destination. They then build guest houses on the sea water. The words 'decrease' and 'increase' indicate an increase or decrease in the area due to human activities.

3.3 Relevance of Land Use Projection Year 2031 with the Spatial Policy of Makassar City

Coastal cities have certain limits and extents, but the demand of built-up area is always high. The land conversion is capable to change the natural configuration of urban land. Urban land use tends to ignore the existence of open space, which is often regarded as uneconomic. Whereas the open spaces, ecologically, is able to balance the functions and work of urban systems. Therefore, it is needed a policy tool that is able to regulate and maintain the existence of the open areas at optimum extent it is required.

In the city's urban spatial plan (RTRW 2010-2030), Makassar City has been divided into 12 Integrated Strategic Areas, namely City Center Area, Integrated Sports Area, Integrated Port Area, Integrated Settlement Area, Integrated Warehousing Area, Research and Integrated Education Area, Integrated Maritime Area, Integrated Cultural Area, Integrated Global Business Area, Integrated Industrial Area, and Integrated Airports Area (Figure 3-4). Each of these areas has been determined the optimal target area that will function as the green open spaces (Table 3-7). In 2015, the City Center has already been deficit in terms of open space area for 187.42 hectares and the spatial projection in 2031 is at392.48 hectares (Table 3-8). In the Integrated settlements area, there are still about 1.366.13 hectares of open space area or remained 297.67 hectares from the target allocation of the open space area. But in 2031, a drastic decline is predicted with 25.49 hectares remains from 1,068.46 Targeted hectares. Table 3-8 also shows several integrated strategic areas that will be deficit of open area in 2031, including the City Center, Integrated Ports, Integrated Warehousing, and Integrated Maritime Zones. These four areas are densely populated areas that require special environmental management, for example by utilizing the roofs or buildings as green areas and integrated waste management systems.

In general, the deviation from the urban spatial plan precisely starts from the inconsistency of government policy. It means that the government as the manager of urban spatial plan has not really referring to the spatial planning maps that have been previously defined. The main cause of ineffectiveness of spatial plan is the lack of inter-institutional coordination and community involvement, so that the aspirations of the people are not accommodated in urban spatial planning (Sunardi 2004).

Determination of a region with a certain purpose must be balanced with the supervision and affirmation. Development permits that are issued by the government often do not conform to the regional regulations, such as green open space areas are permitted for residential areas. The absence of sanctions against violations of the urban spatial plan indicates the uncertainty and inconsistencies of the urban spatial plan. For example, at the present time, Integrated Industrial Zones has many settlements, while the allocated area for open green areas are getting smaller. The

issued construction permit should be aligned with the land allocation based on spatial plan of Makassar City. The data presented in (Table 3-8) shows that the Integrated Industrial and Integrated Warehousing Area has been experiencing a drastic increase of construction in 2031. This could happen not because of industrial and ware housing development, but filled by other land use.

Table 3-7: Land use conditions in Makassar City in 2015 and spatial projection in 2031 at each integrated strategic area

Integrated Strategy Region	Total Area (hectare)	2015		2031	
		Built-up Area (ha)	Open Space (ha)	Built-up Area (ha)	Open Space (ha)
Main City	2.935,22	2.516,39	399,62	2.721,91	194,56
Integrated Sport	883,49	305,65	556,85	308,31	550,80
Integrated Port	292,22	225,91	59,06	255,86	27,36
Integrated Settlement	5.342,28	2.841,57	2.434,59	3.109,76	2.162,41
Integrated Warehouse	1.968,22	860,06	979,13	1.507,44	334,78
Integrated of Research & Education	1.533,17	465,04	929,89	486,90	909,47
Integrated Maritime	354,56	145,32	162,19	246,95	61,58
Integrated Culture	48,02	13,58	34,19	12,70	34,90
Integrated Global Business	420,83	228,88	166,51	253,83	141,67
Integrated Industry	1.391,61	551,36	735,61	862,66	430,89
Integrated Tourism	374,76	192,43	174,20	207,81	158,05
Integrated Airport	1.836,04	919,79	913,73	1.399,49	431,66

Source: Analysis Result (Amri 2017)

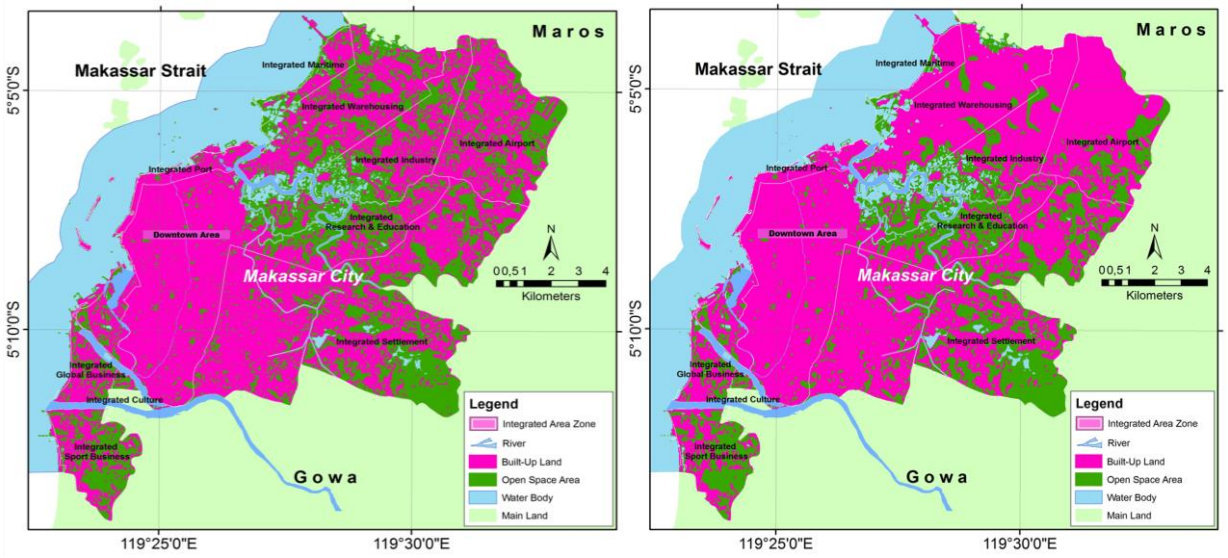

Figure 3-4: The built-up and open space area in 2015 and 2031 in Makassar City base on the integrated strategic area of Makassar City (RTRW 2010-2030)

Table 3-8: Percentage of green open space targeted at each integrated strategic area and realization of target in 2015 and 2031

Integrated Strategy Region	% Target		Difference From Target (hectare)*	
	%	ha	2015	2031
Main City	20	587,04	-187,42	-392,48
Integrated Sport	50	176,70	380,15	374,1
Integrated Port	30	58,44	0,62	-31,08
Integrated Settlement	30	1.068,46	1.366,13	1.093,95
Integrated Warehouse	20	393,64	585,49	-58,86
Integrated of Research & Education	47	306,63	623,26	602,84
Integrated Maritime	50	70,91	91,28	-9,33
Integrated Culture	50	9,60	24,59	25,3
Integrated Global Business	50	84,17	82,34	57,5
Integrated Industry	20	278,32	457,29	152,57
Integrated Tourism	50	74,95	99,25	83,1
Integrated Airport	47	367,21	546,52	64,45

Description : *) Minus (-) means it deviated from the plan target

Sources: Analysis Result (Amri 2017)

This condition would be a serious problem if not solved. The growing of the built-up area that is not proportional to the allocation of green open space, will decrease the carrying capacity of the coastal city (increased pollution, decreased ground water availability, increasing of temperatures, etc.), decreasing the natural beauty and cultural historical artifacts, and at the social level will reduce the urban security and public welfare.

Population density is determinant to the environmental quality of a coastal city. It is an indicator of the high socio-economic activity of the population. The more densely populated area will put greater pressure to the environment and become the cause of environmental degradation. To state how big a region's environmental quality is based on its population density, the Population Density Index (IKP) is used. The density index of Makassar City below 2015 is at 100, which means that the population density of Makassar City is still in the ideal level as recommended by the World Health Organization (WHO) reference (WHO 2014). In 2015 however, the population density index has reached 99.25 which means that the population density level is slightly over the ideal threshold, and this became a warning for Makassar City to more firmly restrict the land conversion efforts that do not consider the ecological factors. Because, if it doesn't start from now, based on the projection of population in 2031 with predicted population of 2,060,309 people, the population density index has reached 82.9. It means that the value indicate a serious pressure on the coastal city environments.

Management of marine areas and islands in Makassar City is regulated in the zoning plan of the coastal area and Small Islands (RZWP3K) for 2014. Spatial plan is very important to do because the

marine and islands in Makassar City is a busy trade and high-traffic area of the ship. With many types of utilization in the sea will cause a lot of potential conflict. RZWP3K of Makassar City is based on the establishment of three utilization zones, among others are Public Utilization Area, Conservation Area, and Cruise Line which each region has zone and subzone (Table 3-9).

The linkages matrix between marine space utilization areas was done to see the connection and harmonization between space utilization and potential conflict (Table 3-10).

Fisheries, port, industry, and cruise line zones are the central of human activities and the ships traffic which are particularly vulnerable to waste disposal. Development of mariculture and conservation areas around the area above is very risky and will cause conflict, because the activities of port and ship traffic will leave an oil spill and fishing gear that can interfere with cultivation activities.

The existence of mariculture and marine tourism zones (especially water recreation zones) will interfere with each other or potentially conflict with the port activities, fishing zones and cruise line zones. Mariculture zones and marine tourism zones (diving and snorkeling) will be contaminated with the port activities, ship traffic, and fishing activities. Negative impacts that may arise are pollution and environmental changes such as the fishing activities that will leave traces of both fishing equipment that is caught in the rocks, oil spills and disposal from fishermen.

Table 3-9: Management of marine areas and islands in Makassar City in RZWP3K document 2014 in Makassar City

No.	Region	Zone	Sub-Zone
1	Common Use	• Aqua Culture	• Mariculture • Deep Sea Aquaculture
		• Fisheries	• Pelagic Fisheries • Demersal Fisheries
		• Port	• DLKp (Collector Port) • DLKr (Collector Port)
		• Tourism	• Water Tourism • Diving • Beach Tourism
		• Others Utilization	
2	Conservation	• Utilization Limited	• Utilization Limited BarrangCaddi Island • Utilization Limited BarrangLompo Island • Utilization Limited of Bonetambung Island
3	Cruise Line	• Cruise Line	• International Cruise Line • National Cruise Line • Regional Cruise Line

Source: Coastal zone planning & small island of Makassar City 2014 (Bappeda Kota Makassar)

Table 3-10: The linkages matrix between marine space utilization areas in Makassar City (Maesaroh *et al.* 2013)

	Aqua Culture	Fisheries	Port	Marine Tourism	Beach Tourism	Conservation	Cruise Line
Aqua Culture							
Fisheries	▲						
Port	○	□					
Marine Tourism	○	○	○				
Beach Tourism	○	○	○	□			
Conservation	◄	◄	◄	□	□		
Cruise Line	▲	○	□	○	○	▲	

Description: ○ potentially conflicting, ▲ threatening to Activities above, □ Positive impacting activities, ◄ Threatening activities on the left

Mariculture zones also have the potential to disrupt diving and snorkeling activities, because it can limits the movement for tourists. The beach recreation zone will also potentially be conflicted with the presence of ports and activities, but the presence of ports with tourism activities on the islands will be crucial as part of the supporting infrastructure for island tourism activities.

4 CONCLUSION

- There has been significant increase of open spaces for a period of 14 years (2001 - 2015). During this observation period, physical development was relatively spreading irregularly and indicated the urban sprawl phenomenon. Spatial growth and movements of the built up areas in 2015-2031 are predicted to be higher especially in two peri-urban sub-districts (sub-district Tamalanrea and Biringkanaya) which are an integrated strategic area for warehousing, industrial, maritime, airport and settlement interests.
- There has been open area deficit for the green open space in 2015, especially in the downtown area, whereas in 2031 it is predicted that land deficits will increase to several designations of integrated strategic areas, such as integrated maritime, ports and warehousing zones.
- Several islands in Makassar City are predicted to have its built-up areas decreased. Especially in Lanjukang Island, Langkai Island, Kodingareng Lompo Island, Bone Tambung Island,

Kodingareng Keke Island and Samalona Island. Meanwhile, the increase on built up area is predicted to occur in Lumu Island, Barrang Caddi Island, Barrang Lompo Island, Lae-lae Island, and Kayangan Island. The land cover is caused by the human activities.

- The plan of development areas or marine utilization zones in Makassar city based on the zoning plan of the coastal area and small islands has the potential of land use conflict, where the plan of conservation area development, maritime tourism and mariculture, will conflict with the port and industry activities, and fishing catch areas.

This study used low resolution to obtain the same spatial resolution at different times. For the future research, to obtain information on land use changes with more detailed land use classification, we recommend using satellite imagery with higher spatial resolution.

ACKNOWLEDGEMENTS

This research was funded by the Marine and Fisheries Ministry of Indonesia through the research scholarship since 2012.

REFERENCES

Amiri F., Rahdari V., Najafabadi SM, *et al.*, (2014), Multitemporal Landsat Images Based on Eco-Environmental Change Analysis in and Around Chah Nimeh Reservoir, Balochestan (Iran). Environ. Earth Sci. 72 (3), 801–809.

Amri SN., (2017), The Land Use Spatial Dynamic of the Coastal City Base on Social Ecological System in Makassar City. Dissertation. Bogor Agriculture University (IPB).

Article 1 of Law No. 27 of 2007 on the Management of the Sea, Coastal, and Small Islands in Indonesia (in Indonesian language)

Baja S., (2012), Land Use Planning in Regional Development. Publisher ANDI, Yogyakarta.

Bambang US, (2012), The Dynamics of Land Use in Urban Areas (Study in Bandar Lampung). Seminar of Research Results. Dies Natalis FISIP Unila 2012.

Barnes KB III, Morgan JM, Roberge MC, *et al.*, (2001), Sprawl Development: its Patterns, Consequences, and Measurement. Towson University, Towson

Boori MS, Vozenilek V., Choudhary K., (2015a), Land Use/Cover Disturbances Due to Tourism in Jeseniky Mountain, Czech Republic: a Remote Sensing and GIS Based Approach. Egypt. J. Remote Sens. Space Sci. 18 (1), 17–26. http://dx.doi.org/10.1016/j.ejrs.2014.12.002. ISSN 1110-9823

Choudhary K., Boori MS, Kupriyanov A., (2017), Spatial Modelling for Natural and Environmental Vulnerability Through Remote Sensing and GIS in Astrakhan, Russia. Egypt. Journal of Remote Sensing Space Sciences.

Courage K., Masamu A., Bongo A., *et al.*, (2009), Rural Sustainability Under Threat in Zimbabwe-Simulation of Future Land Use/Cover Changes in the Bindura District Based on the Markov-Cellular Automata Model. Applied Geography, 29: 435-447. DOI: 10.1016/j.apgeog.2008.10.002.

Dwiyanti, (2013), Study of Land Use Development Related to Trade and Batik Industry in Trusmi Kulon, Plered Village, Cirebon Regency. Jurnal Ruang Ekologi volume 1 No. 2 2013. Semarang: Faculty of Techniques, Diponegoro University.

Farzaneh A., (2007), Application of Image Fusion (Object Fusion) for Forest Classification in Northern Forests of Iran. J. Agr. Sci. Tech. 2007, 9, 43-54.

Jayanth J., Koliwad S., Ashok Kumar T., (2015), Classification of Remote Sensed Data using

Artificial Bee Colony Algorithm. Egypt. J. Rem. Sens. Space Sci. 18, 119– 126.

Jean FM, Melanie K., Martin P., *et al.*, (2014), Modelling Land Use/Cover Changes: a Comparison of Conceptual Approaches and Softwares. Environmental Modelling and Software, Elsevier, 2014, 51, pp.94-111.

Jensen JR., (1996), Introductory Digital Image Processing: a Remote Sensing Perpective, 3rdedn. Prentice-Hall, Upper saddle River, New Jersey.

Kaliraj S., Chandrasekar N., Ramachandran KK, *et al.*, (2017), Coastal Landuse and Land Cover Change and Transformations of Kanyakumari Coast, India using Remote Sensing and GIS. Egypt. J. Remote Sensing Space Sci.

Lu D., Weng QA., (2007), Survey of Image Classification Methods and Techniques for Improving Classification Performance. Int. J. Remote Sens. 2007, 28, 823-870.

Maesaroh S., Barus B., Iman LS, (2013), Analysis of Coastal Areas Utilization in Pandeglang District, Banten Province. Journal of Tanah Lingkungan.15 (2) Oktober 2013: 45-51.

Munibah K., (2008), Spatial Model of Land Use Change and Direction of Environmentally Based Land, Case Study of Cidanau River of Banten Province. Dissertation. Bogor Agriculture University (IPB).

Myint SW, Wang L., (2006), Multicriteria Decision Approach for Land Use Land Cover Change using Markov Chain Analysis and a Cellular Automata Approach. Canad. J. Remote Sens., 32: 390-404. DOI: 10.5589/m06-032.

Peruge TVD, Samsu A., Sakka, (2012), Model of Land Use Change using Cellular Automata - Markov Chain in Mamminasata Area. Study Program of Geophysics, Faculty of Mathematics and Science, Hasanuddin University.

Purwantoa Utomo DH, Kurniawan BR, (2016), Spatio Temporal Analysis Trend of Land Use and Land Cover Change Against Temperature Based on Remote Sensing Data in Malang City. Procedia - Social and Behavioral Sciences 227 (2016) 232 – 238.

Rahmat A., Syadiah N., Subur B., (2016), Smart Coastal City: Sea Pollution Awareness for People in Surabaya Water Front City. Procedia - Social and Behavioral Sciences 227 (2016) 770 – 777.

Romero AF, Abessa DMS, Fontes RFC, *et al.*, (2013), Integrated Assessment for Establishing an Oil Environmental Vulnerability Map: Case Study for the Santos Basin Region, Brazil. Mar. Pollut. Bull. 74 (1), 156–164

Sang L., Zhang C., Yang J., *et al.*, (2011), Simulation of Land Use Spatial Pattern of Towns and Villages Based on CA-Markov Model. Math. Comput.Modell. 54: 938-943. DOI: 10. 1016/j.mcm.2010.11.019

Sunardi, (2004), Reform of Urban Spatial Planning. Materials Discussion on Workshop and Alumni Gathering MPKD-UGM, Yogyakarta. (http://mpkd.ugm.ac.id).

Suweda IW., (2011), Sustainable Urban Spatial Arrangement, Competitive and Autonomy (a Literature Review). Journal Ilmiah Teknik Sipil Vol. 15, No. 2, Juli 2011. Faculty of Techniques, Udayana University Denpasar.

Tong STY, Sun Y., Yang YJ., (2012), Generating a Future Land Use Change Scenario with a Modified Population-Coupled Markov Cellular Automata Model. J. Environ. Inform., 19: 108-119.

Trisasongko BH, Panuju DR, Iman LS., (2009), Analysis of Land Conversion Dynamics Around the Cikampek Toll Road. Technical Publications DATIN. Ministry of Environment Indonesia. Jakarta.

WHO (World Health Organization), (2014), World Health Statistics 2014 - Indicator compendium.

Yikalo HA, Pedro C., (2010), Analysis and Modeling of Urban Land Cover Change in Setúbal and Sesimbra, Portugal. Remote Sensing Journal. 1549-1563; Doi: 10. 3390/rs2061549.

THE EFFECT OF JPEG2000 COMPRESSION ON REMOTE SENSING DATA OF DIFFERENT SPATIAL RESOLUTIONS

Anis Kamilah Hayati[1]*, Haris Suka Dyatmika[2]
[1,2]Remote Sensing Technology and Data Center, LAPAN
*e-mail: anis.kamilah@lapan.go.id

Received: 12 July 2017; Revised: 13 November 2017; Approved: 14 November 2017

Abstract. The huge size of remote sensing data implies the information technology infrastructure to store, manage, deliver and process the data itself. To compensate these disadvantages, compressing technique is a possible solution. JPEG2000 compression provide lossless and lossy compression with scalability for lossy compression. As the ratio of lossy compression getshigher, the size of the file reduced but the information loss increased. This paper tries to investigate the JPEG2000 compression effect on remote sensing data of different spatial resolution. Three set of data (Landsat 8, SPOT 6 and Pleiades) processed with five different level of JPEG2000 compression. Each set of data then cropped at a certain area and analyzed using unsupervised classification. To estimate the accuracy, this paper utilized the Mean Square Error (MSE) and the Kappa coefficient agreement. The study shows that compressed scenes using lossless compression have no difference with uncompressed scenes. Furthermore, compressed scenes using lossy compression with the compression ratioless than 1:10 have no significant difference with uncompressed data with Kappa coefficient higher than 0.8.

Keywords: *compression, effect, spatial resolution, remote sensing, JPEG2000*

1 INTRODUCTION

Rapid improvement in satellite technologies encourages providers to produce various spatial, temporal and radiometric resolution imagery. The advent of new remote sensing platforms and sensors would generate an increasing amount data set day by day (Zabala *et al.* 2012b). The huge size of remote sensing data needs a high capacity of storage, computational resource for processing, and bandwidth channel for transmission. Compressing technique is a possible solution to cope the problem with remote sensing data management.

Compression techniques evolved in recent years from discrete cosine transform (such as JPEG) to wavelet-based algorithm (such as JPEG2000). Previous research on image compression concluded that the latter obtain the better result (Zabala *et al.* 2012a; Zabala and Pons 2013). JPEG2000 became ISO standard in 2000 and revised in 2004 (ISO/IEC 2004). JPEG2000 compression can be performed in a lossless (reversible and no information lost) and lossy (irreversible, allows a higher level of compression with information lost as a trade off). JPEG2000 provides advantages in more various and flexible scalability than JPEG, in which compression ratio is adjustable (Taubman and Marcellin 2002).

Studies about the effect of JPEG compression has been performed in many fields such as in medical (Sung *et al.* 2002; McEntee *et al.* 2013). As for remote sensing, Shrestha *et al.* (2005) has been

giving assessment on JPEG2000 compression for Quickbird data; Zabala *et al.* (2006) compared JPEG and JPEG2000 lossy compression for crops and forest classification using hybrid classification method; Zabala *et al.* (2012a) compared on-board compression at Sentinel-2 and user-side compression at Landsat 8 using JPEG2000 for image quality and land cover classification; Zabala *et al.* (2012b) investigated JPEG2000 compression at orthophotos with 1m spatial resolution for segmentation-based classifications; while Zabala and Pons (2013) studied JPEG and JPEG2000 compression effect for classification at Landsat 5 using hybrid classifier, maximum likelihood, and minimum distance classifiers method.

While previous papers most likely to focus on one type of data to study the effect of compression, this paper tried to investigate the effect of JPEG2000 compression on remote sensing data with different spatial resolution. Therefore remote sensing data users could examine which ratio is best to be applied to their data.

2 MATERIALS AND METHODOLOGY

2.1 Data and Location

Data used in this experiment were Landsat 8 from path 114 row 064 acquired at September 8, 2015; SPOT 6 acquired at July 27, 2016; and two Pleiades data acquired at September 2, 2013 and May 14, 2014. These data were chosen based on location which cover a part of South Sulawesi area with minimum cloud cover. Spectral bands used were the visible bands and NIR band, namely band 2, band 3, band 4 (visible bands) on Landsat-8 and band 1, band 2, band 3 (visible bands) for SPOT 6 and Pleiades.

Those three types of data were chosen to represent different spatial resolutions. Landsat 8 OLI bands have a spatial resolution of 30 meters, while multispectral bands of SPOT 6 and Pleiades bands have 6 meters and 2 meters of spatial resolutions, respectively.

2.2 Assesment Method

Figure 2-1 shows the flow of the study sequence starting from data collection up to accuracy assessment. All data compressed into JPEG2000 format with five different ratios (lossless, 4:1, 10:1, 20:1, 100:1). This study utilized OpenJPEG version 2.1. to perform the JPEG2000 compression. OpenJPEG is an open-source library, which has officially recognized by ISO/IEC as JPEG2000 reference software (ITU-T 2015).

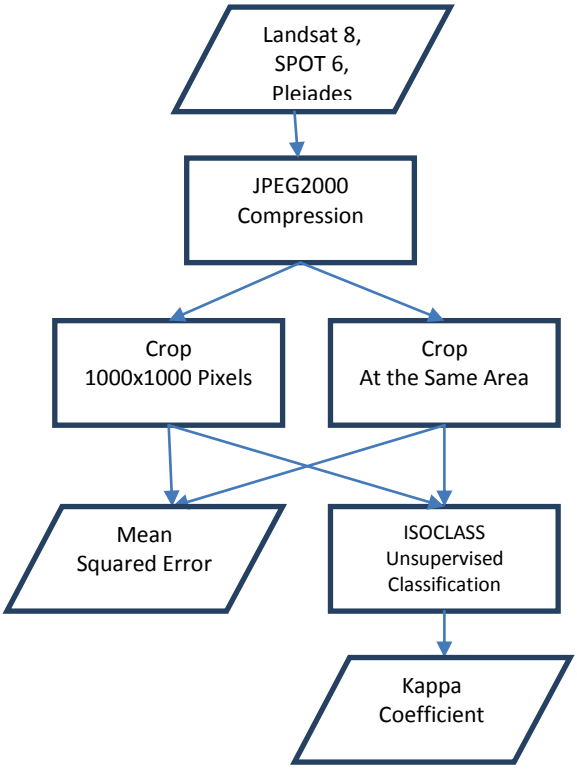

Figure 2-1: Assessment methodology

After compressed, all the data (compressed and uncompressed) were cropped with two different approaches (Figure 2-2). First, these data were cropped into scenes with exactly 1000x1000 pixels-size. Second, all data

were cropped into scenes at the exact same area. The scenes were chosen by considering different land cover, which led to different fragmentation.

MSE values were measured using equation (2-1) where *u(m,n)* and *v(m,n)* represent two scenes of size *MxN*, in this case, *u* represent the uncompressed scene and *v* for the compressed scene. Although MSE criticized for heavily weighting outliers (Bermejo 2001), this study tried to see whether there was any relation between different spatial resolution, different standard deviation, and the MSE escalation at every compression ratio level.

$$MSE(u,v) = \frac{1}{MN}\sum_{m=1}^{M}\sum_{n=1}^{N}|u(m,n) - v(m,n)|^2 \quad (2\text{-}1)$$

All scenes also processed to ISOCLASS unsupervised classification. Classification results then used to calculate Kappa coefficient using equation (2) where p_o represents the actual observed agreement, and p_e represents chance agreement. Both p_o and p_e were calculated from ISOCLASS unsupervised classification results of uncompressed scenes and compressed scenes.

$$\kappa = \frac{p_o - p_e}{1 - p_e} \quad (2\text{-}2)$$

Kappa coefficient introduced in Cohen (1960). Cohen suggested the Kappa result to be interpreted as follows: values ≤ 0 as indicating no agreement and 0.01–0.20 as none to slight, 0.21–0.40 as fair, 0.41– 0.60 as moderate, 0.61–0.80 as substantial, and 0.81– 1.00 as almost perfect agreement. However, this interpretation may be problematic as if 0.61 interpreted as substantial, 40% of the data in dataset represent faulty data (McHugh 2012).

In that way McHugh (2012) suggested interpreting Cohen's Kappa as (Table 2-1).

Landsat 8 SPOT 6 Pleiades

Figure 2-2: Cropped satellite imagery over the study area. at the first row, data cropped into 1000x1000 pixels, at the second row, data cropped in the exact same area

Table 2-1: Interpretation of cohen's Kappa

Value of Kappa	Level of Agreement	% Data that are Reliable
0.00 - 0.20	None	0 – 4%
0.21 - 0.39	Minimal	4 – 15%
0.40 - 0.59	Weak	15 – 35%
0.60 – 0.79	Moderate	35 – 63%
0.80 – 0.90	Strong	64 – 81%
≥ 0.90	Almost Perfect	82 – 100%

Source: McHugh, 2012

3 RESULTS AND DISCUSSION

Figure 3-1 shows that JPEG2000 compression affected the appearance of the data visually. From every tested Landsat 8 scenes, there was no significant visible change up to the ratio 4:1. A notable change was seen at scenes with compression ratio 10:1. Figure 3-1(b) shows compression start to affect at vegetation area, which is more homogenous than other areas (for example city area). Furthermore, SPOT 6 and Pleiades data, which have finer resolution, provided better compression result. Their homogenous area (represented by vegetation) started to blur at compression ratio 20:1 with Pleiades being visibly better than SPOT 6. This result agrees with Shrestha, *et al* (2005) that suggested 10:1 as a save ratio for JPEG2000 compression to Quickbird data which have spatial resolution 1m.

Mean Square Error

As a tradeoff for smaller file size, a higher compression ratio for lossy compression commonly generates a higher error. Nevertheless, lossless compression JPEG2000 proved to be reversible and provide information as it is.

All scenes, which have been cropped to 1000x1000 pixels, then processed to measure their MSE values. Every scene from every data that was compressed with lossless compression has 0 MSE value, which means that lossless compression has not given any effect. Therefore, scenes that compressed using lossless compression have no difference with uncompressed scenes. While scenes that compressed with lossy compression indicate different MSE increment for every data as shown in Figure 3-2.

The effect of compression to MSE value (at each data which cropped at city area) is shown in Figure 3-2. As expected, Landsat 8 is most affected by higher lossy compression ratio, therefore it has the highest MSE value among other data. Significant differences of MSE value between Landsat 8 and another data started to rise at the compression ratio of 4:1. While significant differences of MSE value between SPOT 6 and Pleiades data started at the compression ratio of 20:1. This trend is also implied to other bands (blue and green) and another area (forest area).

Kappa Coefficient

All cropped scenes were classified using ISOCLASS unsupervised classifier and their Kappa coefficient evaluated. Kappa coefficient results from every scene (that cropped into 1000x1000 pixels) in the same data then calculated to get the average of Kappa coefficient.

Table 3-1 shows the average of Kappa coefficient for every data. It stated that scenes which were compressed using lossless compression have Kappa coefficient of 1, which means perfect agreement. While, the compression ratio up to 10:1 provides Kappa coefficient higher than 0.8 which indicates strong agreement with providing more than 64% reliable data.

As shown in Table 3-1, the average of Kappa coefficient from ISOCLASS unsupervised classification does not seem to have a linear correlation with spatial resolution in this case. There are other factors that give influence on Kappa coefficient than just the difference of spatial resolution.

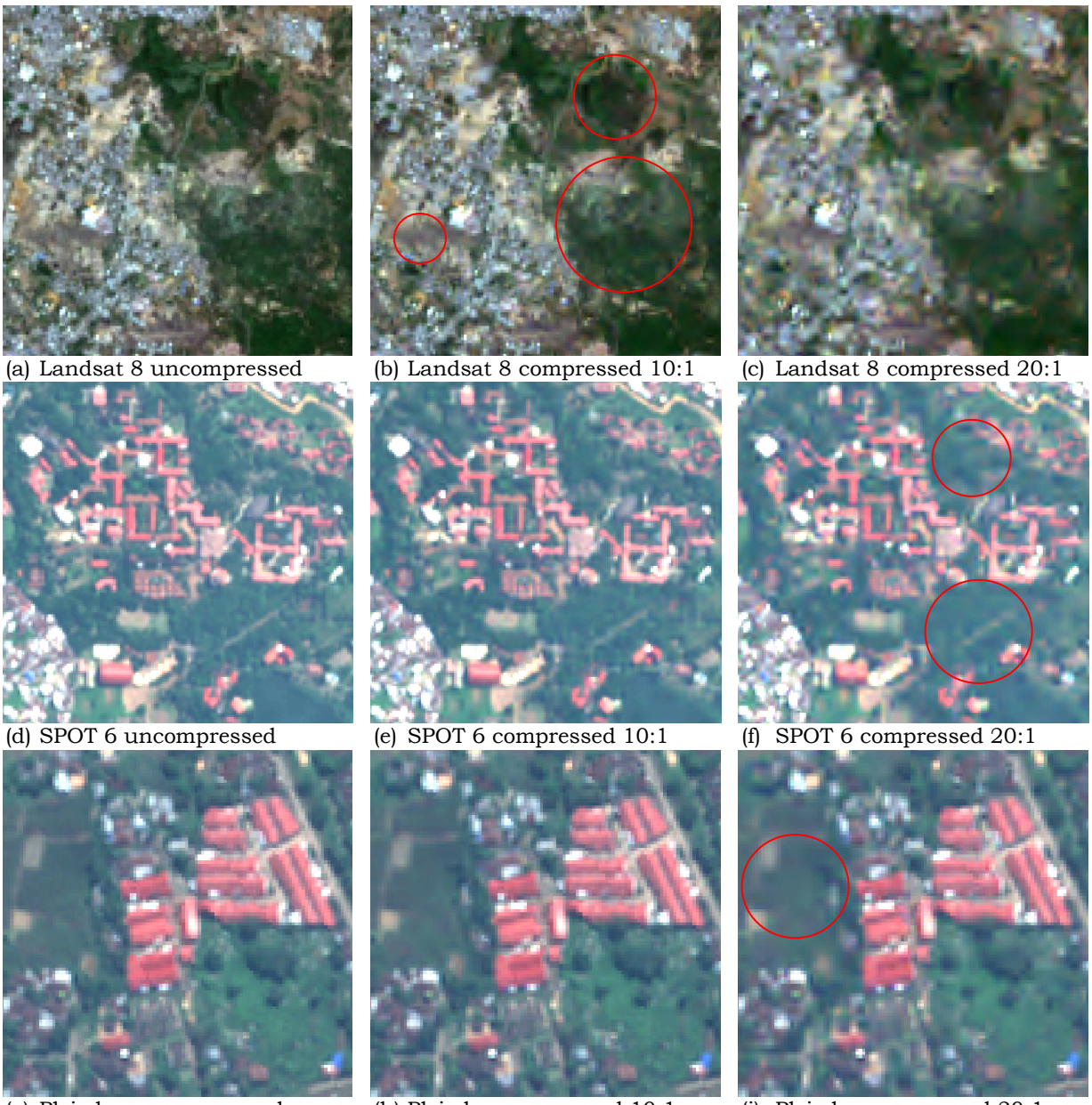

(a) Landsat 8 uncompressed (b) Landsat 8 compressed 10:1 (c) Landsat 8 compressed 20:1

(d) SPOT 6 uncompressed (e) SPOT 6 compressed 10:1 (f) SPOT 6 compressed 20:1

(g) Pleiades uncompressed (h) Pleiades compressed 10:1 (i) Pleiades compressed 20:1

Figure 3-1: JPEG2000 compression effects on Landsat 8 (a, b, c), SPOT6 (d, e, f), and Pleiades (g, h, i). red circles show homogenous areas that are more affected by compression

For instance, Table 3-2 shows result from classification at different areas of SPOT 6 data. Crop area shown in Table 3-2(c) appeared to be less affected by compression, compared to the less fragmented area shown in Table 3-2(a) (forest area). Therefore, Kappa coefficient for more fragmented area tends to have higher Kappa coefficient larger than those with less fragmented areas. In some cases, lower resolution data, which have more fragmentations, generate better MSE values and Kappa coefficients.

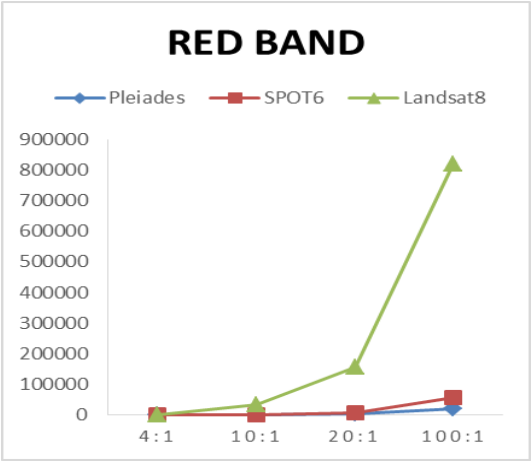

Figure 3-2: Correlation between compression ratio and MSE for Landsat 8, SPOT 6 and Pleiades (red band) data at city area. the x-axis shows compression ratio, while y-axis shows MSE values

Table 3-1: Kappa coefficient measurement

Compression Ratio	Landsat 8			SPOT 6			Pleiades		
	Blue	Green	Red	Blue	Green	Red	Blue	Green	Red
lossless	1	1	1	1	1	1	1	1	1
4:1	0.9786	0.9820	0.9872	0.9217	0.9416	0.9553	0.9286	0.9556	0.9294
10:1	0.8969	0.8772	0.9179	0.8545	0.8560	0.9083	0.8404	0.9081	0.8941
20:1	0.7729	0.6731	0.8236	0.7595	0.7605	0.8286	0.7540	0.8211	0.8365
100:1	0.3804	0.3536	0.2454	0.1254	0.2280	0.4511	0.2001	0.5144	0.5755

Table 3-2: ISOCLASS unsupervised classification result at three different areas from SPOT 6 data

Uncompressed image	Classification on uncompressed image	Classification on CR 10:1	Classification on CR 20:1	Classification on CR 100:1
(a) SPOT 6 cropped at forest area		Kappa coefficient: R: 0.7802 G: 0.7936 B: 0.8588	Kappa coefficient: R: 0.7101 G: 0.7073 B: 0.7725	Kappa coefficient: R: -0.0846 G: -0.0708 B: 0.2182
(b) SPOT 6 cropped at city area		Kappa coefficient: R: 0.8851 G: 0.8827 B: 0.9160	Kappa coefficient: R: 0.7495 G: 0.7539 B: 0.8160	Kappa coefficient: R: 0.2370 G: 0.3084 B: 0.5178
(c) SPOT 6 cropped at crop area		Kappa coefficient: R: 0.8983 G: 0.8917 B: 0.9501	Kappa coefficient: R: 0.8190 G: 0.8203 B: 0.8972	Kappa coefficient: R: 0.2240 G: 0.4465 B: 0.6174

The way fragmented area tends to have higher Kappa coefficient confirmed by Zabala and Pons (2013), which concluded that fragmented images accept less effect from compression. Zabala and Pons (2013) recommended compression ratio 10:1 to 20:1 for more fragmented images and up to 100:1 for less fragmented images depending on the classifier. Zabala and Pons (2013) used Hybrid, Minimum Distance, and Maximum Likelihood classifier.

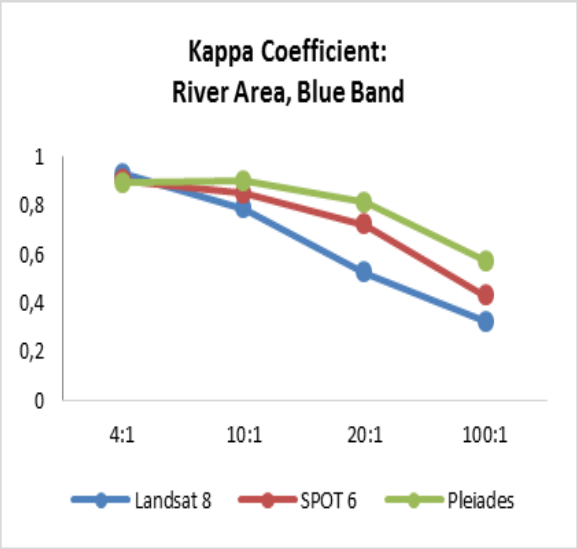

Figure 3-3: Correlation between compression ratio and Kappa coefficient for Landsat 8, SPOT 6 and Pleiades (blue band) data at river area. the x-axis shows compression ratio, while y-axis shows Kappa coefficient

To compare different spatial resolution, scenes that have been cropped at the same area are used. Different with Kappa coefficient result from scenes that cropped with the same size, Kappa coefficient from scenes cropped at the same area indicates a relation with spatial resolution.

Kappa coefficients of the finer spatial resolution generally higher than the coarser spatial resolution. However, at a low compression ratio of 4:1, Kappa coefficient of Landsat 8 was mostly higher than other data (Figure 3-3).

4 CONCLUSION

The study shows that compressed scenes using lossless compression have no difference with uncompressed scenes. Meanwhile, based on visual appearance, sufficient lossy compression ratio for Landsat 8 would be under 10:1 while for the SPOT 6 and Pleiades, the acceptable compression ratios are up to 20:1.

Higher compression ratio generates higher MSE. The MSE value shows a relationship with the spatial resolution where lower spatial resolution tends to have greater MSE than higher resolution.

In accordance with MSE values, higher compression provides lower Kappa coefficient. In general, the compression ratio up to 10:1 are sufficient to be used for ISOCLASS unsupervised classification. Every data (Landsat 8, SPOT 6, and Pleiades) compressed with compression ratio lower than 10:1 presents Kappa coefficient higher than 0.8, which means a strong level of agreement with more than 64% reliable data.

Furthermore, fragmentation of imagery should be considered when choosing lossy compression ratio. Data that have a lower spatial resolution but more fragmented tends to receive better compression result than data that have a higher spatial resolution but less fragmented. However, for a set of data that cropped at the exact same area, higher resolution data get better results, since fragmentation is produced by its resolution.

ACKNOWLEDGEMENTS

This research was funded and facilitated by Remote Sensing Technology and Data Center of LAPAN. We would like to thank everyone who involved in the preparation of this paper, particularly acquisition and management team for providing the access to the Landsat 8,

SPOT6 and Pleiades data. We also would like to offer our gratitude to Prof. Dr. I Nengah Surati Jaya, M.Agr. and Prof. Dr. Rr. Erna Sri Adiningsih, M.Si. for giving us valuable inputs to improve this paper.

REFERENCES

Bermejo S., Cabestany J., (2001), Oriented Principal Component Analysis for Large Margin Classifiers. Neural Networks, 14 (10), 1447–1461.

Cohen J., (1960), A Coefficient of Agreement for Nominal Scales. *Educational and Psychological Measurement, 20,* 37-46. doi: 10.1177/ 001316446002000104.

ISO/IEC 15444-1:2004, (2004) Information Technology – JPEG 2000 Image Coding System: Core Coding System. Geneva, Switzerland, 2004, 194.

ITU-T T.804, (2015), Information Technology - JPEG 2000 Image Coding System: Reference software. Geneva, Switzerland.

McEntee MF, Nikolovski I., Bourne R., *et al.*, (2013), The Effect of JPEG2000 Compression on Detection of Skull Fractures. Academic Radiology. 20(6), 712-720.

McHugh ML, (2012), Interrater Reliability: The Kappa Statistic. Biochem. Med. 22, 276–282. doi: 10.11613/BM.2012.031

Shrestha B., O'Hara CG, Younan NH, (2005), JPEG2000: Image Quality Metrics. ASPRS 2005 Annual Conference.

Sung MM, Kim HJ, Yoo SK, *et al.*, (2002), Clinical Evaluation of Compression Ratios using JPEG2000 on Computed Radiography Chest Images. Journal of Digital Imaging. 15(2):78-83.

Taubman DS, Marcellin MW, (2002), JPEG2000: Standard for Interactive Imaging. Proceedings of the IEEE. 90(8):1336-1357.

Zabala A., Cea C., Pons X., (2012b), Segmentation and Thematic Classification of Color Orthophotos over Non-Compressed and JPEG2000 Compressed Images. International Journal of Applied Earth Observation and Geoinformation Vol. 15.

Zabala A., Pons X., Diaz-Delgado R., *et al.*, (2006), Effects of JPEG and JPEG2000 Lossy Compression on Remote Sensing Image Classification for Mapping Crops and Forest Areas. IEEE International Symposium on Geoscience and Remote Sensing. 781-784

Zabala A., Pons X., (2013), Impact of Lossy Compression on Mapping Crop Areas from Remote Sensing. International Journal of Remote Sensing. Vol. 34, No.8 2796-2813.

Zabala A., Vitulli R., Pons C., (2012a), Impact of CCSDS-IDC and JPEG 2000 Compression on Image Quality and Classification. Journal of Electrical and Computer Engineering, Vol. 2012, 2012.

PRELIMINARY STUDY OF LSU-02 PHOTO DATA APPLICATION TO SUPPORT 3D MODELING OF TSUNAMI DISASTER EVACUATION MAP

Linda Yunita[1], Nurwita Mustika Sari[2], and Dony Kushardono[2]
[1]Physics Department of Universitas Indonesia
[2]Remote Sensing Applications Centre LAPAN
e-mail: linda.yunita@sci.ui.ac.id
Received: 6 November 2017; Revised: 20 November 2017; Approved: 20 December 2017

Abstract. The southern coast of Pacitan Regency is one of the vulnerable areas to the tsunami. Therefore, the map of the vulnerable and safe area from the tsunami disaster is required. Currently, there are many mapping technologies with UAVs used for spatial analysis. One of the UAV technologies which used in this research is LAPAN Surveillance UAV 02 (LSU-02). This study aims to map the evacuation plan area from LSU-02 aerial imagery. Tsunami evacuation area was identified by processing the aerial photo data into orthomosaic and Digital Elevation Model (DEM). The result shows that there are four points identified as the tsunami evacuation plan area. These points are located higher than the surrounding area and are easily accessible.

Keywords: *Aerial remote sensing, photo data of LSU-02, 3D modelling, tsunami*

1 INTRODUCTION

Indonesia is one of the countries located in the Pacific Ring of Fire as well as in between four tectonic plates of the world. This condition makes Indonesia vulnerable to several natural disasters such as earthquakes, tsunami and volcanic eruptions (Siagian *et al.* 2013; Naryanto 2003). Tsunami is one of the natural disasters that have a significant negative impact on the people in the coastal region of Indonesia. Areas along the west coast of Sumatra, southern coast of Java Island to Bali, as well as the coastal areas of Papua and Sulawesi (Sunarto and Marfai 2012). One of the recent examples of the biggest tsunami in Indonesia was the tsunami that occurred in December 2004.

The southern coast of Pacitan regency is one of the areas prone to tsunami. Due to its geographical location, which is near the Indo-Australian plate and Eurasian plates? Based on the USGS earthquake catalog, over the past 100 years, it has been observed that large earthquakes > 7 SR often occur on the seafloor at the depths that are generally less than 30Km. This type of earthquake often found on the epicenter of the Indo-Australian plate that has the potential to generate a tsunami and it is located about 80-100km from the coast of Pacitan. Looking from its distance to the coastline (Islam *et al.* 2014), Pacitan District can be categorized to the vulnerable area of tsunami.

According to Chaeroni *et al.* (2013), the southern region of Pacitan Regency is directly adjacent to the Indian Ocean as well as the ring of fire path because of the convergence of oceanic plates with

effort in case of the tsunami. The evacuation map needs to highlight the terrain elevation, which is used to determine the evacuation plan in case of Tsunami disaster.

Developing a tsunami evacuation map requires high-resolution remote sensing data or high-cost field survey data. The limited availability, high cost, as well as high cloud coverage often disrupts the image acquisition. Unmanned Aerial Vehicle (UAV) technology capable of producing detailed spatial data at relatively low cost (Eisenbeiß 2009; Jones 2007). LAPAN has developed unmanned aircraft known as LAPAN Surveillance UAV (LSU) since 2011. At this time LAPAN has several types of LSU, namely LSU-01, LSU-02, LSU-03, LSU-04 and the largest is the LSU-05 which has a wingspan of 5.5 m and capable of flying up to 8 hours with a flying altitude of 3.6 km. Furthermore, LSU-02 is able to fly under clouds for more than two hours and carry out aerial photography missions, resulting in cloud-free images, with detailed and sharper information than satellite imagery, as well as fast and flexible information acquisition (Kushardono 2014; Sari and Kushardono 2014).

Several studies have examined the ability or potential of aerial photography for the use of the identification and interpretation of coastal area objects (Arifin *et al.* 2015), acquisition of remote sensing data with UAVs (Rosaji *et al.* 2013; Kushardono 2014) modeling of 3-dimensional geometry (Gularso 2013), extraction of DEM data (Purwanto 2016), and land cover classification method with UAV (Sari and Kushardono 2014). DEM extraction from satellite data has been derived using various satellite imagery data such as using ALOS, SPOT and ASTER data (Tadono *et al.* 2014; Al-Rousan *et al.* 1997; Kamp *et al.* 2003).

The accuracy of DEM resulting from photo stereo plotting technique from UAV can be quite high, whereby Purwanto (2017) study finds the accuracy of DEM is up to 0.073 m, whereas Uysal *et al.* (2015) obtain a vertical DEM accuracy of 6 cm. A good flight plan that controls the direction of flight and the different altitude (cross flight) of shooting with UAVs can improve the accuracy of acquired DEM (Mark and Heinz-Jürgen 2016). Meanwhile, Matthesen and Schmidt (2016) have proposed the method of making DTM (digital terrain model) from DSM data (digital surface model) of UAV photo data by conducting point cloud filter. However, there is a limited amount of research on the use of DEM and ortho-photo from UAV related to the processing and data analysis for 3D modeling in making tsunami disaster evacuation map. The digital elevation model (DEM) in question is data with raster format that describes the elevation of an area (Siwi 2009). The assessment of the tsunami evacuation area has been conducted for the determination of the tsunami evacuation route by taking into account the nearest distance but not yet at the stage of making evacuation map for tsunami (Madona and Irmansyah 2013; Pratomo and Rudiarto 2013).

This study aims to provide an overview of 3D modeling to create a tsunami disaster evacuation map using the results of processing LSU-02 photo data that has been previously processed into orthomosaic and Digital Elevation Model (DEM).

2 MATERIALS AND METHODOLOGY

2.1 Location and Data

The main data used in this study was the LSU-02 air photo data. The data acquired by LAPAN Aviation Technology Center Tea on April 7th, 2016. The LSU-02 was equipped with a SONY ILCE-6000

camera that flown by 2 lanes along the southern coastal area of Pacitan as shown in Figure 2-1. The average speed of flying LSU-02 during the acquisition was 100 km per hour at 500 m above ground level as well as traveling a range of about 250 km.

Figure 2-1: Flight LSU-02 acquisition of data based on GPS photo results

Figure 2-2: LSU-02 photo data is used

The aerial photographs obtained went as much as 2210 photos with 6000x4000 pixels each and spatial resolution of 10 cm. Front-rear photos overlapped by 80%, while left-right photos overlapped by 60%. Each photo contained coordinate position recorded by the onboard GPS. LSU-02 photo data used in this study located at Watukarung Beach of Pacitan Regency (Figure 2-2) and amounted to 33 photos.

Location data obtained on the field combined with Google map was used as the reference. The GPU specification used in this study was as follows; Core i7 3.40 GHz CPU and 32 Gb RAM. The hardware equipped with data mosaic processing devices, stereoplotting, and data analysis.

2.2 Methods

The data processing conducted in several stages as shown in Figure 2-3. All of the LSU-02 photos were mosaicked and stereo-plotted using the coordinate information stored within each photo. It was then created two products: mosaicked image and DEM. Afterwards, the data were masked to only include the observation target. DEM correction uses field measurement data as the reference. Furthermore, the 3D analysis is derived using corrected DEM data and ortho-image to get the result of disaster evacuation map based on photo interpretation and height of the land.

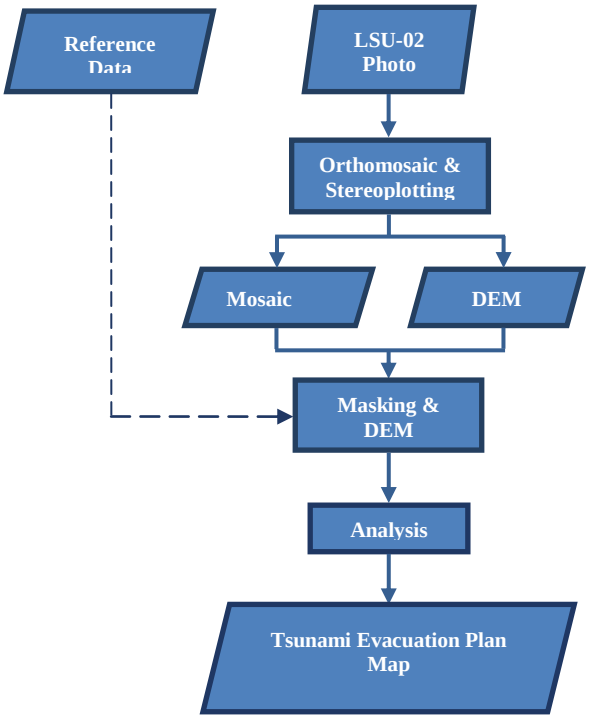

Figure 2-3: Flow of data processing

2.2.1 Mosaic Photo Data

The mosaic process was conducted by combining 33 photo data from the LSU-02. The process begun with Align Photos, followed by Build Dense Cloud, Build Mesh, Build Texture, Build Tiled Model, Build DEM, and Build Orthomosaic. The Align Photos aimed to perform the matching process between the overlapped photos. In addition, Align Photos can also improve the position of the camera for each photo and build a model point dot coordinate system (point cloud model). After the dense point cloud successfully reconstructed, a polygonal mesh model then generated based on the dense cloud data.

Orthomosaic was derived to perform the matching process at the same point on two or more photos. The process was continued by repairing the camera position for each photo and establishing point cloud. Based on the camera position estimation, the program calculated the information from each camera's position to be combined into a dense point cloud that forms the basis for 3D and DEM modelling.

2.2.2 Masking and DEM Correction

The masking process was performed to subset the image only contained the observation area. Afterwards, the DEM value was corrected, using reference data to determine the 0 mdpl value. This process was conducted by taking and calculating the average elevation of some samples taken and creates a linear regression between the DEM and the reference data. Using minimum height value method, the DSM was converted into DTM.

2.2.3 3D Analysis

From the corrected DTM result and orthomosaic images, the 3D model was developed to highlight the relief within the study area. Potential evacuation point was then identified. Nearest highland around the coast identified from DTM data, whereas the least obstacle pathway was identified from orthomosaic images due to its high spatial resolution. The potential obstacle such as buildings and trees as well as the infrastructure critical for an evacuation plan (road, sidewalk) were also identified. These parameters then analyzed to determine the gathering point.

3 RESULTS AND DISCUSSION

Figure 3-1 shows the orthomosaic image created from 33 LSU-02 overlapped photos. Figure 3-1 also shows that the research area is a coastal region. The land cover mainly consists of settlement, forest, and moor. In general, the morphology consists of coastal plains which are dominantly occupied by residential areas, some hilly region around the coastal plains with forest land cover, and bare land on some of the hills.

Figure 3-1: Image of orthomosaic result of study area

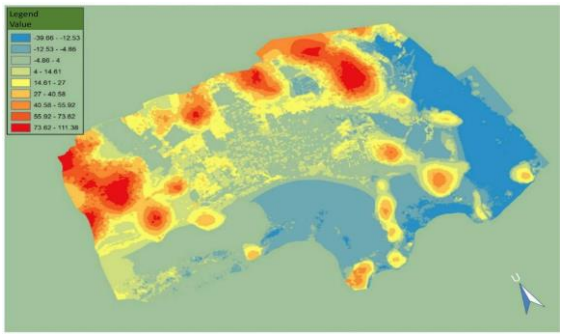

Figure 3-2: The DEM extraction results have been corrected and the contour lines are altitudinal

Figure 3-2 shows the DTM as the product of DEM generation, masking, and elevation correction explained in section 2.2. Elevation correction was performed using field data as the reference. The linear regression analysis, resulted in the linear equation, and the results are as follow:

$$y = 0.2553x + 73.861 \text{ (meters)} \quad R^2 = 0.9413 \qquad (2\text{-}1)$$

The DEM obtained is the Digital Surface Model (DSM). For identification of the evacuation path, the DEM needs to be transformed into a Digital Terrain Model (DTM). By utilizing the minimum elevation value of the transect on the DSM data (assuming the maximum DSM elevation value is the height of the tree or the building above the ground).

Figure 3-2 shows the DTM with the elevation ranging from 0 to 111.38. Based on the image, it appears that the residential area is generally located at an altitude of 0-4 meters. This makes it vulnerable to tsunami threats. The result of previous research indicates that the accuracy of DEM created from UAV with stereoplotting technique reaches 0.073m (Purwanto 2013). This study employed the same technique.

Figure 3-3 visualizes the terrain within the study area. A near-shore residential area on a low coastal plain and a forest on the hill behind have the potential to become the evacuation site in the event of a tsunami disaster. There is also a difference in DSM where tree height and buildings are still visible and flattened to the soil surface at DTM. However, there are slight errors on the seafront that corrected the sea level altitude. This is because the method used is still very simple that based the minimum elevation only.

The 3-D image shown in Figure 3-3 is used to determine the evacuation path to the evacuation point. The DSM data used to identify the effective evacuation path and avoid obstacles such as trees or overly steep slopes. Meanwhile, the DTM was used to assist the creation of an effective path to the evacuation points.

a) 3-Dimensional images of orthomosaic and DSM data

b) 3-Dimensional images of orthomosaic and DTM data

Figure 3-3: 3-Dimensional image of beach Watukarung photos of LSU-02 camera data

Figure 3-4 shows four sites have been identified as the feasible evacuation points. These points located more than 25 meters above sea level. The evacuation route was made from the beach or seafront on the grounds at Watukarung Beach. This is a tourist attraction, so it is likely densely populated by tourists.

The distance between the evacuation points to the seafront are shown in Figure 4-5. Point 1 on Figure 3-4 is located 269 meters from the seafront. Point 2, 3, and 4 are located 360, 343, and 525 meters from the seafront, respectively. But in the implementation, the map of Figure 3-4

shows that in the event of a tsunami, the flow of evacuation can be interchanged, so that people located in area A can reach point 2, the people in area B can reach point 2 or point 3, and the community in area C can go to point 3 or point 4 as an effort to save them from the danger of the tsunami.

Figure 3-5 is also shows the slope for each evacuation point, which appears on the evacuation route to Point 1 of the uphill road, while on the evacuation route to the gathering points 2, 3 and 4 have a similar pattern of land slope through a road that is up to hundreds of meters flat at low altitudes then in the last 30 to 50 meters through a very uphill road. In this preliminary study, the very uphill tracks approaching the gathering point, still need to be studied in more detail to determine alternative paths or made stairs to facilitate climbing to the gathering point above. The most effective evacuation paths are available to each evacuation point for each settlement group in regions A, B and C.

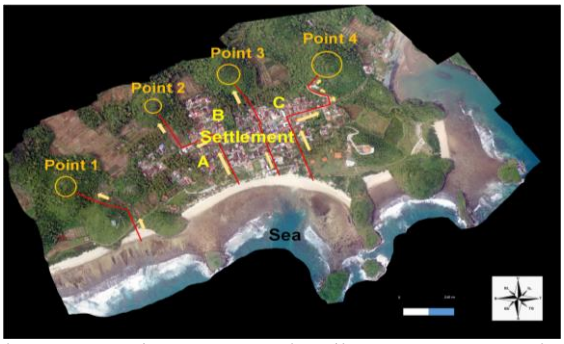

Figure 3-4: The tsunami disaster evacuation map of the research results

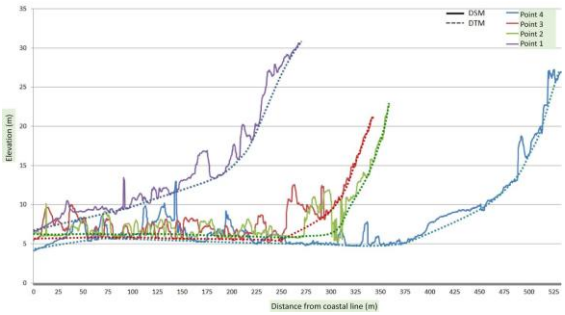

Figure 3-5: Profiles and the distance of each evacuation path to each point of the gathering location and the height of the land

Table 3-1 shows the accuracy assessment for the DEM data created by LSU-02. Fifteen points were created. The elevation for both LSU-02 DEM and the reference data were taken and analyzed. The points represented several types of land cover, from bare land, road and beach area. The highest error was found on point number 5. This point located in the elevated area. The average error was at 1.5 meters. This suggests that in relation to the tsunami disaster evacuation recommendation, errors with these values are still be tolerated, although for the DEM generated from the UAV the error rate is high. However, this is also affected by the accuracy of the reference data used.

Table 3-1: Accuracy assessment of DEM

No.	DEM 9m resolution	DEM LSU-02	Error
1	5	4.1	0.9
2	7	5.4	1.6
3	7	6.2	0.8
4	9	6.8	2.2
5	33	27	6
6	15	14.3	0.7
7	14	11	3
8	12	12.6	0.6
9	11	12	1
10	8	6.9	1.1
11	7	8.3	1.3
12	17	18.44	1.44
13	16	16.7	0.7
14	2	2.33	0.33
15	9	10.5	1.5
Mean ERROR			**1.545**

4 CONCLUSION

This study has shown the potential of LSU-02 aerial photograph data to generate DEM data and high spatial orthomosaic resolution images, from which the DEM data and ortho-images can be utilized for 3D land modeling.

Based on 3D modeling of land and its interpretation, it can be used to determine evacuation points for tsunami disaster, as well as the most effective path to these points.

ACKNOWLEDGEMENTS

The authors would like to thank Aeronautics Technology Centre of LAPAN for the opportunity to use LSU-02 data for this research. We also would like to thank Dr. Adhi Harmoko Saputro S.Si., M.Kom from Physics Department of Universitas Indonesia and Dr. Rokhis Khomarudin as Director of Remote Sensing Applications Centre LAPAN for the support of this research.

REFERENCES

Al-Rousan N., Cheng P., Petrie G., *et al.*, (1997), Automated DEM Extraction and Orthoimage Generation from SPOT Level 1B lmagery. Photogrammetric Engineering & Remote Sensing, Vol 63, No. 8, August 1997, 965-974.

Arifin S., Anas A., Sari NM, *et al.*, (2015), Identifikasi dan Interpretasi Visual Citra Kamera Digital Multispektral untu Obyek Wilayah Pesisir. Seminar Nasional Penginderaan Jauh 2015, 560-566.

Chaeroni Hendriyono W., Kongko W., (2013), Pemodelan Tsunami dan Pembuatan Peta Rendaman untuk Keperluan Mitigasi di Teluk Teleng, Pacitan. Jurnal Penanggulangan Bencana Vol. 4, No.2, 23-33.

Eisenbeiβ H., (2009), UAV Photogrammetry. (Doktor Sains Disertasi), University of Technology Dresden, Zurich. http:// citeseerx.ist.psu.edu/messages/downloads exceeded.html. Accessed August 2017.

Gularso H., Subiyanto S., Sabri, LM, (2013), Tinjauan Pemotretan Udara Format Kecil Menggunakan Pesawat Model Skywalker 1680, Jurnal Geodesi Undip, Vol.2, No.2, 78-94.

Islam F., Subiyanto S., Sabri LM, (2014), Penentuan Resiko dan Kerentanan Tsunami di Kebumen dengan Citra ALOS. Jurnal Geodesi UNDIP Vol. 3, No 1, Tahun 2014, (ISSN: 2337-845X) Pp. 141-154.

Jones BT, (2007), An Evaluation of a Low-Cost UAV Approach to Noxious Weed Mapping. Master Thesis. Department of Geography Brigham Young University, Hawaii. http:// scholarsarchive.byu.edu/cgi/viewcontent.cgi?article=2219&context=etd Accessed August 2017.

Kamp U., Bolch T., Olsenholer J., (2003), DEM Generation from Aster Satellite Data for Geomorphometric Analysis of Cerro Sillajhuay, Chile/Bolivia. ASPRS 2003 Annual Conference Proceedings.

Kushardono D., (2014), Teknologi Akuisisi Data Pesawat Tanpa Awak dan Pemanfaatannya untuk Mendukung Produksi Informasi Penginderaan Jauh. Inderaja, Vol. V, No. 7, 24-31.

Madona E., Irmansyah M., (2013), Aplikasi Metode Nearest Neighbor pada Penentuan Jalur Evakuasi Terpendek untuk Daerah Rawan Gempa dan Tsunami. Jurnal Elektron Vol. 5 No. 2, Edisi Desember 2013.

Markus G., Heinz-Jürgen P., (2016), Accuracy Analysis of Photogrammetric UAV Image Blocks: Influence of Onboard RTK-GNSS and Cross Flight Patterns, Photogrammetrie, Fernerkundung, Geoinformation, vol.1, 17 – 30, DOI: 10.1127/pfg/2016/0284.

Matthesen AW, Schmidt K., (2016), DTM Generation-UAV Point Cloud Classification. Master Thesis, Aalborg University, Denmark. 158p. http://projekter.aau.dk/projekter/files/198676072/SM4_report_DTM_generation.pdf diakses September 2017.

Naryanto HS, (2003), Mitigasi Kawasan Pantai Selatan Kota Bandar Lampung, Provinsi Lampung terhadap Bencana Tsunami. Alami Vol. 8 No. 2 Tahun 2003.

Pratomo RA, Ruadiarto I., (2013), Permodelan Tsunami dan Implikasinya Terhadap

Mitigasi Bencana di Kota Palu. Jurnal Pembangunan Wilayah dan Kota Vol. 9 (2): 174-182 Juni 2013.

Purwanto HT, (2017), Pemanfaatan Foto Udara Format Kecil untuk Ekstraksi Digital Elevation Model dengan Metode Stereoplotting, Majalah Geografi Indonesia, Vol. 31, No.1, 73 – 89.

Rosaji FSC, Handayani W., Nurteisa YT, *et al.*, (2013), Aerial/Terrestrial Videography: Alternatif Teknologi Penginderaan Jauh untuk Survey dan Akuisisi Data Spatial. Prosiding Simposium Nasional Sains Geoinformasi III – 2013, ISBN 978-979-98521-4-4.

Sari NM, Kushardono D., (2014), Klasifikasi Penutup Lahan Berbasis Obyek pada Data Foto UAV untuk Mendukung Penyediaan Informasi Penginderaan Jauh Skala Rinci. Jurnal Penginderaan Jauh Vol.11 No.2, Desember 2014, 114-127.

Siagian TH, Purhadi, Suhartono, *et al.*, (2013), Social Vulnerability to Natural Hazards in Indonesia: Driving Factors and Policy Implications. Natural Hazards, Vol. 69 October 2013 DOI 10.1007/s11069-013-0888-3.

Siwi SE, (2009), Analisis Luas Penutup Lahan Berbasis Citra 2-Dimensi dan 3-Dimensi Studi Kasus: Daerah Tangkapan Air Danau Toba, Pemanfaatan Data Inderaja untuk Pemantauan Sumberdaya Alam dan Lingkungan (pp. 1-13). Jakarta: Massma Publishing.

Sunarto, Marfai MA, (2012), Potensi Bencana Tsunami dan Kesiapsiagaan Masyarakat Menghadapi Bencana Studi Kasus Desa Sumberagung Banyuwangi Jawa Timur. Jurnal Forum Geografi, Vol. 26 No.1, Juli 2012. Universitas Muhammadiyah Surakarta, Surakarta.

Tadono T., Ishida H., Oda F., *et al.*, (2014), Precise Global DEM Generation by ALOS PRISM. ISPRS Annals of the Photogrammetry, Remote Sensing and Spatial Information Sciences, Vol. II-4, 2014.

Uysal M., Toprak AS, Polat N., (2015), DEM Generation with UAV Photogrammetry and Accuracy Analysis in Sahitler hill, Measurement, Vol. 73, 539-543, DOI: 10.1016/j.measurement.2015.06.010.

DETERMINATION OF THE BEST METHODOLOGY FOR BATHYMETRY MAPPING USING SPOT 6 IMAGERY: A STUDY OF 12 EMPIRICAL ALGORITHMS

Masita Dwi Mandini Manessa[1]*, Muhammad Haidar[2], Maryani Hastuti[3], Diah Kirana Kresnawati[1]

[1]Geodesy Department, Pakuan University, Bogor, Indonesia

[2]Thematic Mapping Division, Geospatial Information Agency of Indonesia, Bogor, Indonesia

[2]Remote Sensing Application Center, Indonesian National Institute of Aeronautics and Space, Jakarta, Indonesia

*e-mail: m.manessa@outlook.com

Received: 8 November 2017; Revised: 22 December 2017; Approved: 22 December 2017

Abstract. For the past four decades, many researchers have published a novel empirical methodology for bathymetry extraction using remote sensing data. However, a comparative analysis of each method has not yet been done. Which is important to determine the best method that gives a good accuracy prediction. This study focuses on empirical bathymetry extraction methodology for multispectral data with three visible band, specifically SPOT 6 Image. Twelve algorithms have been chosen intentionally, namely, 1) Ratio transform (RT); 2) Multiple linear regression (MLR); 3) Multiple nonlinear regression (RF); 4) Second-order polynomial of ratio transform (SPR); 5) Principle component (PC); 6) Multiple linear regression using relaxing uniformity assumption on water and atmosphere (KNW); 7) Semiparametric regression using depth-independent variables (SMP); 8) Semiparametric regression using spatial coordinates (STR); 9) Semiparametric regression using depth-independent variables and spatial coordinates (TNP), 10) bagging fitting ensemble (BAG); 11) least squares boosting fitting ensemble (LSB); and 12) support vector regression (SVR). This study assesses the performance of 12 empirical models for bathymetry calculations in two different areas: Gili Mantra Islands, West Nusa Tenggara and Menjangan Island, Bali. The estimated depth from each method was compared with echosounder data; RF, STR, and TNP results demonstrate higher accuracy ranges from 0.02 to 0.63 m more than other nine methods. The TNP algorithm, producing the most accurate results (Gili Mantra Island RMSE = 1.01 m and R^2=0.82, Menjangan Island RMSE = 1.09 m and R^2=0.45), proved to be the preferred algorithm for bathymetry mapping.

Keywords: *bathymetry; SPOT 6; empirical methodology; multispectral image*

1 INTRODUCTION

Bathymetry data is important for ship traffic, conservation, coastal zoning and other environmental issues. Traditional bathymetric charts are collected using a single multibeam echo-sounders of ship-borne surveying. This method gives a satisfactory accuracy in water depths of up to 200 m. Instead, these methods are limited by their high costs, areal coverage, and time consumption. This limitation became an important issue especially for a nation that has a long coastal area, such as Canada, Indonesia, Russia, and Philippine.

Remote sensing has been suggested as an alternative tool for mapping the bathymetry especially for shallow water environment (Lyzenga 1978; Kanno *et al.*

2011). In this study, satellite derives bathymetry (here and after as SDB) term was used to define the remote sensing method for bathymetry extraction. The SDB technique for multispectral image start appear in 1970 proposed by Polycin *et al.* (1970), a prototype model based on a ratio of reflected radiation in at least two spectral bands in the visible region of the spectrum, was used to determine water depth. A decade after, for the first time used a commercial satellite data LANDSAT TM to extract the depth of using a linearized regression of single band (Lyzenga 1985), this method was based on previous publication (Lyzenga 1978). Since that time the algorithm has been re-developed and applied to the newest multispectral image: LANDSAT-TM and ETM (Clark *et al.* 1987; Van Hengel and Spltzer 1991; Bierwirth *et al.* 1993; Daniell 2008), SPOT 4 and SPOT 5 (Melsheimer and Chin 2001; Lafon *et al.* 2002; Liu *et al.* 2010; Sánchez-Carnero *et al.* 2014), IKONOS (Stumpf *et al.* 2003; Hogrefe *et al.* 2008; Su *et al.* 2014), QuickBird (Conger *et al.* 2006; Mishra *et al.* 2006; Lyons *et al.* 2011), LANDSAT-OLI (Pacheco *et al.* 2015; Vinayaraj *et al.* 2016; Kabiri 2017; Pushparaj and Hegde 2017), and Worldview-2 (Lee and Kim 2011; Deidda and Sanna 2012; Doxani *et al.* 2012; Bramante *et al.* 2013; Kanno *et al.* 2013; Yuzugullu and Aksoy 2014; Eugenio *et al.* 2015; Manessa *et al.* 2016b; Guzinski *et al.* 2016; Hernandez and Armstrong 2016; Kibele and Shears 2016; Manessa *et al.* 2016a).

Overall, SDB empirical algorithm can be divided into two types, first, the empirical algorithm that based on pixel radiance/reflectance value and second the combination of pixel radiance/reflectance value and the spatial information. This study focus on an empirical algorithm that based on pixel radiance/reflectance value and the set up was inspired by previous studies (Arya *et al.* 2016; Mohamed *et al.* 2017). But even so, both studies compared less number of an empirical algorithm. Early investigators analyzing SPOT 6/7 data for its utility in assessing bathymetry assessed the four extensions of Lyzenga's SDB algorithm for turbid water (Arya *et al.* 2016) and a new statistical approach (Mohamed *et al.* 2017), those studies have concluded that SPOT 6/7 performed accurately in the bathymetry mapping.

Afterwards, no published work exists on comparing all published empirical SDB algorithm on the use of SPOT 6 data for bathymetry mapping. Our research focuses on the finding the best empirical SDB algorithm for SPOT 6 multispectral data. Twelve empirical SDB algorithm was intensionally chosen: 1) Ratio transform (henceforth named "RT") by Stumpt *et al.* (2003); 2) Multiple linear regression (henceforth named "MLR") by Lyzenga *et al.* (2006); 3) Multiple non-linear regression (henceforth named "RF") by Manessa *et al.* (2016a); 4) Second-order polynomial of ratio transform (henceforth named "SPR") by Mishra *et al.* (2006); 5) Principle component (henceforth named "PC") by Van Hengel and Spitzer (1991); four extension of Lyzenga's SDB algorithm by Kanno *et al.* (2011): 6) Multiple linear regression using relaxing uniformity assumption on water and atmosphere (henceforth named "KNW"); 7) Semiparametric regression using depth-independent variables (henceforth named "SMP"); 8) semiparametric regression using spatial coordinates (henceforth named "STR"); 9) Semiparametric regression using depth-independent variables and spatial coordinates (henceforth named "TNP"), and three statistic new statistical approach of Mohamed *et al.* (2017): 10) Bagging Fitting

Ensemble (henceforth named "BAG"); 11) Least Squares Boosting Fitting Ensemble (henceforth named "LSB"); and 12) support vector regression (henceforth named "SVR").

2 MATERIALS AND METHODOLOGY

2.1 Location and Data

2.1.1 Location

This study assesses the performance of twelve empirical models for bathymetry calculations in two different areas: Gili Mantra Islands, West Nusa Tenggara and Menjangan Island, North Bali. First, the Gili Mantra Islands located on the off the coast of Lombok Island. The Gili Mantra Marine Natural Park includes three islands: Gili Trawangan, Gili Meno, and Gili Air (Figure 2-1B). Tourism is the dominant economic activity in the islands. Second, North Bali is the driest area in Bali Islands, due to low rainfall intensity. This condition became a perfect condition for a coral reef to grow. Menjangan Island (Figure 2-1A) is taken as the sample of the site that represent North Bali coral reef area.

2.1.2 Data

2.1.2.1 Single beam sonar

Bathymetry data were measured using a single-beam echo sounder and a differential global positioning system (D-GPS) (plotted as a red dot in Figure 2-1). The bathymetry data of the Gili Islands Island and Menjangan Island is individually collected for research purposed on September 25th, 2011 and September 1st, 2010, respectively. The depth data was strongly affected by tide and wave. Then this study applied a tidal correction (explain further in subchapter 3.1) to reduce the tide effect. But the wave effect is un-corrected and became the drawback issue.

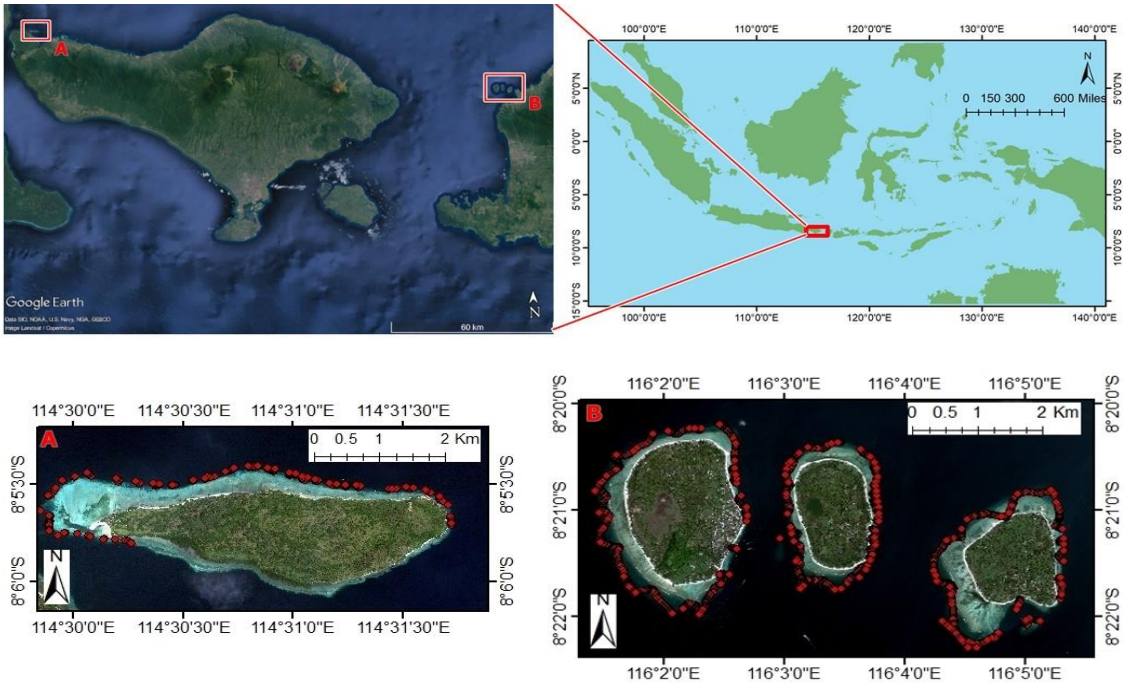

Figure 2-1: Study Site: Indonesia map (upper right), satellite image of Bali island and part of Lombok island (upper left), spot 6 image of Gili Mantra island (under right) and Menjangan island (under left). the red dot shows the depth measurement data

2.1.2.2 Multispectral imagery

The SPOT 6 high-resolution commercial imaging satellite was launched on September 9, 2012. The satellite is in a nearly circular, sun-synchronous orbit with a period of 98.97 minutes at an altitude of approximately 694 km. SPOT 6 acquires 12-bit data in five spectral bands covering blue, green, red, panchromatic, and near-infrared. SPOT 6 image used in this study is shown in Figure 2-1.

2.2 Methods

2.2.1 Tidal Correction

The measured depth data and Multispectral Imagery were affected by the tide. Hence, it necessary to convert the measured depth to zero mean sea levels (MSL) by subtracting the measured depth from the tide level of tide gauge. Also, the Imagery data should tide corrected up to the zero MSL. The tidal data was collected from the Indonesia Geospatial Agency tidal station.

2.2.2 Image Pre-rocessing: Atmospheric and Surface Scattering Correction

The SPOT 6 imagery passed three steps of image pre-processing. The first step was sensor calibration from digital numbers to the units of band-averaged spectral radiance or TOA (Top of Atmosphere) radiance. The equations and calibration coefficients applied were based on the technical note about the radiometric use of SPOT 6 imagery. The physical units of band-averaged spectral radiance are $W \cdot m^{-2} \cdot sr^{-1} \cdot \mu m^{-1}$. Secondly, the atmospheric and surface noise then TOA radiance were corrected (Lyzenga *et al.* 2006). Then, the formula of Lyzenga *et al.* (2006)'s atmospheric dan surface scattering correction is written as:

$$L_{c_i} = L_{TOA_i} - \alpha_{iNIR} \cdot (L_{TOA.NIR} - \bar{L}_{TOA.NIR}) \quad (2\text{-}1)$$

Where $L_{TOA.NIR1}$ is the measured TOA radiance in NIR band, $\bar{L}_{TOA.NIR}$ is that average over the deep water pixels, and α_{iNIR} is the slope of the simple regression line between the visible radiance and NIR radiance for the deep-water pixels.

Lastly, the relationship between radiance and depth was linearized to create the transformed radiance (X_i). Based on Lyzenga *et al.* (1978), the transformed radiance (X_i) is a linear value of radiance and depth and written as:

$$X_i = log\left(L_{c_i} - \overline{L_{c_{\infty,i}}}\right) \quad (2\text{-}2)$$

Where $\overline{L_{c_{\infty,i}}}$ is the mean of surface radiance deep water area for each band i. The X_i for three visible bands are used as the input for Lyzenga's based model.

2.2.3 Empirical Satellite Derive Bathymetry Algorithm

The twelve empirical algorithm has been choosing intentionally, this algorithm is the most commonly used and also the newest proposed. Several algorithms is a modification of and the first proposed SDB algorithm (Lyzenga 1978; Lyzenga *et al.* 2006). Most of the modification is based on statistical model improvement to nail several unrealistic assumptions, such as the number of bottom types and is based on a premise that bottom radiance is discrete, non-linear relation due to noise influence, and spatial uncorrelatedness of the error term. The summary of SDB empirical algorithm shown in Table 2-1.

2.2.4 Accuracy Assessment

The depth estimation accuracy of each model is measured by (Walpole 1968):

$$R^2 = 1 - \sum_i (h_i - \hat{h}_i)^2 \Big/ \sum_i (h_i - \bar{h})^2 \quad (2\text{-}3)$$

$$\text{RMSE} = \left(\sum_{i=1}^{n} (h_i - \hat{h}_i)^2 / n \right)^{0.5} \quad (2\text{-}4)$$

where h is measurement depth, $\hat{h}$ is estimated depth, $\bar{h}$ is the mean of depth measurement value, and n is the number of input data.

3 RESULTS AND DISCUSSION

Table 3-1 shows the accuracy assessment for the twelve algorithms mention in Table 2-1. In the case of Gili Mantra Island, the RMS errors of the eleven extended methods (PC, LR, LRSPO,

Table 2-1: Summary of 12 models reviewed in this paper

Model	Description and Equation	Source
Principle Component (PC)	Modification algorithm based on Lyzenga's SDB method, based on a rotational transformation of the transformed radiance (X_i), resulting in a depth-dependent variable, i.e. the relative water depth (digital counts), in the direction of the highest variance.	Van Hengel and Spitzer 1991
Linear Ratio (LR)	Proposed to nails the problem of mapping shallow-water areas with significantly lower radiance than adjacent. Accordingly, the change in ratio because of depth is much greater than that caused by a change in bottom albedo, suggesting that different bottom albedoes at a constant depth will still have the same ratio.	Stumpt *et al.* 2003
Second-order Polynomial of Ratio Transform (LRSPO)	Identified a ratio of wavebands (blue and green) that is constant for all bottom types. With these bands having different water absorptions, one band will have arithmetically lesser values than the other. Then, the log ratio of the two bands (blue, green) was plotted against known depth data to develop a second-order polynomial regression.	Mishra *et al.* 2005
Multiple Linear Regression (MLR)	Modified from the simple linear regression (Lyzenga, 1978). In before Lyzenga (1978) used the single band to build the prediction algorithm. The MLR analysis was conducted to depth as the dependent variable and the X_i of all visible bands as the independent variables.	Lyzenga *et al.* 2006
Multiple Linear Regression using Relaxing Uniformity Assumption on Water and Atmosphere (KNW)	Modified the Lyzenga, *et al* 2006, assumed that the water and atmosphere is uniform.	Kanno *et al.* 2011
Semiparametric Regression using Depth-Independent Variables (SMP)	The assumption in Lyzenga *et al.*'s method about the number of bottom types and is based on a premise that bottom radiance is discrete, is unrealistic. Then the elements of the bottom-type-dependent are included and used the semiparametric regression.	Kanno *et al.* 2011
Semiparametric Regression using Spatial Coordinates (STR)	Explicitly model by the spatial dependency of error (ε) due to the assumption of spatial uncorrelatedness of the error term.	Kanno *et al.* 2011
Semiparametric Regression using Depth-Independent Variables and Spatial Coordinates (TNP)	Combined the extension of Relaxing Uniformity Assumption on Water and Atmosphere, Depth-Independent Variables, Spatial Coordinates and uses the semiparametric regression model.	Kanno *et al.* 2011
Multiple Non-Linear Regression (RF)	Theoretically, the relation between depths and linearize surface radiance should be linear but a noise could cause a non-linear condition. Then random forest algorithm is used nail the nonlinear relation between depth and linearized radiance.	Manessa *et al.* 2016a
Bagging Fitting Ensemble (BAG)	The ensemble methods aim at improving the predictive performance of a given statistical learning or model fitting technique. A model is fitted to each bootstrap sample and the models are finally aggregated by majority voting for classification or averaging for regression.	Mohamed *et al.* 2017
Least Squares Boosting Fitting Ensemble (LSB)	The Least Squares Boosting Fitting Ensemble estimation algorithm is built by combining the concept of boosting, ensemble, and least square.	Mohamed *et al.* 2017
Support Vector Regression (SVR)	SVR model is used because of their ability to generalize well with limited training sample that commonly delead with remote sensing. This regression model applied to estimate the depth based on the several pixels with known depth.	Mohamed *et al.* 2017

MLR, KNW, SMP, STR, RF, LSB, BAG, and SVR) were higher compared to TNP method by 1.14, 1.16, 1.15, 0.78, 0.8, 0.65, 0.09, 0.66, 0.99, 0.78, and 0.77m, or in relative terms, 112.9%, 114.9%, 113.9%, 77.2%, 79.2%, 64.4%, 8.9%, 65.3%, 98%, 77.2% and 76.2%, respectively.

In the case of Menjangan Island, the RMS errors of the eleven extended methods (PC, LR, LRSPO, MLR, KNW, SMP, STR, RF, LSB, BAG, and SVR) were also higher compared to TNP method by 0.26, 0.28, 0.28, 0.25, 0.22, 0.18, 0.21, 0.04, 0.24, 0.24, and 0.21 m, or in relative terms, by 23.9%, 25.7%, 25.7%, 22.9%, 20.2%, 16.5%, 19.3%, 3.7%, 22%, 22% and 19.3% respectively. These results indicate that the TNP algorithm effectively improve the accuracy of the other methods.

Based on the results obtained from the image of two evaluated sites, the estimated depth was less accurate in Menjangan Island site. Two processes may have caused these accuracy problems. First, a measurement error of the single beam echo-sounder occurred especially in reef areas with significant morphology different such as Menjangan Island reef, where there were some delays in receiving the signal. Secondly, the significant error of depth measurement due to the data obtained in the afternoon, so high wave occurred. This shows that SDB for coral reef areas has a limitation under a specific condition, proper survey plan (times, instrument, and site) give a significant influence to produce an accurate SDB model.

Scattergrams of the estimated water depth against the measured water depth for Gili Mantra Islands and Menjangan Island are shown in Figure 3-1. The superior accuracy of the TNP algorithm is obvious. Even the other eleven algorithms is based on physical and statistical principles, but still includes several assumptions that are often unrealistic and also not effective or appropriate statistical analysis, details as follows. MLR algorithm assumed that water quality and atmospheric condition is uniform, and the number of bottom types is less than a number of used bands are unrealistic for much shallow water environment

Table 3-1: Statistic value of RMSE and R^2 for depth estimation accuracy of twelve evaluated SDB algorithm (values in bold shows the model with the best accuracy)

Method		Gili Mantra Island		Menjangan Island	
		RMSE [m]	**R^2**	**RMSE [m]**	**R^2**
Van Hengel and Spitzer (1991)	PC	2.15	0.21	1.35	0.16
Stumpt *et al.* (2003)	LR	2.17	0.20	1.37	0.14
Mishra *et al.* (2005)	LRSPO	2.16	0.21	1.37	0.14
Lyzenga *et al.* (2006)	MLR	1.79	0.45	1.34	0.18
Kanno *et al.* (2011)	KNW	1.81	0.44	1.31	0.22
	SMP	1.66	0.53	1.27	0.27
	STR	1.10	0.79	1.30	0.23
	TNP	**1.01**	**0.82**	**1.09**	**0.45**
Manessa *et al.* (2016a)	RF	1.67	0.53	1.13	0.44
Hassan *et al.* (2017)	LSB	2.00	0.32	1.33	0.17
	BAG	1.79	0.44	1.33	0.18
	SVR	1.78	0.48	1.30	0.22

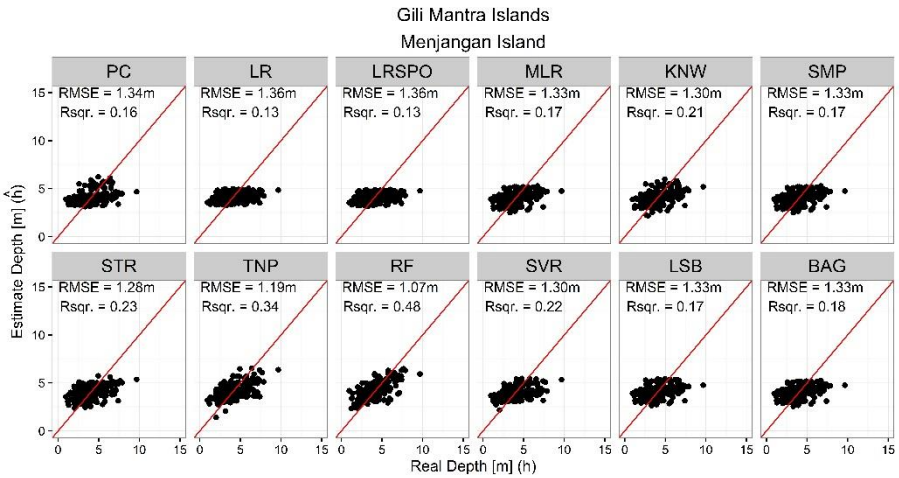

Figure 3-1:Scatter plot between estimated depth and real depth (Rsqr. is equal with R^2) and redlines x=y

(Kanno *et al.* 2011). RF algorithm used in this study is run on auto-tuning mode, however, to get the best result of random forest algorithm, it is necessary to do an optimization on the hyper-parameters (Manessa *et al.* 2016a). LR and PC algorithm focused on noise reduction (Stumpt *et al.* 2003 and Van Hengel and Spitzer 1991) but not consider that the linear regression works well with a number of explanatory variables. The ratio analysis on LR and PC analysis reduces the number of bands (explanatory variables), cause a linear regression of single explanatory variable. LRSPO algorithm used the same assumption with LR algorithm, where a ratio between the blue and green band is plotted with the known depth. Even Mishra *et al.* (2003) in the publication shows that the LRSPO algorithm works well (RMSE = 2,711 m and R^2 = 0.92) but in this study, this algorithm could not produce a good accuracy (RMSE = 1.37 – 2.16 and R^2 = 0.14 – 0.21). KNW algorithm only focuses on non-uniform of surface and atmospheric condition (Kanno *et al.* 2011). SMP algorithm only including the elements of the bottom-type-dependent to nails the premise that bottom radiance is discrete (Kanno *et al.* 2011). STR is proposed only to overcome the assumption of spatial uncorrelatedness of the error term in Lyzenga's method (Kanno *et al.* 2011). Finally, TNP algorithm is a model that nail all the unrealistic assumption mention above (Kanno *et al.* 2011) and also used an advanced statistical analysis (semiparametric regression) to get a satisfactory result. However, it still has a limitation, which requires longer execution times than the other algorithm.

The TNP algorithm used in this study provided a better estimation of depth (Gili Mantra Island RMSE = 1.01 m, Menjangan Island RMSE = 1.09 m) than the other eight algorithms (Gili Mantra Island RMSE = 1.10 - 2.17 m, Menjangan Island RMSE = 1.09 - 1.37 m) under the conditions represented in the study region and images analyzed. This result is in line with the previous studies (Kanno *et al.* 2011, and Arya *et al.* 2017). In the case of the same multispectral image with three visible bands (SPOT-7), the TNP algorithm yielded lower accuracy (RMSE = 1.14 m) (Arya *et al.* 2016) than those reported in this study. The higher RMSE in this study is likely due to differences in environmental conditions, including lower levels of suspended solids of coral reef environment. While for a multispectral image with higher spatial resolution,

namely Worldview-2, the TNP algorithm shows higher RMSE value (ranging from 0.2 – 0.8 m) (Kanno *et al.* 2011). This underline just how important the spatial resolution and environment condition on depth estimation accuracy.

4 CONCLUSION

Various empirical models have been developed to convert multispectral image pixel values into depth estimates. This study compares twelve empirical SDB model in two coral reef environment of Indonesia shallow water. In the case of Gili mantra, Islands and Menjangan Island illustrated that depth estimation can be derived from the SPOT 6 multispectral image with accuracy about 1-2 m (RMSE) in water depth down to 15 m. These depth estimation data are useful for many purposes, such as conservation, wave simulation, and coastal zoning. Moreover, as shown in this study, a correct empirical algorithm to be chosen is played an important role to produce an accurate bathymetry map. The accuracy different could reach 3.7 - 114.8% more or less accurate for each empirical algorithm. The result of comparisons suggests that the overall performance of Semiparametric Regression using Depth-Independent Variables and Spatial Coordinates algorithm can produce more accurate depth estimation. This study also found that the effect of wave gave a negative effect on the accuracy of SDB model. Then a wave correction is strongly suggested to be applied to a site with a strong wave influence or exclude an image with that condition.

ACKNOWLEDGEMENTS

The authors extend their appreciation for the support provided by the National Institute of Aeronautics and Space (LAPAN). We would like to thank the Geospatial Information Agency of Indonesia for providing the Gili Mantra Islands and Menjangan Island tidal data. We are very grateful to field survey team and Miko Raharjo. Most importantly, we thank Dr. Ing. Widodo S. Pranowo and Mr. Syarif Budhiman for the scientific advice to improve our manuscript.

REFERENCES

Arya A., Winarso G., Santoso AI, (2016), Ekstraksi Kedalaman Laut Menggunakan Data SPOT 7 di Teluk Belangbelang Mamuju (Accuracy Assesment of Satellite Derived Bathymetry using Lyzenga Method and it's Modification using SPOT 7 Data at the Belangbelang Bay Waters Mamuju). J Ilm Geomatika 22:9–19.

Bierwirth PN, Lee TJ, Burne RV, (1993), Shallow Sea-Floor Reflectance and Water Depth Derived by Unmixing Multispectral Imagery. Photogramm Eng Remote Sensing 59:331–338.

Bramante JF, Raju DK, Sin TM, (2013), Multispectral Derivation of Bathymetry in Singapore's Shallow, Turbid Waters. Int J Remote Sens 34:2070–2088. doi: 10.1080/01431161.2012.734934.

Clark RK, Fay TH, Walker CL, (1987), Bathymetry Calculations with Landsat 4 TM Imagery Under a Generalized Ratio Assumption. Appl Opt 26:4036. doi: 10.1364/AO.26.4036_1.

Conger CL, Hochberg EJ, Fletcher CH, Atkinson MJ, (2006), Decorrelating Remote Sensing Color Bands from Bathymetry in Optically Shallow Waters. IEEE Trans Geosci Remote Sens 44:1655–1660. doi: 10.1109/TGRS. 2006.870405.

Daniell JJ, (2008), Development of a Bathymetric Grid for the Gulf of Papua and Adjacent Areas: A Note Describing its Development. J Geophys Res Earth Surf 113:1–8. doi: 10.1029/2006JF000673.

Deidda M., Sanna G., (2012), Bathymetric Extraction using Worldview-2 High Resolution Images. ISPRS - Int Arch

Photogramm Remote Sens Spat Inf Sci XXXIX-B8:153–157. doi: 10.5194/ isprsarchives-XXXIX-B8-153-2012.

Doxani G., Papadopoulou M., Lafazani P., *et al.,* (2012), Shallow-Water Bathymetry Over Variable Bottom Types Using Multispectral Worldview-2 Image. In: ESA 2nd Space for Hydrology Workshop. 159–164.

Eugenio F., Marcello J., Martin J., (2015), High-Resolution Maps of Bathymetry and Benthic Habitats in Shallow-Water Environments Using Multispectral Remote Sensing Imagery. IEEE Trans Geosci Remote Sens 53:3539–3549. doi: 10.1109/ TGRS.2014.2377300.

Guzinski R., Spondylis E., Michalis M., *et al.,* (2016), Exploring the Utility of Bathymetry Maps Derived With Multispectral Satellite Observations in the Field of Underwater Archaeology. Open Archaeol 2:243–263. doi: 10.1515/opar-2016-0018.

Hernandez W., Armstrong R., (2016), Deriving Bathymetry from Multispectral Remote Sensing Data. J Mar Sci Eng 4:8. doi: 10.3390/jmse4010008.

Hogrefe KR, Wright DJ, Hochberg EJ, (2008), Derivation and Integration of Shallow-Water Bathymetry: Implications for Coastal Terrain Modeling and Subsequent Analyses. Mar Geod 31:299–317. doi: 10.1080/01490410802466710.

Kabiri K., (2017), Accuracy Assessment of Near-Shore Bathymetry Information Retrieved from Landsat-8 Imagery. Earth Sci Informatics 10:235–245. doi: 10.1007/ s12145-017-0293-7.

Kanno A., Koibuchi Y., Isobe M., (2011), Shallow Water Bathymetry from Multispectral Satellite Images: Extensions of Lyzenga'S Method for Improving Accuracy. Coast Eng J 53:431–450. doi: 10.1142/S057856341 1002410.

Kanno A., Tanaka Y., Kurosawa A., Sekine M., (2013), Generalized Lyzenga's Predictor of Shallow Water Depth for Multispectral Satellite Imagery. Mar Geod 36:365–376. doi: 10.1080/01490419.2013.839974.

Kibele J., Shears NT, (2016), Nonparametric Empirical Depth Regression for Bathymetric Mapping in Coastal Waters. IEEE J Sel Top Appl Earth Obs Remote Sens 9:5130–5138. doi: 10.1109/JSTARS.2016. 2598152.

Lafon V., Froidefond J-MM, Lahet F., *et al.*, (2002), SPOT shallow water bathymetry of a moderate turbid tidal inlet based on field measurements. Remote Sens Environ 81:136–148. doi: 10.1016/S0034-4257(01) 00340-6.

Lee K., Kim A., (2011), Determination of bottom-type and bathymetry using WorldView-2. In: Proc. SPIE Ocean Sens. Monitoring III. p 80300D–1.

Liu S., Zhang J., Ma Y., (2010), Bathymetric Ability of SPOT 5 Multi-Spectral Image in Shallow Coastal Water. In: Proc. 18th International Conference on Geoinformatics. 2–6

Lyons M., Phinn S., Roelfsema C., (2011), Integrating Quickbird Multi-Spectral Satellite and Field Data: Mapping Bathymetry, Seagrass Cover, Seagrass Species and Change in Moreton Bay, Australia in 2004 and 2007. Remote Sens 3:42–64. doi: 10.3390/rs3010042.

Lyzenga DR, (1978), Passive Remote Sensing Techniques for Mapping Water Depth and Bottom Features. Appl Opt 17:379. doi: 10.1364/AO.17.000379.

Lyzenga DR, (1985), Shallow-Water Bathymetry Using Combined Lidar and Passive Multispectral Scanner Data. Int J Remote Sens 6:115–125. doi: 10.1080/014311685 08948428.

Lyzenga DR, Malinas NP, Tanis FJ, (2006), Multispectral Bathymetry Using a Simple Physically Based Algorithm. IEEE Trans Geosci Remote Sens 44:2251–2259. doi: 10.1109/TGRS.2006.872909.

Manessa MDM, Kanno A., Sekine M., *et al.,* (2016a), Satellite-Derived Bathymetry Using Random Forest Algorithm and Worldview-2 Imagery. Geoplanning J Geomatics Plan 3:117. doi: 10.14710/geoplanning.3.2.117-126.

Manessa MDM, Kanno A., Sekine M., *et al.*,

(2016b), Lyzenga Multispectral Bathymetry Formula for Indonesian Shallow Coral Reef: Evaluation and Proposed Generalized Coefficient. In: Bostater CH, Neyt X, Nichol C, Aldred O (eds) Proc. Remote Sensing of the Ocean, Sea Ice, Coastal Waters, and Large Water Regions 2016. SPIE, Edinburgh, UK, 99990O.

Melsheimer C., Chin LS, (2001), Extracting Bathymetry from Multi-Temporal SPOT Images. In: Proc. The 22nd Asian Conference on Remote Sensing.

Mishra D., Narumalani S., Rundquist D., Lawson M., (2006), Benthic Habitat Mapping in Tropical Marine Environments Using QuickBird Multispectral Data. Photogramm Eng Remote Sensing, 72:1037–1048. doi: 10.14358/PERS.72.9.1037.

Mohamed H., Abdelazim Negm, Salah M., *et al.*, (2017), Assessment of Proposed Approaches for Bathymetry Calculations Using Multispectral Satellite Images in Shallow Coastal/Lake Areas: a Comparison of Five Models. Arab J Geosci 10:1–17. doi: 10. 1007/s12517-016-2803-1.

Pacheco A., Horta J., Loureiro C., Ferreira, (2015), Retrieval of Nearshore Bathymetry From Landsat 8 Images: A Tool for Coastal Monitoring in Shallow Waters. Remote Sens Environ 159:102–116. doi: 10.1016/j.rse. 2014.12.004.

Pushparaj J., Hegde AV, (2017), Estimation of Bathymetry Along the Coast of Mangaluru using Landsat-8 Imagery. Int J Ocean Clim Syst 8:71–83. doi: 10.1177/17593 131166 79672.

Sánchez-Carnero N., Ojeda-Zujar J., Rodríguez-Pérez D., Marquez-Perez J., (2014), Assessment of Different Models for Bathymetry Calculation using SPOT Multispectral Images in a High-Turbidity Area: The Mouth of the Guadiana Estuary. Int J Remote Sens 35:493–514. doi: 10.1080/01431161.2013.871402

Stumpf RP, Holderied K., Sinclair M., (2003), Determination of Water Depth with High-Resolution Satellite Imagery Over Variable Bottom Types. Limnology Oceanogr 48:547–556. doi: 10.4319/lo.2003.48.1_part_2. 0547.

Su H., Liu H., Wang L., *et al.,* (2014), Geographically Adaptive Inversion Model for Improving Bathymetric Retrieval from Satellite Multispectral imagery. IEEE Trans Geosci Remote Sens 52:465–476. doi: 10.1109/TGRS.2013.2241772.

Van Hengel W., Spltzer D., (1991), Multi-Temporal Water Depth Mapping by Means of Landsat TM. Int J Remote Sens 12:703–712. doi: 10.1080/01431169108929687.

Vinayaraj P., Raghavan V., Masumoto S., (2016), Satellite-Derived Bathymetry using Adaptive Geographically Weighted Regression Model. Mar Geod 39:458–478. doi: 10.1080/01490419.2016.1245227.

Walpole RE., (1968), Introduction to Statistics. Macmillan, Madison.

Yuzugullu O., Aksoy A., (2014), Generation of the Bathymetry of a Eutrophic Shallow Lake Using WorldView-2 Imagery. J. Hydroinformatics 16:50. doi: 10.2166/ hydro.2013.133.

CARBON STOCK ESTIMATION OF MANGROVE VEGETATION USING REMOTE SENSING IN PERANCAK ESTUARY, JEMBRANA DISTRICT, BALI

Amandangi Wahyuning Hastuti[1]*, Komang Iwan Suniada, Fikrul Islamy
[1]Institute for Marine Research and Observation – Perancak, Bali
*e-mail: amandangi.wahyuning@gmail.com
Received: 7 November 2017; Revised: 20 November 2017; Approved: 22 December 2017

Abstract. Mangrove vegetation is one of the forest ecosystems that offers a potential of substantial greenhouse gases (GHG) emission mitigation, due to its ability to sink the amount of CO_2 in the atmosphere through the photosynthesis process. Mangroves have been providing multiple benefits either as the source of food, the habitat of wildlife, the coastline protectors as well as the CO_2 absorber, higher than other forest types. To explore the role of mangrove vegetation in sequestering the carbon stock, the study on the use of remotely sensed data in estimating carbon stock was applied. This paper describes an examination of the use of remote sensing data particularly Landsat-data with the main objective to estimate carbon stock of mangrove vegetation in Perancak Estuary, Jembrana, Bali. The carbon stock was estimated by analyzing the relationship between NDVI, Above Ground Biomass (AGB) and Below Ground Biomass (BGB). The total carbon stock was obtained by multiplying the total biomass with the carbon organic value of 0.47. The study results show that the total accumulated biomass obtained from remote sensing data in Perancak Estuary in 2015 is about 47.20±25.03 ton ha^{-1} with total carbon stock of about 22.18±11.76 tonC $ha^{-1}$and CO_2 sequestration 81.41±43.18 tonC ha^{-1}.

Keywords: *Perancak Estuary, carbon stock estimation, mangrove, CO_2 sequestration, NDVI*

1 INTRODUCTION

Global warming is one of the strategic issues in the world today, as marked by the incidence of rising earth temperatures related to greenhouse gases. Several researchers noted that the major contributors to global warmings, such as carbon dioxide (CO_2), and methane (CH) gases are anthropogenic, mainly produced from the human activities like fossil fuels burning, industry, deforestation, forest degradation and other forest conversion through combustion (Giri and Mandla 2017; Vicharnakorn *et al.* 2014). The accumulation of these gases causes the earth's temperature to rise, triggering climate change on Earth (Manuri *et al.* 2011).

Sutaryo (2009) describes the forest biomass as highly relevant to climate change issues. Forest biomass has an important role in the biogeochemical cycle, especially in the carbon cycle. Of the total forest carbon, about 50% is stored in forest vegetation. As a consequence, if there is forest damage, forest fire, logging and etc., it will increase the possibility to have larger -amount of carbon in the atmosphere. The dynamics of carbon in nature can be explained simply by the carbon cycle. The carbon cycle is a biogeochemical cycle that includes the exchanged/transferred of carbon between the biosphere, the

pedosphere, the geosphere, the hydrosphere and the earth's atmosphere. The carbon cycle is actually a complex process and every process related to other processes. The global carbon describes the exchanges of carbon between the Earth's atmosphere, oceans, land and fossil fuels, which are both sources of emissions and sinks that contain carbon. One important function of the carbon cycle is the regulation of earth's climate (Bennington 2009).

Mangrove ecosystems, like other forest ecosystems, have a potential -ability to absorb carbon dioxide better than other forest ecosystems due to its ability to grow faster than any other forest vegetation. It is noted that mangrove forests have an important role in reducing the concentration of carbon dioxide in the air. Mangrove forest is one of the highest carbon-storage forests in the tropics and it is very high compared to the average carbon storages in other kinds of forest in the world (Donato *et al.* 2012). Although mangroves are known to have good assimilation capabilities with environmental components and have a high rate of carbon sequestration, data and information on carbon storage for some components, especially for tree biomass are very limited (Komiyama *et al.* 2008), so it is important to know that biomass information in the mangroves for sustainable forest management. In forest carbon inventories, carbon pools are accounted for by at least 4 carbon bags: surface biomass, subsurface biomass, dead organic matter and soil organic carbon. According to Donato *et al.* (2011), carbon is mostly stored in the sediments, aerial vegetal biomass, and below-ground biomass in the descending order. However recent studies suggest the importance of the carbon stock in the below-ground biomass of mangrove forests (Abohassan *et al.* 2012), there a few estimates regarding this compartment (Komiyama *et al.* 2008).

According to Lu (2006), field or terrestrial measurement is the most accurate way to collect biomass data, but this method is generally very expensive, time-consuming, labor-intensive and difficult to apply into remote and broad areas. Therefore there is another alternative solution in knowing the potential information of biomass that is by using aerial approach through remote sensing technology. The advantage of the remote sensing technology is to provide information needed quickly and completely at a relatively cheaper cost. In addition, the use of remote sensing technology in finding information on potential estimation of mangrove biomass as CO_2 absorber can be monitored effectively and efficiently every year. One of the remote sensing data that can be utilized is Landsat satellite data.

Situmorang *et al.* (2016) found that there was a high correlation (R^2=0.729) between vegetation index resulted from satellite data and carbon stock estimation calculated using allometric equation. This high determination coefficient indicates that the satellite data is feasible to use to estimate carbon stock. Many studies on carbon stocks in mangrove vegetation by using remote sensing techniques have been conducted. In mangrove forest carbon stock (Mariana *et al.* 2015; Alemayehu *et al.* 2014; Sitoe *et al.* 2014; Hamdan *et al.* 2013; Murdiyarso *et al.* 2009) carbon sequestration (e.g. Bouillon *et al.* 2008; Khan *et al.* 2007) and organic carbon dynamics (Kristensen *et al.* 2008; Machiwa and Hallberg 2002) have been studied much. Carbon stock in mangrove ecosystem varies with species (Fu and Wu 2011; Laffoley and Grimsditch 2009), vegetation type (Sahu *et al.* 2016; Cerón-Bretón *et al.* 2011; Mitra *et al.* 2011; Sapit

et al. 2011) and salinity (Adame *et al.* 2013).

Perancak Estuary is one of the four main mangrove ecosystems in Bali Island besides West Bali National Park, Benoa Bay and Nusa Lembongan. In addition to feeding, spawning and nursery ground, information on the ability of mangrove forest in Perancak Estuary to store carbon utilizing of remote sensing technology is still very low, so this research becomes very important to do. The objective of this research is to identify the biomass and potential carbon stock of mangroves vegetation in Perancak Estuary by using remote sensing approach. This information is very useful for Jembrana district government to support sustainable development planning based on low carbon, especially for the coastal area.

2 MATERIALS AND METHODOLOGY

2.1 Location and Data

The research is located in Perancak Estuary, Jembrana District, Bali as shown in Figure 2-1. Geographically, Perancak Estuary is located between 8°22'30"S to 8°24'18"S and 114°36'18"E to 114°38'31.2"E. Perancak Estuary has an area of 2512.69 ha, with land use in the form of fishponds and mangroves.

Data used in this research is Landsat 8 OLI/TIRS with acquisition date 13 September 2015 and path/ row 117/ 66 which obtained from United States Geological Survey (USGS) through website https://earthexplorer.usgs.gov.

2.2 Data Analysis

2.2.1 Converting digital values into reflectance

The Landsat sensor is converted into reflectance value by using the variable factors that provided in the metadata. Landsat suggests to converting the digital value into Radian using the following formula:

$$\rho\lambda' = M\rho Qcal + A\rho \quad (2\text{-}1)$$

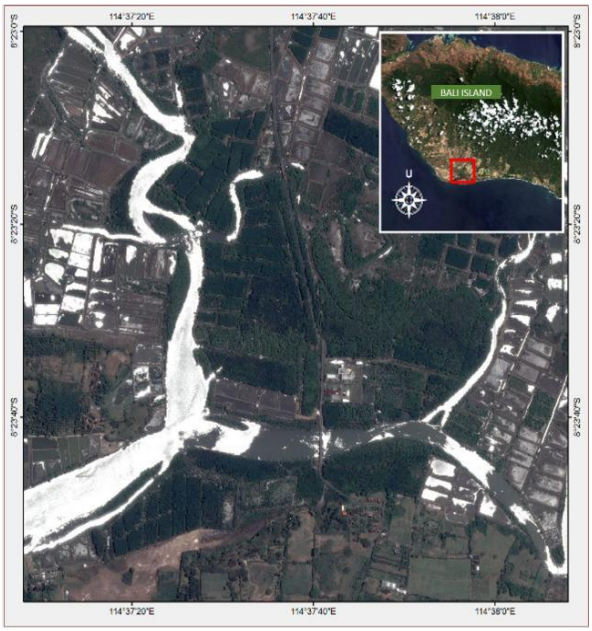

Figure 2-1: Location of the research area

$\rho\lambda'$ = a reflectance value without correction to the sun's elevation, $M\rho$ = band specific multiplicative rescaling factor (where*x* is *Band* (*REFLECTANCE_MULT_ BAND_x*), $A\rho$ = Band-specific additive rescaling factor from the metadata (where *x* is *Band* (*REFLECTANCE_ADD_BAND_x*,), *Qcal* = quantized and calibrated standard product pixel values(DN).

Conversion of reflectance value to the sun elevation follows equation (2-2).

$$P\lambda' = \frac{\rho\lambda'}{cos(\theta SZ)} = \frac{\rho\lambda'}{sin(\theta SE)} \quad (2\text{-}2)$$

$P\lambda'$ = reflectance, θSE = a local sun elevation. The scene center sun elevation in degrees (SUN_ELEVATION); θSZ = local solar zenith angle, $\theta SZ=90°-\theta SE$.

2.2.2 Vegetation index

Calculation of land covers vegetation index using Normalized Difference Vegetation Index (NDVI). NDVI is a

calculation of visible light and near infrared which is reflected by vegetation. The classification of pixel values for NDVI ranges from -1 to 1. The low (negative) NDVI values identify areas of water bodies, rocks, sand, and snow. High NDVI values (positive) identify areas of vegetation in the form of savanna, bush, and forests, whereas the NDVI value near 0 generally identifies bare land (Saputra 2007). This value of NDVI can be calculated using the equation 2-3.

$$NDVI = \frac{NIR - RED}{NIR + RED} \quad (2\text{-}3)$$

where *NIR* = near infrared band, *RED* = red band.

The NIR reflectance is affected by leaf internal structure and leaf dry matter content. RED is the reflectance or radiance in a visible wavelength channel (0.63 - 0.69 µm) and corresponds to band 3 for ETM+ images.

In this paper, NDVI images were generated to enhance mangrove forest that has higher NIR reflectance, and lower red light reflectance. Also, NDVI images were produced to eliminate water bodies, those of low red light reflectance, and those of very low NIR reflectance.

2.2.3 Image classification of mangrove land

Image classification is performed to separate the spectral values contained in the pixel image unit. The unit of the pixel value is explained into several classes of land cover. The method of satellite image classification guided using imagery classification method to distinguish between mangrove area and non-mangrove area. Guided classification uses the maximum likelihood method which assumes that the class statistics in each band are normally distributed. The manual visual analysis classification is performed when the data is cloud-covered and the absence of other data available as the closing or graph fill data so that the edge of limitation digit to classify using the 563 composite band approach with mangrove-looking conditions as seen in Figure 2-2.

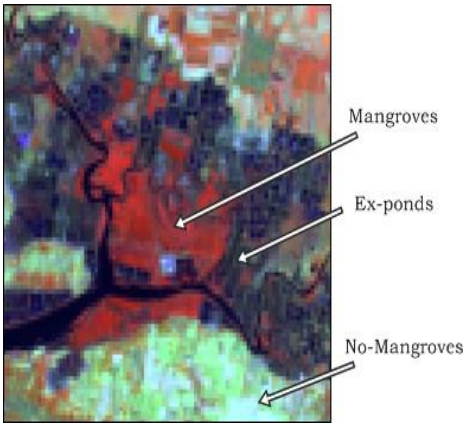

Figure 2-2: The mangrove vegetation shown in the composite image of 5-6-3 (NIR-WSIR 1-Green)

The pixel class is determined by the highest probability level. The results of guided data and manual visual analysis can then be converted to measure the area of land cover.

2.2.4 Above Ground Biomass (AGB) estimation

Estimation of above the ground surface biomass value was done using the approach of NDVI result of equation correlation with Above Ground Biomass (AGB) of mangrove that is equal to 0.787 by Jha *et al.* (2015) as follows:

$$AGB = 305.9 * NDVI^{4.864} \quad (2\text{-}4)$$

NDVI = the value of Vegetation Index,
AGB = the Above Ground Biomass Value (ton ha^{-1}).

2.2.5 Below Ground Biomass (BGB) estimation

The estimated value of Below Ground Biomass (BGB) is obtained from the estimation of AGB which is

formulated using the equation compiled by Cairns, *et al* (1997) as follows:

$$BGB = \exp(-1.0587 + 0.8836 * Ln(AGB)) \quad (2\text{-}5)$$

AGB = the value of Above Ground Biomass (ton ha^{-1}), *BGB* = the Below Ground Biomass value (ton ha^{-1}).

2.2.6 Total Accumulated Biomass (TAC) Calculation

Total Accumulation Biomass (TAB) is formulated by using:

$$TAB = AGB + BGB \quad (2\text{-}6)$$

TAB = Total Accumulated Biomass (ton ha^{-1}).

2.2.7 Total Carbon Stock (TCS) calculation

Calculation of total carbon stock based on Westlake (1963) using the following formula:

$$TCS = TAB * \%\, C\ organic \quad (2\text{-}7)$$

TCS = the value of Total Carbon Stock (ton C ha^{-1}), *TAB* = the value of Total Accumulated Biomass (ton ha^{-1}), *%C organic* = the percentage value of carbon stock (0.47) or using the value of carbon emitted from the measurement results in the laboratory.

2.2.8 Amount of CO_2 Sequestration (ACS) calculation

IPCC (2001) suggests converting carbon stock from biomass to carbon dioxide uptake using the following conversion:

$$ACS = 3.67 * TCS \quad (2\text{-}8)$$

ACS = the Amount of CO_2 Sequestration (ton C ha^{-1}), *TCS* = the value of Total Carbon Stock (ton C ha^{-1}).

The biomass or carbon stock unit can be converted from unit ton ha^{-1} into kg/Landsat Pixel (kg/900m^2) by using the equation (9).

$$Data\left(\frac{kg}{Landsat\ Pixel}\right) = Data\left(\frac{ton}{ha}\right) * 90 \quad (2\text{-}9)$$

2.2.9 Estimation of biomass, carbon stock and CO_2sequestration

The biomass, carbon stocks, and carbon sequestration are calculated by constructing the equation above using ArcGIS Geoprocessing toolbox application for Landsat Image 7 and 8.

3 RESULTS AND DISCUSSION

From the image analysis, we found that the extent of mangrove vegetation within the research area is approximately 101.16 ha. Green, *et al* (1998) did the assessment of mangrove area using NDVI to estimate of percent canopy, the accuracy of the percent canopy closure image was 80%. High accuracy to assess mangrove using NDVI also reported by Otero, *et al* (2016) with the overall accuracy of 87% ± 2%. The ability of the NDVI method to detect mangrove vegetation conducted by Guha (2016) has an overall accuracy of 88.75% for 1989 image and 86.25% for 2010 images, and the overall Kappa coefficient of 0.81 and 0.76.

Based on the area of mangrove forest, the range of mangrove vegetation index in Perancak Estuary is 0.0025 – 0.78 (Table 3-1). This range of NDVI values differs from Prameswari *et al.* (2015), where the minimum value of NDVI obtained from the measurement using ALOS AVNIR-2 image data is -0.723 and maximum of 0.530 with the standard deviation 0.127.

A variety of vegetation index has been developed by retrieving vegetation

density from optical remote sensing. Li *et al.* (2007) are used the most common one method is NDVI to predict the biomass of trees. NDVI is based on the characteristics that vegetation has noticeable absorption in the near read infrared spectrum.

In addition to NDVI, there are also several image data processing methods for determining vegetation index such as Simple Ratio (SR), Triangular Vegetation Index (TVI), Enhanced Vegetation Index (EVI), Ratio Vegetation Index (RVI), and Soil Adjusted Vegetation Index (SAVI) (Frananda *et al.* 2015). Furthermore, the vegetation index values were used for the determination value of AGB, BGB, TAB, TCS and ACS using equation (4) to (9) above.

Based on Table 3-1, it can be seen that the AGB value is 38.60±20.79 ton ha^{-1} and the value of BGB is 8.60±4.24 ton ha^{-1}. Based on the value of AGB and BGB it can be said that the AGB is bigger than BGB. This is consistent with the results of a study conducted by (BPOL 2015) which states that by conducting field measurements in Perancak Estuary, the average value of AGB is higher than the BGB's.

The value of AGB and BGB on this research still representative with the research about assessment of mangrove forest carbon stock monitoring in Indonesia conducted by Yenni*, et al* (2014), which the average of AGB in Subang, West Jawa 1.65 ton ha^{-1}; Cilacap, Central Java 4.62 ton ha^{-1}; Badung, Bali 12.87 ton ha^{-1}; and Merauke, Papua 3.97 ton ha^{-1}.

AGB will give the best estimation using diameter breast height (DBH) as a parameter (Alemayehu *et al.* 2014). The determination of the AGB value is an important step in the planning of the protection and utilization of natural mangrove resources (Meideros and Sampaio 2008). The differences in AGB and BGB valuescan also be seen among mangrove species, depending on geographical location, tree density and ecology (Sahu *et al.* 2016; Alongi 2012).

Total accumulated biomass (TAB) is the total amount of biomass on above and below the soil surface. The value TAB in Perancak Estuary is 18.67 ton ha^{-1}. If the ratio between BGB and AGB is bigger, then the plant undergoes substantial root growth (below ground) which is quite dominant rather than trunk growth (above ground). Plant biomass is closely related to photosynthesis, biomass increases as plants absorb CO_2 from the air and convert it into organic compounds through photosynthesis. Biomass in each part of the plant increases proportionately with the larger diameter of the tree. The high ability of trees to store carbon free from air depends on the diameter of trees (Imani *et al.* 2017) and tree height (Fu and Wu 2011).

Table 3-1: Average values of AGB, BGB, TAB, ACS and ACS in Perancak Estuary

Average Values	Statistics (t ha^{-1})		
	Mean±SD	Max	Min
NDVI	0.63±0.11	0.78	0.0025
AGB	38.60±20.79	93.43	0
BGB	8.60±4.24	19.11	0
TAB	47.20±25.03	112.54	0
TCS	22.18±11.76	52.89	0
ACS	81.41±43.18	194.12	0

The estimated of total carbon stock value in the Perancak Estuary is 22.18±11.76 tonC ha^{-1} and the amount of CO_2 sequestration estimation is 81.41±43.18 tonC ha^{-1}. The estimated total carbon stock value obtained from the remote sensing measurements is much higher than the field measurements conducted by (Sidik *et al.* 2014) in Perancak Estuary.

Regarding of (Sidik *et al.* 2014), there is a difference in carbon stock value between natural mangrove forest and re-plantation mangroves in ex-ponds. Carbon stock produced by natural mangroves is higher than re-plantation mangroves in ex-ponds. The carbon stock value in natural mangrove forest is 171±43 MgC ha^{-1} while the carbon stock from mangrove that grows in ex-pond is 52±15 MgC ha^{-1}.

The estimated value of carbon stocks in Perancak Estuary can be done by remote sensing approach with a good result, even the value is still low compared with other studies (Table 3-2). The average biomass of live trees found from (Sitoe *et al.* 2014) is below the lower limit 58.38±19.1Mg ha^{-1} and the average carbon 28.02±9.2 Mg ha^{-1}.

Table 3-2 shows, the estimation of carbon stock using remote sensing data at Perancak estuary is still reasonable. Existing mangrove forest is usually producing a higher value of carbon stock comparing to the replanted mangrove.

Table 3-2: Carbon stock estimation of mangrove vegetation found in the literature

Reference	Carbon Stock (tonC ha^{-1})
This study	22.18±11.76
Estrada and Soares (2016)	78.0±64.5
Hutchinson *et al.* (2014)	74.5±54.6
Hamdan *et al.* (2013)	1.01 – 259.68
Komiyama *et al.* (2008)	78.3±51.0

Variations of carbon stock value depend on several physical factors of environmental chemistry, the diversity and density of existing plants, soil types and how they are managed. Besides on those factors, mangroves in Perancak Estuary are from rehabilitated mangroves in 2001 and 2009. The dominant mangroves found in Perancak Estuary are *Rhizopora mucronata*, *Rhizopora apiculata*, *Sonneratia alba*, *Avicennia alba* and *Avicennia marina* (Proisy *et al.* 2015).

Mangroves in Perancak Estuary area grow on the mud-soil type substrate mixed with organic material (Kartikasari and Sukojo 2015). The size of the carbon stored in vegetation depends on the amount of biomass contained in the tree, soil fertility and the absorption of the vegetation (Ati *et al.* 2014).

Figure 3-1 shows the location of natural and rehabilitation (re-plantation) mangroves in Perancak Estuary. In the natural mangroves dominated by *Avicennia* sp. and *Sonneratia alba.* While the dominant mangrove grown in the former location of ponds (rehabilitation mangroves) estimated to be around 8-10 years old is *Rhizopora* sp. (BPOL 2015). Based on the result of this research, the variation values of carbon stock in Perancak Estuary due to the age of the relatively young mangrove trees. Almost 70% of carbon stock variability is explained by age (Estrada and Soares 2017), species, management regime, as well as the climate (Kairo *et al.* 2008). It has been reported that the highest carbon stock for > 80-year-old *R. apiculata* - dominated mangrove forest was 230.0 t C ha^{-1} (Putz and Chan 1986) while those of 20- and 28-year-old *Rhizopora* forests were 114 and 105.9 t C ha^{-1} respectively (Ong *et al.* 1995). The standing biomass

for the 12-year-old *Rhizopora mucronata* plantation was 106.7±24.0 t/ ha, giving a biomass accumulation rate of 8.9 t/(ha year) (Kairo *et al.* 2008). The condition of mangrove vegetation in Perancak Estuary shown in Figure 3-2**.**

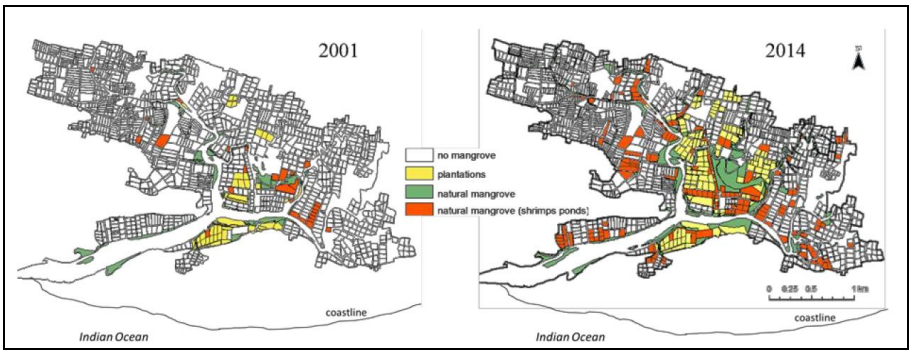

Figure 3-1: Fine-scale maps of changes in mangrove cover between 2001 (left) and 2014 (right) over the whole Perancak Estuary (Rahmania *et al.* 2014)

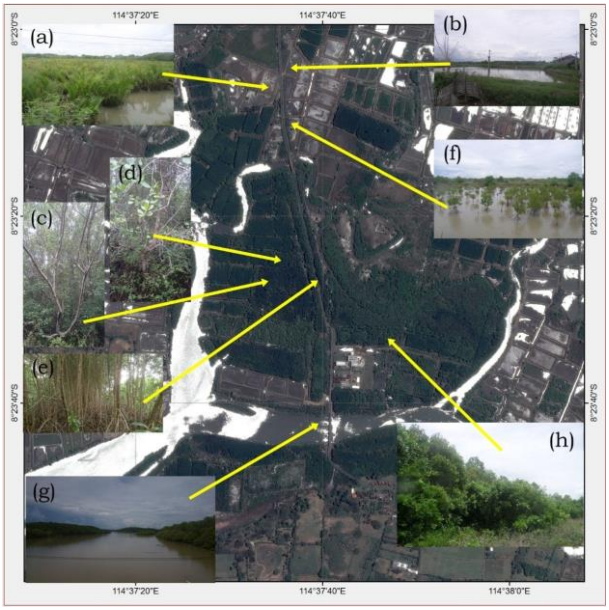

Figure 3-2: Mangrove vegetation condition in Perancak Estuary which surrounded by river and ponds (a) *nypa* sp. which grow in ex-ponds (b) active ponds (c) *avicennia* sp. (d) *sonneratia* sp. (e) *rhizopora* sp. (f) *rhizopora* sp. re-plantation in the ex-ponds (g) natural mangrove vegetation that grows along the river (h) natural mangrove vegetation

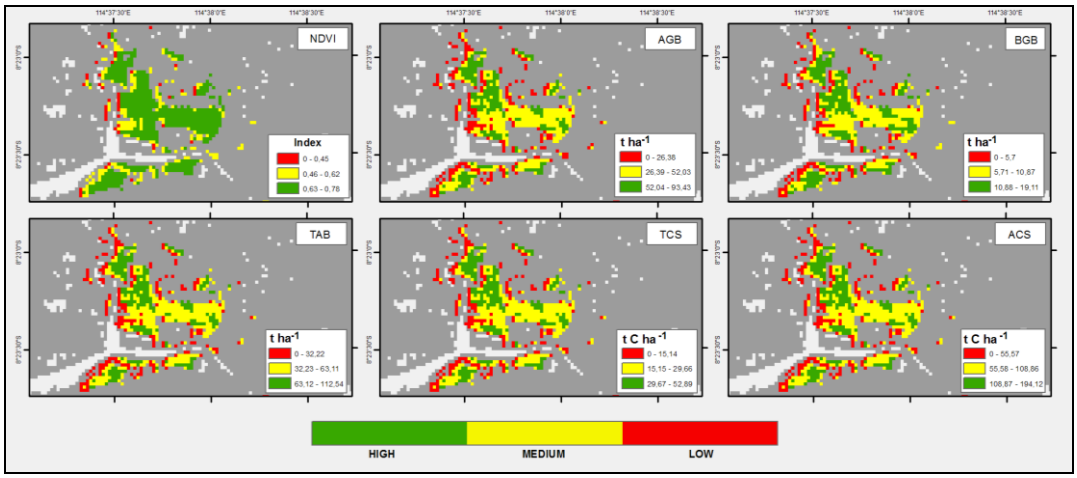

Figure 3-3: Map of value and distribution of NDVI, AGB, BGB, TAB, TCS and (ACS) in Perancak Estuary in 2015

Figure 3-3 shows the values and distributions of NDVI, AGB, BGB, TAB, TCD and ACS in the Perancak Estuary. Spatially viewed of the distribution of NDVI value, the range value of AGB, BGB, TAB, TCD and ACS are different. Variations of the distribution of these values are speculated because of the different types of mangroves, namely mangroves that grow naturally and rehabilitated mangroves. Value of NDVI, the average value of AGB, BGB, TAB, TCD and ACS in natural mangroves is higher than mangroves that grow in the former location of ex-fishponds and rehabilitation mangrove (Figure 3-3).

NDVI value generated for each pixel on the images was converted to carbon stock will give a different result. The higher NDVI will produce a high biomass value as well. The relationship between NDVI and biomass is also reported (Hamdan *et al.* 2013), which states that there are different relationships between AGB and NDVI. Linear regression produced higher correlation coefficients but not represent the real distribution, especially when the NDVI value approaches 0.

Optic data approach commonly used vegetation indices for mangrove biomass estimation (Sahu *et al.* 2016; Hamdan *et al.* 2013; Wicaksono *et al.* 2011; Li *et al.* 2007) and for the common forest (Laurin *et al.* 2016; Jha *et al.* 2015). Vegetation indices are highly related to net primary productivity (Li *et al.* 2007).

Given that optical imagery cannot obtain tree height as a crucial parameter in biomass estimation, detailed and accurate estimation of mangrove forest AGB still presents a challenge when parameters derived from optical imagery are applied to biomass estimation. Studies of plant allometry indicated that biomass is determined not only by canopy parameters but also by other factors such as wood density, trunk taper and tree height (Komiyama 2008; Chave *et al.* 2006; Niklas 1995) which are closely relevant to the floristic characteristics of the species.

The results of research on estimation of carbon stock by using remote sensing method still require the accuracy and field test to mangrove type and density. The NDVI method is not the best method for estimation of carbon stocks, but the method has relatively consistent accuracy at various levels of radiometric correction (Wicaksono *et al.* 2011). According to Frananda (2015), measuring the vegetation index using TVI has the best accuracy. In addition, the use of high-resolution image data is necessary to be applied in assessing the condition and dynamics of mangroves properly (Rodriguez and Feller 2004), classification of tree species based on their reflectance value (Wang *et al.* 2004; Dahdouh-Guebas *et al.* 2005) and the other necessities.

4 CONCLUSION

Estimated carbon stocks in Perancak Estuary can be done using remote sensing data with the good enough result, which is 22.18±11.76 tonC ha^{-1}. The use of NDVI is still relevant for biomass and carbon stock estimation in a mangrove ecosystem. Moreover, the difficulty of distinguishing mangrove vegetation is due to relatively small research areas. Field measurement and high-resolution satellite data in carbon stock estimation, especially in Perancak Estuary still need further study to improve the accuracy of carbon stock estimation results.

ACKNOWLEDGEMENTS

The authors are thankful to Institute of Marine Research and Observation. Acknowledge to I Nyoman Radiarta, Nuryani Widagti and Frida Sidik for advice and support. We also thank to the reviewers, Prof. Dr. I Nengah Surati Jaya, M.Agr. and Dr. Indah Prasasti for their constructive comments and suggestions.

REFERENCES

Abohassan RAA, Okia CA, Agea JG, *et al.*, (2012), Perennial Biomass Production in Arid Mangrove Systems on the Red Sea Coast of Saudi Arab. Environ Res J 6(1): 22-31.

Adame MF, Kauffman JB, Medina I., *et al.*, (2013), Carbon Stocks of Tropical Coastal Wetlands within the Karstic Landscape of the Mexican Caribbean. PLoS One 8(2):e56569. doi.10.1371/ journal. pone.0056569.

Alemayehu F., Richard O., James KM, *et al.*, (2014), Assessment of Mangrove Covers Change and Biomass in Mida Creek, Kenya. Open Journal of Forestry, 4:398-413. http://dx.doi.org/ 10.4236/ojf.2014.44045.

Alongi DM, (2012), Carbon Sequestration in Mangrove Forests. Carbon Management 3(3), 313-322.

Ati RNA, Rustam A., Kepel TL, *et al.*, (2014), Stok Karbon dan Stuktur Komunitas Mangrove Sebagai Blue Carbon di Tanjung Lesung, Banten. Jurnal Segara. Vol. 10 No. 2, Desember 2014: 119-127.

Bennington JB., (2009), The Carbon Cycle and Climate Change. Hofstra University – USA.

Bouillon S., Borges AV, Eda-Moya EC, *et al.*, (2008), Mangrove Production and Carbon Sink: a Revision of Global Budget Estimates. Global Biogeochem Cycles 22:1-12. doi:10.1029/ 2007GB003052.

Cairns MA, Brown S., Helmer EH, *et al.*, (1997), Rootbiomass Allocation in the World's Upland Forests. Oecologia (1997) 111:1 - 11.

Cerón-Bretón RM, Cerón-Bretón JG, Sánchez-Junco RC, *et al.*, (2011), Evaluation of Carbon Sequestration Potential in Mangrove Forest at Three Estuarine Sites in Campeche Mexico. Int J Energy Environ 5(4):487-494.

Chave J., Muller-Landau HC, Baker TR, *et al.*, (2006), Regional and Phylogenetic Variation of Wood Density Across 2456 Neotropical Tree Species. Ecol. Appl. 16, 2356–2367.

Dahdouh-Guebas F., Hiel EV, Chen JCW, *et al.*, (2005), Qualitative Distinction of Congeneric and Introgressive Mangrove Species in Mixed Patchy Forest Assemblages using High Spatial Resolution Remotely Sensed Imagery (IKONOS). Systematics and Biodiversity, 2, 113- 119.

Deng S., Shi Y., Jin Y., *et al.*, (2011), A GIS-Based Approach for Quantifying and Mapping Carbon Sink and Stock Values of Forest Ecosystem: A case study. Energy Procedia, 5:1535-1545.doi:10.1016/ j.egypro.2011.03.263.

Donato D., Kauffman JB, Murdiyarso D., *et al.*, (2012), Mangrove adalah Salah Satu Hutan Terkaya Karbon di Kawasan Tropis (No. CIFOR Infobrief no. 12, p. 12p). Center for International Forestry Research (CIFOR), Bogor, Indonesia.

Donato DC, Kauffman JB, Murdiyarso D., *et al.*, (2011), Mangroves Among the Most Carbon-Rich Forests in the Tropics. Nature Geosci 4: 293-297.

Estrada GCD, and Soares MLG, (2017), Global Patterns of Abgove Ground Carbon Stock and Sequestration in Mangroves. Anais de Academia Brasileira de Ciencias 89(2): 973-989.

Frananda H., Hartono, Jatmiko, RH, (2015), Komparasi Indeks Vegetasi untuk Estimasi Stok Karbon Hutan Mangrove Kawasan Segoro Anak pada Kawasan Taman Nasional Alas Purwo Banyuwangi, Jawa Timur. Majalah Ilmiah Globe. Vol. 17 No 2. Desember 2015: 113 – 123.

Fu W., Wu Y., (2011), Estimation of Above Ground Biomass of Different Mangrove Trees Based on Canopy Diameter and Tree Height. 3rd International Conference on Environmental Science and Information Application Technology (ESIAT 2011). Procedia Environmental Sciences, 10 (2011) 2189 - 2194.

Giri RKKV, Madla VR., (2017), Study and Evaluation of Carbon Sequestration using Remote Sending and GIS: A Review on Various Techniques. International Journal of Civil Engineering and Technology, 8(4), 287-300.

Green EP, Mumby PJ, Edwards AJ, *et al.*, (1998), The Assessment of Mangrove Areas using High Resolution Multispectral Airborne Imagery. Journal of Coastal Research, 14(2), 433-443. Royal Palm Beach (Florida), ISSN 0749-0208.

Guha S., (2016), Capability of NDVI Technique in Detecting Mangrove Vegetation. International Journal of Advanced Biological Research. Vol. 6(2): 253-258.

Hamdan O., Khairunnisa MR, Ammar AA, *et al.*, (2013), Mangrove Carbon Stock Assessment by Optical Satellite Imagery. Journal of Tropical Forest Science 25(4): 554-565.

Huete A., Didan K., Leeuwen WV, *et al.*, (2011), MODIS Vegetation Indices. Land Remote Sensing and Global Environmental Change. Springer. New York.

Hutchison J., Manica A., Setnam R., *et al.*, (2014), Predicting Global Patterns in Mangrove Forest Biomass. Conserv Let 7:233-240.

Imani G., Boyemba F., Lewis S., *et al.*, (2017), Height-Diameter Allometry and Above Ground Biomass in Tropical Montane Forests: Insights from the Albertine Rift in Africa. PLOS ONE 12(6): e0179653. https://doi.org/10.1371/journal.pone.0179653.

IPCC., (2001), Climate Change 2001. Intergovernmental Panel on Climate Change National Greenhouse Gas Inventories Programme downloaded on 15 June 2017 from http://www.ipcc.ch/ipccreports/tar/wg3/index.php?idp=477S.

Jha CS, Fararoda R., Rajashekar, *et al.*, (2015), Spatial Distribution of Biomass in Indian Forests using Spectral Modelling (No.Technology Trends: Multi-Scale Remote Sensing Using Optical Sensorsno. 3, 138p). The International Centre for Integrated Mountain Development (ICIMOD), Nepal.

Kairo JL, Lang'at JKS, Dahdouh-Guebas F., *et al.*, (2008), Structural Development and Productivity of Replanted Mangrove Plantations in Kenya. For. Ecol. Manag. 255, 2670-2677.

Kartikasari AD, Sukojo BM, (2015), Analisis Persebaran Ekosistem Hutan Mangrove Manggunakan Citra Landsat-8 di Estuari Perancak Bali. GEOID. Vol. 11 No. 01.

Khan MNI, Suwa R., Hagihara A., (2007), Carbon and Nitrogen Pools in a Mangrove Stand of Kandelia obovate (S., L.) Yong: vertical distribution in the soil-vegetation system. Wetl. Ecol. Manag 15(2):141-153. doi:10.1007/s11273-006-9020-8.

Komiyama A., Ong JE, Poungparn S., (2008), Allometry, Biomass, and Productivity of Mangrove Forests. Aquatic Botany. Vol. 89: 128–137.

Kristensen E., Bouillon S., Dittmar T., *et al.*, (2008), Organic Carbon Dynamics in Mangrove Ecosystem: a review. Aquat Bot 89:201-219. doi:10.1016/j.aquabot.2007.12.005.

Laffoley DDA, Grimsdicth G., (2009), The Management of Natural Coastal Carbon Sink. IUCN Gland, Switzerland.

Li XA, Yeh GO, Wang S., *et al.*, (2007), Regression and Analytical Models for Estimating Mangrove Wetland Biomass in South China Using Radarsat Images. International Journal of Remote Sensing 28:5567-5582.

Lu D., (2006), The Potential and Challenge of Remote Sensing-Based Biomass Estimation. International Journal of Remote Sensing. Vol. 27(7), 1297-1328.

Machiwa JF, Hallberg RO., (2002), An Empirical Model of the Fate of Organic Carbon in a Mangrove Forest Partly Affected by Anthropogenic Activity. Ecol Model 147:69-83. Doi:10.1016/S0304-3800(01)00407-0.

Manuri S., Putra CAS, Saputra AD., (2011), Teknik Pendugaan Cadangan Karbon Hutan. Merang REDD Pilot Project, German International Cooperation – GIZ. Palembang.

Mariana, Felix F., Sukendi, *et al.*, (2015), Estimation of Mangrove Forest's Carbon Stock in Kuala Indragiri Coastal Riau Province – Indonesia. International Journal of Oceans and Oceanography. 9(2), 117-126. ISSN 0973-2667.

Meideros TCC, Sampaio E., (2008), Allometry of Above Ground Biomasses in Mangrove Species in Itamaraca, Pernambuco, Brazil. Wetlands Ecology and Management 16 (4): 323-330.

Mitra A., Sengupta K., Banerjee K., (2011), Standing Biomass and Carbon Storage of Above-Ground Structures in Dominant Mangrove Tress in the Sundarbans. For Ecol Manag 261:1325-1335. doi:10.1016/j.foreco. 2011.01.012.

Mudiyarso D., Donato D., Kauffman JBD, *et al.*, (2009), Carbon Storage in Mangrove and Peatland Ecosystems – A Preliminary Account from Plots in Indonesia. No. CIFOR-Center for International Forestry Research (CIFOR), Bogor, Indonesia. Working paper 48.

Niklas KJ, (1995), Size-Dependent Allometry of Tree Height, diameter and trunk-taper. Ann. Bot. 75, 217–227.

Ong JE, Gong WK, Clough BF, (1995), Structure and Productivity of a 20-year-old Stand of Rhizopora Apiculata BI. Mangrove forest. Journal of Biogeography 22: 417-424.

Otero V., Quisthoudt K.. Koedam N., *et al.*, (2016), Mangroves at Their Limits: Detection and Area Estimation of Mangroves Along the Sahara Desert Coast. Remote Sensing. 8: 512; doi: 10.3390/rs8060512.

Parmeswari AASG, Hariyanto T., Sidik F., (2014), Analisis Indeks Vegetasi Mangrove Menggunakan Citra Satelit ALOS AVNIR-1 (Studi Kasus: Estuari Perancak, Bali). Geiod Vol. 11, No. 1 Agustus 2015.

Proisy C., Rahmania R., Viennois G., *et al.*, (2015), Monitoring Changes on Mangroves Coats using High Resolution Satellite Images. A Case Study in The Perancak Estuary, Bali. 12th Biennial Conference of Pan Ocean Remote Sensing Conference (PORSEC 2014). 04 - 07 November 2014. Bali - Indonesia.

Putz F., Chan HT, (1986), Tree Growth, Dynamics, and Productivity in a Mature Mangrove Forest in Malaysia. Forest Ecology and Management 17: 211-230.

Rahmania R., Proisy C., Viennois G., *et al.*, (2015), 13 Years of Changes in the Extent and Physiognomy of Mangroves After Shrimp Farming Abandonment, Bali. 2015 8th International Workshop on the Analysis Multitemporal Remote Sensing Images (Multi-Temporal). IEEE Explore. doi:10.1109/Multi-Temp.2015. 7245801.

Rodriguez W., Feller IC, (2004), Mangrove Landscape Characterization and Change in Twin Cays, Belize Using Aerial Photography and IKONOS Satellite Data. Atoll Research Bulletin. 513: 1-22.

Sahu SC, Kumar M., Ravindranath NH, (2016), Carbon Stocks in Natural and Planted Mangroves Forests of Mahanadi Mangrove Wetland, East Coast of India. Current Science, Vol. 110, No. 12, 25 June 2016.

Sapit D., Damrong S., Ladawan P., *et al.*, (2011), An Assessment of Stand Structure and Carbon Storage of a Mangrove Forest in Thailand. IUFRO World Ser 29:28-30.

Saputra GR, (2007), Model Penduga Potensi Hutan Rakyat Menggunakan Citra Aster dan Sistem Informasi Geografis di Beberapa Wilayah Kabupaten Bogor

Bagian Barat. (Skripsi). Bogor (ID): Departemen Manajemen Hutan Fakultas Kehutanan, IPB (Bogor Agricultural University), Bogor.

Sidik F., Widagti N., Kadarusman HP, *et al.*, (2015), Laporan Teknis Penelitian dan Pengambangan: Aplikasi Sistem Observasi Adaptasi Mangrove Terhadap Perubahan Iklim (Technical Report: Enhancement of Research for Adaption of Wetlands in Indonesia to Projected Impacts of Sea Level Rise). Balai Penelitian dan Observasi Laut. Pusat Pengkajian dan Perkeyasaan Teknologi Kelautan dan Perikanan. Badan Penelitian dan Pengembangan Kelautan dan Perikanan. Kementerian Kelautan dan Perikanan.

Sitoe AA, Mandlate LJC, Guedes BS, (2014), Biomass and Carbon Stocks of Sofala Bay Mangrove Forests. Forest. 5, 1967-1981; 10.3390/f5081967. ISSN 1999-4907.

Situmorang JP, Sugiatnto S., Darusman, (2016), Estimation of Carbon Stock Stands using EVI and NDVI Vegetation Index in Production Forest of Lembah Seulawah Sub-District, Aceh Indonesia. Aceh Int. Sci. Technol, 5(3):126-139. doi: 10.13170/aijst. 5.3.5836.

Sutaryo D., (2009), Perhitungan Biomassa, Sebuah Pengantar untuk Studi Karbon dan Perdagangan Karbon. Bogor (ID) : Wetlands International Indonesia Programme.

Vicharnakorn P., Shrestha RP, Nagai M., *et al.*, (2014), Carbon Stock Assessment using Remote Sensing and Forest Inventory Data in Savannakhet, Lao PDR. Remote Sensing. 6: 5452-5479. doi: 10.3390/ rs6065452.

Wang L., Sousa WP, Gong P., (2004), Integration of Object-Based and Pixel-Based Classification for Mapping Mangroves with IKONOS imagery. Int. J. Remote Sens. 25: 5655-5668.

Westlake DF, (1963), Comparison of Plant Productivity. Biological Reviews. 38(3): 385-425.

Wicaksono P., Danoedoro P., Hartono H., *et al.*, (2011), Preliminary Work of Mangrove Ecosystem Carbon Stock Mapping in Small Island using Remote Sensing: Above and Below Ground Carbon Stock Mapping on Medium Resolution Satellite Image. Proceedings of SPIE: Vol. 8174. Remote Sensing for Agriculture, Ecosystems, and Hydrology XIII. International Society for Optics and Photonics.

Yenni V., Parwati E., Winarso G., *et al.*, (2014), Assessment of Mangrove Forest Carbon Stock Monitoring of Indonesia using Remote Sensing Approach. SAFE Workshop. Tokyo. 1st December 2014.

DETECTING THE AREA DAMAGE DUE TO COAL MINING ACTIVITIES USING LANDSAT MULTITEMPORAL (Case Study: Kutai Kartanegara, East Kalimantan)

Suwarsono*, Nanik Suryo Haryani, Indah Prasasti, Hana Listi Fitriana
M. Priyatna, M. Rokhis Khomarudin
Remote Sensing Application Center
Indonesian National Institute of Aeronautics and Space (LAPAN)
*e-mail: suwarsono@lapan.go.id / landsono@yahoo.com
Received: 29 November 2017; Revised: 22 November 2017; Approved: 25 December 2017

Abstract. Coal is one of the most mining commodities to date, especially to supply both national and international energy needs. Coal mining activities that are not well managed will have an impact on the occurrence of environmental damage. This research tried to utilize the multitemporal Landsat data to analyze the land damage caused by coal mining activities. The research took place at several coal mine sites in East Kalimantan Province. The method developed in this research is the method of change detection. The study tried to know the land damage caused by mining activities using NDVI (Normalized Difference Vegetation Index), NDSI (Normalized Difference Soil Index), NDWI (Normalized Difference Water Index) and GEMI (Global Environment Monitoring Index) parameter based change detection method. The results showed that coal mine area along with the damage that occurred in it can be detected from multitemporal Landsat data using NDSI value-based change detection method. The area damage due to coal mining activities can be classified into high, moderate, and low classes based on the mean and standard deviation of NDSI changes (ΔNDSI). The results of this study are expected to be used to support government efforts and mining managers in post-mining land reclamation activities.

Keywords: *damage area, coal mining, landsat multitemporal*

1 INTRODUCTION

Mining activities cause serious impacts on ecosystems worldwide (Schroeter and Gläber 2011). The Government has a mandate to control pollution and environmental damage based on Indonesia Law Number 32 the Year 2009 on Environmental Protection and Management. According to the Law, environmental protection and management is a systematic and integrated effort undertaken to preserve environmental functions and prevent pollution and/or environmental damage including planning, utilization, control, maintenance, supervision and law enforcement.

One of the activities that have great potential to cause environmental pollution is mining activities. Mining activities have two opposite sides, namely as a carrier of the country's economic prosperity and as an environmental impact carrier that requires considerable energy, thought, and cost for its recovery process (Marganingrum and Noviardi 2010).

Coal is one of the most mining commodities to date, especially to supply both national and international energy

needs. Indonesia's coal production has shown a significant increase in production. Indonesia's coal production in 2009 reached about 254 million tons. About 94.4% of them are from Kalimantan, and 75% of the national coal production is exported to abroad (Ginting 2010).

Environmental problems arising from coal mines in Indonesia are, as is generally done by open pit mines, although there are some who use underground mining, it will have an impact on changes in the landscape, physical, chemical, and biological properties of the soil, and generally cause damage to the earth's surface. Thus, this condition will cause disruption to the ecosystem above it (Subardja 2007).

Based on the Act, one of the efforts to protect and manage the environment is to supervise activities that have the potential to cause environmental damage. Remote sensing data can be used to provide the informations about changes in surface water and land cover over time, which is essential for environmental monitoring in mining areas. Remote sensing data are also ideal for environmental impact assessment due to their broad spectral range, affordable cost, and rapid coverage of large areas. Remote sensing data enables the identification, delineating, and monitoring of pollution sources and affected areas, including derelict land, and changes in surface land use and to water bodies (Charou *et al.* 2010). Remote sensing allows for cost- and time-efficient monitoring of landscapes vital to the conservation of natural resources, ecosystems, and biodiversity (Willis 2015). Taking into account the advantages possessed by the use of remote sensing data, the authors are interested to use remote sensing methods to monitor the environmental damage caused by mining activities in Indonesia.

Landsat data is the optical data that historically has the best recording among other data. The existence of this data has been available since Landsat 1 was launched in 1972. Until now, it has been pretty well available Landsat data archive to the latest recording by Landsat 8 the satellite launched since 2013. The results of research at several locations abroad have shown the result that Landsat data is very useful to be used to monitor the impacts of coal mining (Schroeter and Gläber 2011), (Erener 2011) (Chitade and Katyar 2010). In Kütahya Turkey, multi-temporal Landsat TM data sets were used to assist in identifying and monitoring the progress in the rehabilitation field and the evaluation was based on analyzing varying vegetation indices (Erener 2011).

This research tries to raise the topic of utilization of multitemporal Landsat data to know the damaged area caused by coal mining activity in Indonesia region. Research on this topic is rarely done by taking a location in Indonesia.

2 MATERIALS AND METHODOLOGY

2.1 Location and Data

The research took place at several coal mine sites in Kutai Kartanegara, East Kalimantan Province (Figure 1-1). In more detail, these locations can be seen in Figure 3-1. The image data used is a pair of multitemporal Landsat data, namely Landsat 7 path/row 116/060 recording date of May 15, 2000, and Landsat 8 recording dated February 7, 2014.

2.2 Standardization of data

Landsat 8 data were obtained from Remote Sensing Technology and Data Center of Indonesian National Institute of Aeronautics and Space (LAPAN) through

website http://landsat-catalog.lapan.go.id/. The data format is GeoTIFF. Level of Landsat 8 is level one terrain-corrected product (L1T). L1T available to users is a radiometrically and geometrically corrected image. The image is also radiometrically corrected to remove relative detector differences, dark current bias, and some artifacts. The level one image is presented in units of Digital Numbers (DNs) which can be easily rescaled to spectral radiance or top of atmosphere (TOA) reflectance (USGS 2015).

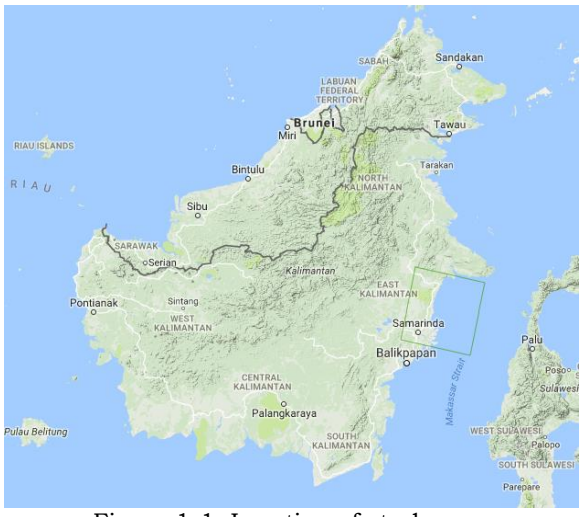

Figure 1-1: Location of study area
(source: http://landsat-catalog.lapan.go.id/)

2.3 Methods

The method developed in this research is the method of change detection. By doing a review of many studies, in the context of ecological monitoring, Willis (2015) suggested that change detection has historically been used to look at changes in land use/land cover and disturbance using binary comparisons contrasting conditions during two discrete time periods. In assessing changes in environmental changes, NDVI is a commonly used indicator, especially for monitoring plant phenology changes. The study tried to know the land damage caused by mining activities using NDVI parameter based change detection method. Besides NDVI, this study also extracts other indices such as NDSI, NDWI, and GEMI which will be used for mine area damage analysis.

Processing steps, interpretation, and analysis of data covering three main stages (Figure 2-1), namely:

a. Radiometric correction. The radiometric correction involves converting the DN data into a TOA reflectance both Landsat 7 (USGS 1998) and Landsat 8 (USGS 2015). The atmospheric correction is done by the DOS (Dark Object Subtraction) model (Chavez 1988; 1988; Chavez 1989),
b. Preparation of the Landsat 7 image dataset (bands 2, 3, 4, 5, and 7) and Landsat 8 (bands 3, 4, 5, 6, and 7),
c. Extraction of NDVI, NDSI, NDWI, and GEMI values,
d. Preparation of Landsat 7 RGB-543 color composite image and Landsat 8 RGB-654. Then followed by contrast enhancement and spatial filtering (using high pass filter),
e. Interpretation of mining areas. Done by comparing Landsat 7 image (2000) with Landsat 8 image (2014). The mining area is identified from the image based on the visual visibility changes of Landsat 7 image 2000 and Landsat 8 in 2014, especially the colors, shapes, patterns, and associations,
f. Analysis of mine area damage is done by: sampling, calculation of pixel value statistics, determination of the most sensitive parameters for damage detection, the threshold determination, and classification of the damage level.

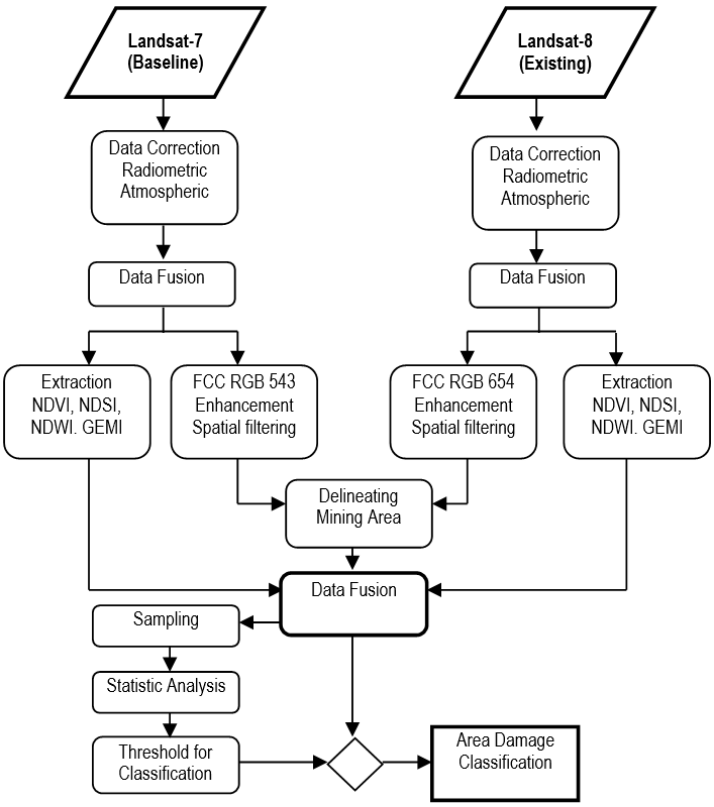

Figure 2-1: Flowchart of processing, interpretation and data analysis

NDVI, NDWI, NDSI, and GEMI values can be derived from Landsat 8 images using the following formula:

a. NDVI is derived from band 4 (Red) and 5 (NIR). The formula was modified from Rouse , *et al* (1974):

$$NDVI = \frac{\rho 5 - \rho 4}{\rho 5 + \rho 4} \quad (2\text{-}1)$$

b. NDSI is derived from band 4 (Red) and 7 (SWIR). The formula was modified from Rogers and Kearney (2004):

$$NDSI = \frac{\rho 7 - \rho 4}{\rho 7 + \rho 4} \quad (2\text{-}2)$$

c. NDWI is derived from band 3 (Green) and 5 (NIR). The formula was modified from McFeeters (1996):

$$NDWI = \frac{\rho 3 - \rho 5}{\rho 3 + \rho 5} \quad (2\text{-}3)$$

d. GEMI is derived from band 4 (Red) and 5 (NIR). The formula was modified from Pinty and Verstraete (1992):

$$GEMI = \delta(1 - 0.25\delta) - \frac{(\rho RED - 0.125)}{(1 - \rho RED)} \quad (2\text{-}4)$$

$$\delta = \frac{2(\rho NIR^2 - \rho RED^2) + 1.5\rho NIR + 0.5\rho RED}{(\rho NIR + \rho RED + 0.5)}$$

Normalized distances (D-values) were calculated to measure and to test the discrimination ability of the index (Kaufman and Remer 1994). In this research, the D-values > 1 will represent good separability of the index to discriminate the changes of pre-mining and during or post-mining.

$$D = \left| \frac{\mu 2 - \mu 1}{\sigma 2 + \sigma 1} \right| \quad (2\text{-}5)$$

where D is Normalized Distance (Kaufman and Remer 1994), μ1 and μ2 are mean values of samples pre-mining and

during/post-mining respectively, σ1 and σ2 are the standard deviation of samples pre-mining and during/post-mining respectively. The calculation resulted D-values for all indices which are NDVI, NDSI, NDWI and GEMI.

3 RESULTS AND DISCUSSION

3.1 Identifying the Mining Area

The mining area is identified from the image based on the visual visibility changes of Landsat 7 image 2000 and Landsat 8 in 2014. In general, the mining area can be identified from Landsat 7 (the Year 2000) and Landsat 8 (in 2014). There is a change of color from greenness to redness. In the image of 2000, generally, still greenish color, while in the image of 2014, has undergone many changes, which turned into redness. In the mining area, around red pixels, there are found the dark blue pixels. These pixels are the body of water that was stored. In the Landsat 8 image, the coal outcrop appears to be reddish in color, since this object is dominant to have a high reflectance for the SWIR (Short Wave Infra Red) wavelength. In this composite image, the vegetation is greenish because this object is dominant to have high reflectance for the NIR wavelength. While the object of water for this composite image tends to be blackish black because this dominant object has a high reflectance for the wavelength of Visible (Red) (Figure 3-1).

3.2 Extracting and analyzing the index NDVI, NDSI, NDWI, and GEMI

The results of sampling and statistical measurements, obtained a list of NDVI, NDSI, NDWI and GEMI values at the time pre-mining, while still being mined/post-mining, as presented in Table 3-1, Table 3-2, Table 3-3, and Figure 3-2.

Taking into account the formulas for generating NDVI, NDWI, NDSI, and GEMI, it is known that, respectively, NDVI, NDSI, and NDWI data would be most appropriate for analyzing vegetation objects, open land (coal and soil outcrops), and water. While GEMI data will tend to be similar to NDVI, which is to analyze vegetation objects.

The results of the measurement show that in general, mining activities cause a decrease in the value of NDVI and GEMI. Otherwise for NDSI and NDWI increased.

Based on the results of the measurement of separability, it can be seen that basically NDVI, NDSI, and GEMI have values above 1 and can be used as parameters to measure the extent of damage to mine land. However, since the NDSI value has the highest value, then further to classify the level of mine land damage is used NDSI parameters. Why NDSI has the greatest separability value, this is probably because NDSI is more sensitive to open land objects (coal and soil) than other indices.

By using the assumption of the normal distribution of the value of the increase of NDSI, it can be the classified the estimation of damage level of mining area with criteria based on the mean and standard deviation of NDSI changes (ΔNDSI) as follows:

- High, if $\Delta NDSI_{ij} \geq m\Delta NDSI + 1St.Dev$
- Moderate, if $m\Delta NDSI - 1St.Dev \leq \Delta NDSI_{ij} < m\Delta NDSI + 1St.Dev$
- Low, if $\Delta NDSI_{ij} \leq m\Delta NDSI - 1St.Dev$

Where ΔNDSI is $NDSI_{ij}$ changes of a given pixel, mΔNDSI and St.Dev are the mean and standard deviation of NDSI changes respectively.

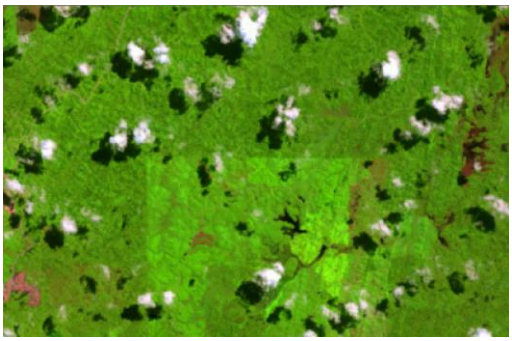

Landsat 7 image RGB 543
15 May 2000

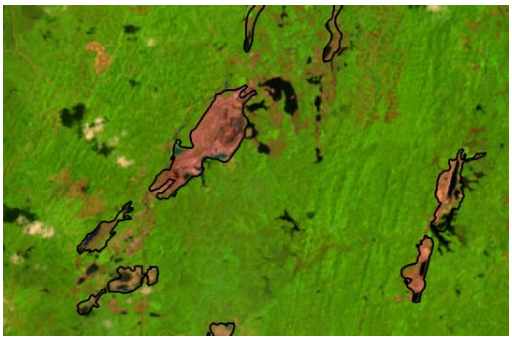

Landsat 8 image RGB 654
7 February 2014

Figure 3-1: The results of the mining area identification of Landsat 7 image RGB 543 on 15 May 2000 and Landsat 8 RGB 654 on 7 February 2014. dark polyline shows the boundaries of the mining area

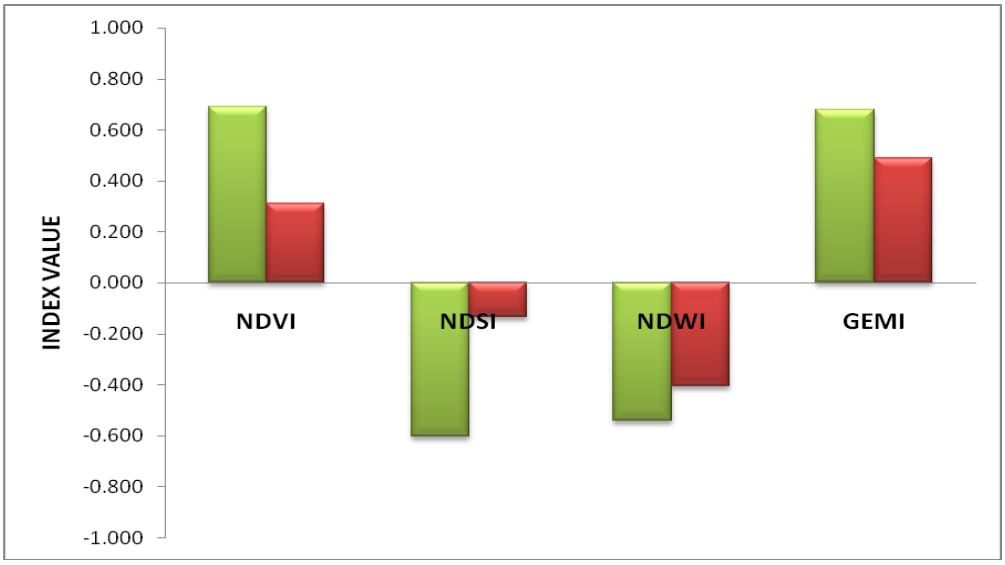

Figure 3-2: Graph of average change of index value, from baseline (green) and existing (red)

Tabel 3-1: Index value at baseline condition, existing and change with sample location of mining areas in East Kalimantan Province

	BASELINE				EXISTING			
INDEX	**NDVI**	**NDSI**	**NDWI**	**GEMI**	**NDVI**	**NDSI**	**NDWI**	**GEMI**
Mean	0.691	-0.602	-0.541	0.678	0.311	-0.136	-0.406	0.488
St.Dev	0.045	0.043	0.032	0.042	0.212	0.199	0.170	0.114

Tabel 3-2: Index value at baseline condition, existing and change with sample location of mining areas in East Kalimantan Province

CHANGES				
INDEX	**NDVI**	**NDSI**	**NDWI**	**GEMI**
Mean	-0.380	0.467	0.135	-0.191
St.Dev.	0.216	0.201	0.174	0.120

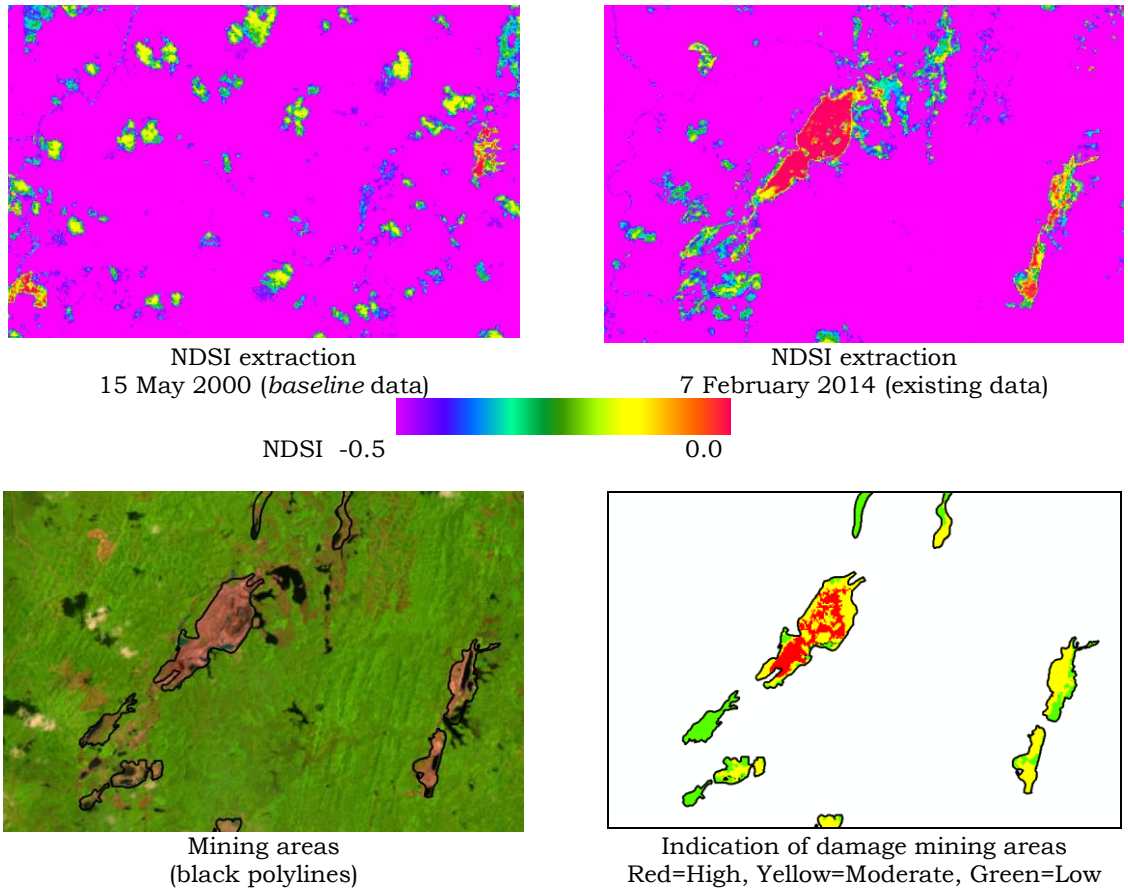

Figure 3-3: Image analysis for mining area identification and indication of damaged area. (location: Kutai Kartanegara)

Tabel 3-3: Separability (D-values) of several indices (NDVI, NDSI, NDWI, and GEMI)

NDVI	NDSI	NDWI	GEMI
-1.477	1.931	0.666	-1.221

Based on above criteria, the indication of mining damage areas in the study area are determined i.e, High if ΔNDSI ≥ 0.668, Medium if 0.266 ≤ ΔNDSI <0.668 and Low if ΔNDSI <0.266. Figure 3-3 shows the result image analysis for the indication of damaged areas in the study area based on ΔNDSI.

The use of NDSI value to know the indication of land damage due to mining activities is based on the understanding that the occurrence of land conversion from vegetation opened to coal excavation will decrease the NIR reflectance and increase SWIR reflectance.

The main weakness in this research is the limitation of spatial resolution of Landsat multitemporal image, which is 30 meters. So the resulting information is not so detailed. With this resolution, Landsat data will only be able to be used to analyze relatively large and extensive mine land. For more detailed analysis or smaller mining areas, a higher resolution image is required, such as SPOT 5, SPOT 6 or SPOT 7. This weakness will be an input for further research.

4 CONCLUSIONS

The results showed that coal mine area along with the damage that occurred in it can be detected from multitemporal Landsat data using NDSI value-based change detection method. The area

damage due to coal mining activities can be classified into high, moderate, and low classes based on the mean and standard deviation of NDSI changes (ΔNDSI). The results of this study are expected to be used to support government efforts and mining managers in the post-mining land reclamation activities.

ACKNOWLEDGEMENT

The paper is part of the research results of "Development of Remote Sensing Data Utilization Model for the Environment" at Remote Sensing Application Center of LAPAN in 2017. The Research is a follow up of the results of "Satellite Image Analysis and Establishing the Spatial-based of Damage Criteria" project, a cooperation activity between Remote Sensing Application Center of LAPAN, Aerospace Technology Application Center of LAPAN and Directorate of Open Access Recovery of Ministry of Environment and Forestry in 2016. Thank Director of Aerospace Technology Application Center of LAPAN and Director of Open Access Recovery of Ministry of Environment and Forestry. Thank also Drs. Taufik Maulana, MBA who has given useful advices and suggestions in this research.

REFERENCES

Charou E., Stefouli M., Dimitrakopoulos D., *et al.*, (2010), Using Remote Sensing to Assess Impact of Mining Activities on Land and Water Resources. *Mine Water Environ* 29:45–52.

Chavez Jr. PS, (1988), An Improved Dark-Object Subtraction Technique for Atmospheric Scattering Correction of Multispectral Data. *Remote Sensing of Environment* 24:459–79.

Chavez Jr. PS, (1989), Radiometric Calibration of Landsat Thematic Mapper Mutispectral Images. *Photogrammetric Engineering and Remote Sensing* 55(9):1285-1294.

Chitade AZ, Katyar SK, (2010), Impact Analysis of Open Cast Coal Mines on Land Use/Land Cover using Remote Sensing and GIS Technique: A Case Study. International Journal of Engineering Science and Technology 2(12):7171–76.

Erener A., (2011), Remote Sensing of Vegetation Health for Reclaimed Areas of Seyitömer Open Cast Coal Mine. *International Journal of Coal Geology* 86:20–26.

Ginting D., (2010), Makalah Ilmiah. Buletin Sumber Daya Geologi 5(1).

Kaufman YJ, Remer LA, (1994), Detection of Forests using Mid-IR Reflectance: An Application for Aerosol Studies. IEEE 32(3):1994.

Marganingrum D., Noviardi R., (2010), Pencemaran Air Dan Tanah di Kawasan Pertambangan Batubara di PT. Berau Coal, Kalimantan Timur. *Riset Geologi dan Pertambangan* 20(1):11–20.

McFeeters SK, (1996), The Use of the Normalized Difference Water Index (NDWI) in the Delineation of Open Water Features. International Journal of Remote Sensing17(7):1425–1432.

Pinty B., Verstraete MM, (1992), GEMI: A Non-Linear Index to Monitor Global Vegetation from Satellites. Vegetatio 101:15–20.

Rogers AS, Kearney M., (2004), Reducing Signature Variability in Un-Mixing Coastal Marsh Thematic Mapper Scenes using Spectral Indices. International Journal of Remote Sensing 25:2317–2335.

Rouse JW, Haas RW, Schell JA, *et al.*, (1974), Monitoring the Vernal Advancement and Retrogradation (Greenwave effect) of natural vegetation. Greenbelt, MD. USA: NASA/GSFC.

Schroeter L., Gläber C., (2011), Analyses and Monitoring of Lignite Mining Lakes in Eastern Germany with Spectral Signatures of Landsat TM Satellite Data. International Journal of Coal Geology 86:27–39.

Subardja A., (2007), *Pemulihan Kualitas Lingkungan Penambangan Batubara: Karakterisasi dan Pengendalian Air Asam Tambang di Berau*. Laporan Teknis, Puslit Geoteknologi LIPI TA 2007.

USGS, (1998), Landsat 7 Science Data Users Handbook. Sioux Falls, South Dakota.

USGS, (2015), Landsat 8 (L8) Data Users Handbook. version 1. Sioux Falls, South Dakota.

Willis KS, (2015), Remote Sensing Change Detection for Ecological Monitoring in United States Protected Areas. *Biological Conservation* 182:233–42.

MACHINE LEARNING-BASED MANGROVE LAND CLASSIFICATION ON WORLDVIEW-2 SATELLITE IMAGE IN NUSA LEMBONGAN ISLAND

Aulia Ilham[1]* and Marza Ihsan Marzuki[2]

[1]Program Studi Oseanografi, Fakultas Ilmu dan Teknologi Kebumian, Institut Teknologi Bandung, Jl. Ganesha No. 10, Bandung 40132, Indonesia.

[2]Badan Riset dan Sumber Daya Manusia, Kementerian Kelautan dan Perikanan, Jl. Pasir Putih 1, AncolTimur, Jakarta 14430, Indonesia.

*e-mail: aulia.ilham27@gmail.com

Received: 7 November 2017; Revised: 25 November 2017; Approved: 26 December 2017

Abstract. Machine learning is an empirical approach for regressions, clustering and/or classifying (supervised or unsupervised) on a non-linear system. This method is mainly used to analyze a complex system for wide data observation. In remote sensing, machine learning method could be used for image data classification with software tools independence. This research aims to classify the distribution, type, and area of mangroves using Akaike Information Criterion approach for case study in Nusa Lembongan Island. This study is important because mangrove forests have an important role ecologically, economically, and socially. For example is as a green belt for protection of coastline from storm and tsunami wave. Using satellite images Worldview-2 with data resolution of 0.46 meters, this method could identify automatically land class, sea class/water, and mangroves class. Three types of mangrove have been identified namely: *Rhizophora apiculata*, *Sonnetaria alba*, and other mangrove species. The result showed that the accuracy of classification was about 68.32%.

Keywords: *clustering, machine learning, remote sensing data*

1 INTRODUCTION

Remote sensing system consists of data collection (image) by the sensor, followed by the initial processing of image, analysis and extraction of information to produce thematic maps that will be further utilized by the user for various purposes (Wicaksono 2009). In General, remote sensing systems can be distinguished by the energy source used, the recording mode, the wavelength spectrum region, and the type of platform that is used as the basis of sensor placement. One of the remote sensing utilization is for multi-temporal analysis of mangrove area, which effective to monitor changes in the condition of mangrove forests (Suk-ueng *et al.* 2017).

Machine Learning is an empirical approach to regression or classification (supervised or unsupervised) on a nonlinear system (David *et al.* 2015) and excellent for processing large amounts of data. Machine Learning began to be developed since the 1950s, where in the early stages only conducted by a simple algorithm. According to Rhee (2016), machine learning method has a better advantage than the interpolation method for classification and regression. Machine learning approach (statistical approach) is so prominent in analyzing a complex system that has wide observations (Ashkezari 2016).

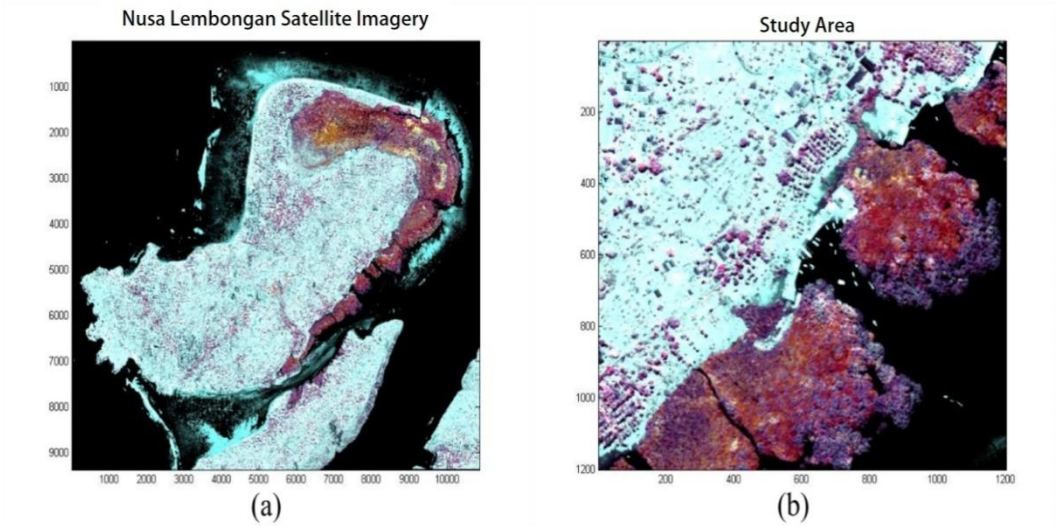

Figure 2-1: Worldview-2 satellite imagery. (a) Nusa Lembongan Island, and (b) The study area

To perform the data processing from unsupervised to be supervised can be done using algorithm of Akaike Information Criterion (AIC). The AIC model is the best choice for doing linear data processing (Bracher *et al.* 2015). AIC is used to perform processing with statistical approaches on large data. Hosseini *et al.* (2015) said this AIC can be used to achieve high predictive power from statistical models, which requires a substantial set of training and spatial data.

Mangrove forests in Nusa Penida sub-district are mostly concentrated on the northern side of Nusa Lembongan. The existence of mangroves along the coast of an island has an important role as a green belt or a protector against tsunami waves or hurricanes (Nuryani 2011). To manage mangrove areas in Nusa Lembongan and Nusa Ceningan effectively, basic information on the extent of mangrove forests, mangrove species that grow in the area, and fauna that live in the mangroves are necessary (Marthen *et al.* 2010).

This study aims to classify the determination of the distribution, type and extent of the mangrove area using the AIC approach on the satellite image data Worldview-2 in the Nusa Lembongan Island area. The assumption used is the study area is that selected sample location could represent the total area extent. The AIC approach is used as a reference to determine the number of existing classes resulted by unsupervised clasification as new features, followed by supervised classification with the Gaussian Mixture Model (GMM) approach. The level of accuracy is analyzed using Cohen's calculation Kappa.

2 MATERIALS AND METHODOLOGY

This research used satellite imagery data Worldview-2 of 2013 over Nusa Lembongan Island, Bali. The research sites include Nusa Lembongan Island and part of Nusa Ceningan Island as shown in Figure 2-1.a. The area of interest in this study is an area of study that can represent mangrove, terrestrial, and ocean vegetation as shown in Figure 2-1.b.

Satellite imagery Worldview-2 itself is usually used to perform spatial analysis as mapping, land use, and some needs requiring spectral data. This satellite is equipped with a high-resolution sensor that is 0.46 meters and 8 multispectral bands (Figure 2-2) which are capable to acquire image data in wide coverage

of 1 million km^2 in a day.

The research method is to classify the land cover types using high resolution image data. This land classification can distinguish between land, sea, and mangrove. The mangrove land itself can later be differentiated by type and compared with previous studies that processed the same data with GIS method. An example of mangrove classification using GIS method obtained by Gaëlle *et al.* (2013) is shown in Figure 2-3.

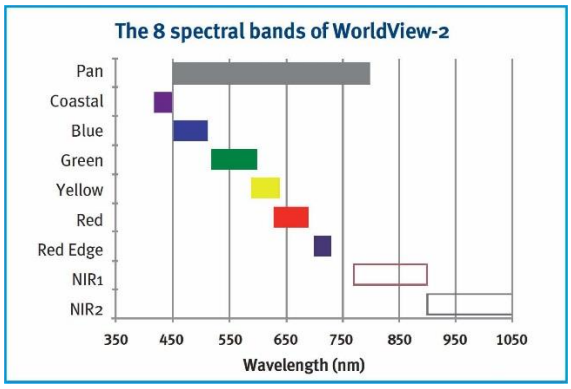

Figure 2-2: Wavelength for each bands (source: satimagingcorp.com)

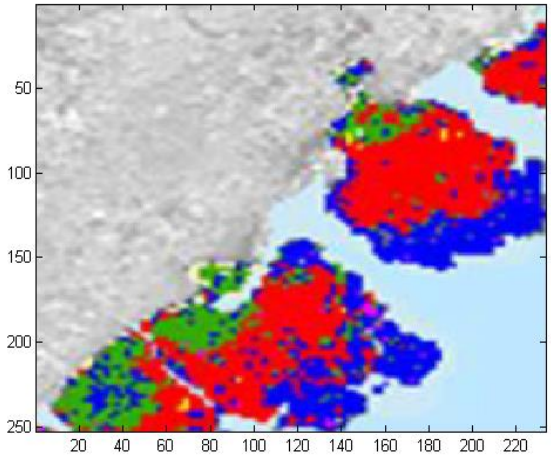

Figure 2-3: Mangrove classification using GIS method (Source: Gaëlle *et al.* 2013)

The data validation used the results of previous research conducted by Gaëlle *et al.* (2015), which also did the mangrove land classification in Nusa Lembongan Island using GIS method. In the area of interest, Figure 2-3, which corresponds to the current research site, the previous study revealed that there were 3 dominant mangrove species, namely: *Sonneratia alba* (blue), *Rhizophora apiculata* (red), and other types of mangroves (green). And there are also land and water/sea that have not been taken into account into the classification. Previous studies have classified mangrove land using the Worldview-2 satellite image data by matching field data results, so the results can be more accurate.

In this research, image data is processed by statistical learning approach that we developed using MATLAB software. The method used is with the AIC to determine the number of clusters of the image data. By having a collection of statistical data, AIC can help to determine the best quality model for certain data without guidance. According to Parviainen *et al.* (2013), AIC works by examining the sampled or whole data repeatedly to determine the parameters (clusters) in order to obtain the best results for the whole data. The AIC formulation used in this study is as shown in formula (1).

$$AIC = -2 \log[\pounds(\theta \mid y) + 2k] \qquad (2\text{-}1)$$

Then we used the GMM approach to conduct a supervised classification with the number of classes according to the calculation results from AIC. GMM is a probabilistic model to represent the existence of a parameter against the parameters as a whole, without using the data set previously calculated by the AIC. The function of this approach is used to calculate the probability of each data in each cluster which will then be grouped by the largest probability value.

3 RESULTS AND DISCUSSION

Data processing conducted by AIC approach has resulted 14 clusters. The cluster number is derived from the

process of calculating the parameter determination, which value is generated from the data input processed is taken from the smallest value among the input numbers.

After clustering, then the data is merged according to the existing class in the reference for the same result, from the 14 clusters, there are 2 clusters 2 and 6 which cannot represent any classification because of the number of pixels and unspecified spatial depiction. In Table 3-1 it is seen that clusters 1 and 3 go into class 1 i.e Mangrove Other Types.

Then clusters 4 and 5 go into *Sonneratia alba* (SA) class, as well as clusters 7,8,10, and 12 belong to the *Rhizophora apiculata* (RA) class. In addition to be distinguished from the types of mangrove, the subsequent classes are differentiated to land and water/sea each consisting of clusters 9 and 11. While there are several clusters that are classified into other classes because they do not represent any class of clusters 2 and 6. Thus, clustering obtained from AIC can be considered to function as a new feature that can help ease the process of classification to be performed by GMM rather than its original feature, the spectral values of 8 bands of Worldview-2 image.

The incorporation of these clusters is carried out using supervised classification by utilizing spatial depictions that can represent classes in validation data.

3.1 Mangrove Land Classification

From unstructured land classification process based on calculation of AIC over study area, we obtained 14 clusters of mangrove land covers as shown in Figure 3-1.

Table 3-1: Distribution of clusters in each class

Cluster	*Class (pixel)*					
(pixel)	*OM*	*SA*	*RA*	*Water/Ocean*	*Land*	*Other*
1	13067					
2						4119
3	27775					
4		10160				
5		19498				
6						14719
7			131330			
8			52582			
9				65768		
10			38628			
11					27337	
12			42258			
13		39837				
14		76923				

In Figure 3-1, there are 14 clusters of classification without AIC supervised and GMM supervised classification. The details of each class are shown in Table 3-2. Among all clusters, there is 1 green cluster representing the water class, 1 orange cluster representing the land class, and 10 other color clusters representing the mangrove class. While cluster 1 (dark blue) and cluster 14 (dark red) do not represent the five classes, so these two clusters could be ignored and we used only 12 clusters for further analysis.

By combining several clusters it could produce the same pattern with reference results. The number of generated classes is divided into 5 land cover types, namely *Sonneratia alba*, *Rizhopora apicullata*, other types of mangrove, land, and water/sea, as shown in Figure 3-2.

In the area of interest it can be seen that mangrove land is presented by green, light blue, and dark blue color. While the yellow and orange color represent water/sea and land with the largest percentage of area is 26% and 33% of the total area respectively. The extent of mangrove distinguished by type has an area of OM 3.5%, SA 17%, and RA 20.5%. Comparing with the reference, the results obtained by this research are not fully similar because we used statistical approach in the calculation process. So that some points can be read as mangrove by the system and the resulting image is purely based on the value of each pixel that has not done smoothing process data. To see the relationship between the two methods, then calculate the accuracy value of AIC-GMM method to reference.

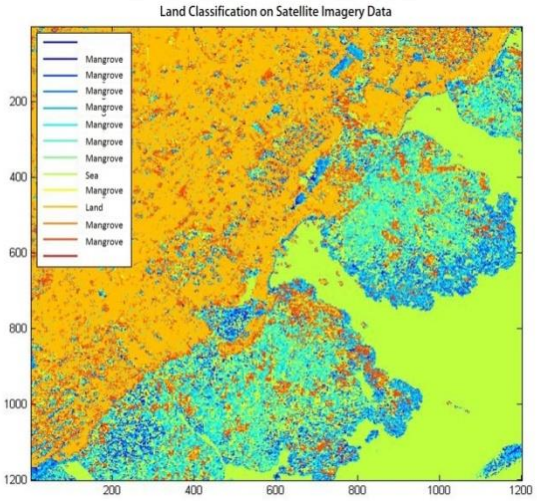

Figure 3-1: Supervised Field Classification Results Used AIC with 14 Clusters

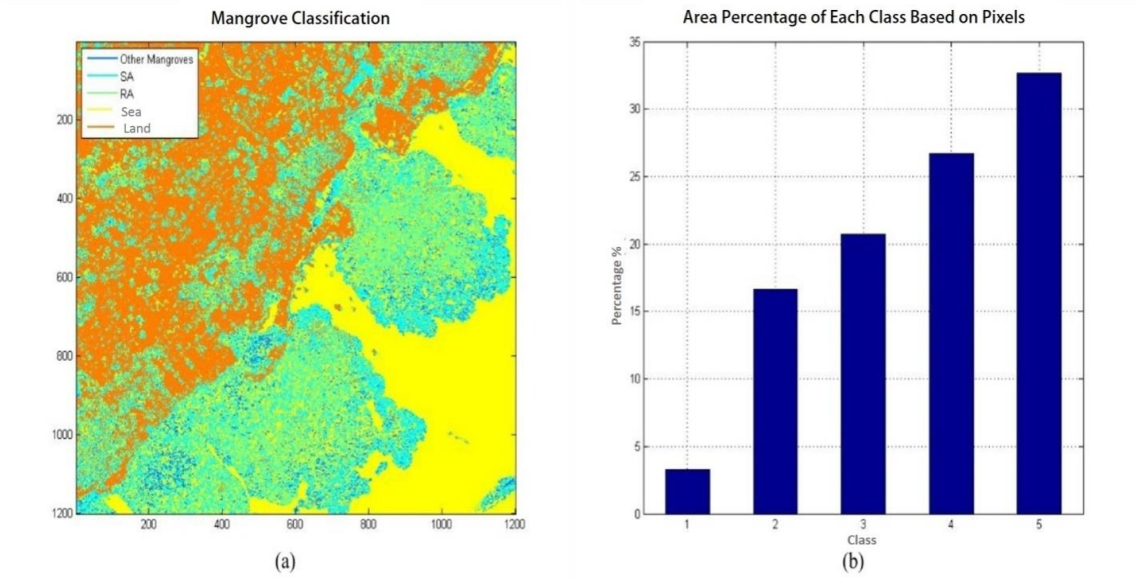

Figure 3-2: Results of land classification by type of mangrove. (a) types of mangroves, and (b) percentage of each class

Table 3-2: Accuracy table from Cohen's Kappa coefficient calculation

Classification	*1*	*2*	*3*	*4*	*5*	*Total*
OM	**14125**	26275	31600	7800	15200	95000
SA	4800	**88600**	28900	30150	1550	154000
RA	4450	33950	**178825**	21325	1700	240250
Water/Sea	1825	14875	7725	**228875**	4200	257500
Land	9625	75712.5	90787.5	12775	**501750**	690650
Total	34825	239412.5	337837.5	300925	524400	**1437400**
Agreement	14125	88600	178825	228875	501750	1012175
By Chance	2301.6384	15823.144	22328.205	19888.601	34658.411	95000
Kappa	**0.6832353**					

Accuracy of the results can be calculated using Cohen's Kappa Coefficient method by considering all factors contained in each classification column. The calculation results can be seen in Table 3-2. The calculation is done to analyze the influence of AIC-GMM calculation with comparison in previous study using field data validation.

The accuracy resulted by Cohen's Kappa coefficient calculation is of 68.32% comparing with the reference result. The accuracy result is good enough for the AIC-GMM method that applies supervised/unsupervised classification simply by using pixel values as statistical data. There is a difference in the calculation process of each component, as we found in other types of mangrove classes having pixel values which were quite different from the appropriate classes. This may cause decreasing percentage of the accuracy.

3.2 Discussion

In this study we used the AIC method to determine the number of clusters from satellite imagery over the study area that were accounted as the new features in the further supervised and unsupervised classification processes. After obtaining the number of classes from the satellite image, then the selection of each pixel value to be classified into the appropriate class. GMM method has been successfully used to handle limited test data across multiple applications, including in remote sensing (Davari 2017). The method used a statistical learning approach for clustering. The output of the process is shown in the processed image that has been classified according to their respective classes.

AIC is used as a link between unsupervised and supervised processing. AIC is functioned to generate of new features to replace the original features. The new feature will be used in classification using GMM. Determination of the cluster number of spatial data is quite difficult to do. So this could be done by the statistical approach using AIC. The processing result is then used as the reference for the grouping of each data against the existing cluster. According to Liu, the advantage of using a combination

between unsupervised and supervised is that the user can determine the parameters or the number of clusters that exist on the data quickly and minimize errors.

The AIC method could provide good result to classify mangrove over imagery data, both on large and small scales. For high resolution image data (Worldview-2 of 0.46 m resolution), the processing results showed almost the same density but different cluster readings. This is because in high resolution data, resulted image will be very detailed and the reading of values in each region will greatly affect the reflectance of the sensor. Image data classification is done for each pixel value, so the results of some pixels could differ from the result of other method. To obtain maximum results, it is necessary to conduct data smoothing into the results obtained, so the later results could be classified more clearly.

In this study, for validation we used is the data resulted by the previous works using GIS method. In the same study area, the results show similarity, so it can be said that the results obtained from processing using machine learning can be received well.

In the reference results, there are 3 mangrove types outside the study area, namely: *Rhizophora apiculata* (red), *Sonneratia alba* (blue), and other mangroves (green). The same result was also shown if we used the AIC method. The result of GIS method had better density when compared with machine learning method. This is because at the end process could smoothen the data so the areas could be distinguished clearly. The basic difference of both methods is on data processing. The AIC method is not limited by the tools provided by the processing software in conducting the classification, because the statistical approach is based on each pixel value. The model we applied in this research is the best choice for the data we used. Meanwhile, image data processing using other methods is usually limited by the tools of data processing software.

Using Cohen's Kappa we obtained the accuracy by considering the other components beside the main ones. This will produce different numbers if it is done with confusion matrix only. The advantage of image data processing method in this research is that we can identify spatial data without determining the parameters manually. The process can be conducted automatically using the GMM model. This method is also able to process large data with fast and efficient computing capabilities, which makes it suitable for processing high resolution satellite imagery. While the constraints are on the initial classification which is based on pixel spectral value, so the processing is not as good as GIS. In some cases, the AIC method still cannot distinguish water classes of sea water, pond water, or pond water, because the pixel values are similar. In addition, the texture variables is expected to provide a solution to solve the problem in water classification. This method could also perform big data processing which requires adequate device.

4 CONCLUSION

Based on the merger of several clusters from the AIC calculation, we obtained another type of mangrove classes consisting of clusters 1 and cluster 3; *Sonneratia alba* class consists of clusters 4,5, and 13; the *Rhizophora apiculata* class consists of clusters 7, 8, 10, and 12; while the water/sea and terrestrial classes consist of clusters 9 and 11 respectively. There were also two clusters that could not be identified because they did not represent any classes in clusters 2 and 6. Using the Akaike Information Criterion

method, we obtained data accuracy calculations with Cohen's Kappa Coefficient which is equal to 68.32%. Akaike Information Criterion is one step ahead in image data processing, which is from unsupervised into supervised classification.

For better results in future research using AIC for supervised and unsupervised classification process, it is necessary to perform repetitive testing of the data samples. This testing is necessary, so that resulted parameters can be tested based on the actual data.

ACKNOWLEDGEMENT

Thanks to the Indeso Project which has provided the image of the Worldview-2 satellite and the Research and Human Resources Agency, the Ministry of Marine Affairs and Fisheries which supported this research, as well as the relevant parties contributing to the research implementation.

REFERENCES

Ashkezari MD, Hill CN, Follett CN, (2016), Oceanic Eddy Detection and Life Time for Ecast using Machine Learning Methods. Department of Earth, Atmospheric and Planetary Sciences, Massachusetts Institute of Technology.

Bracher A., Taylor MH, Taylor B., *et al.*, (2015). Using Empirical Orthogonal Functions Derived from Remote-Sensing Reflectance for the Prediction of Phytoplankton Pigment Concentrations. Ocean Science, Germany.

Davari AA, Christlein V., Vesal S., *et al.*, (2017), GMM Supervectors for Limited Training Datain Hyperspectral Remote Sensing Image Classication. Friedrich-Alexander-University Erlangen-Nuremberg, Erlangen, Germany.

Hosseini R., Newlands NK, Dean CB, *et al.*, (2015), Statistical Modeling of Soil Moisture, Integrating Satellite Remote-Sensing (SAR) and Ground-Based Data. Remote Sensing Journal.

Lary DJ, Alavi AH, Gandomi AH, *et al.*, (2015), Machine Learningin Geosciences and Remote Sensing. University of Texas.

Liu X., (2005), Supervised Classification and Unsupervised Classification, ATS 670 Class Project.

Parviainen M., Zimmermann NE, Heikkinen RK, *et al.*, (2013), Using Unclassified Continuous Remote Sensing Data to Improve Distribution Models of Red-Listed Plant Species. Biodivers Conserv.

Rhee J., Im J., Park S., (2016), Drought Forecasting Based on Machine Learning of Remote Sensing and Long-range Forecast Data, APEC Climate Center, Republic of Korea.

Suk-ueng K., Buranaprattheprat A., Gunbua V., *et al.*, (2017), Applicationof Remote Sensing Technique for Mangrove Mapping at the Welu Estuary, Thailand. Chiangrai Rajabhat University.

Viennois G., Proisy C., Feret JB, *et al.*, (2015), Multitemporal Analysis of High-Spatial-Resolution Optical Satellite Imagery for Mangrove Species Mappingin Bali, Indonesia. France.

Welly M., Sanjaya W., (2010), Identifikasi Flora dan Fauna Mangrove Nusa Lembongan dan Nusa Ceningan. Coral Triangle Center.

Wicaksono P., Danoedoro P., Hartono, *et al.*, (2015), Mangrove Biomass Carbon Stock Mapping of the Karimun Jawa Islands using Multispectral Remote Sensing. ITT.

Widagti N., Triyulianti I., Manessa MDM, (2011), Changesin Density of Mangrove Forestin Nusa Lembongan, Bali. Institute for Marine Research and Observation.

AUTHORS INDEX

KEYWORDS INDEX

INTERNATIONAL JOURNAL OF REMOTE SENSING AND EARTH SCIENCES

Instruction for Authors

Scope

International Journal of Remote Sensing and Earth Sciences (IJReSES) publishes research results on remote sensing and earth sciences, with special interest in Asian region.

Manuscript Submission

Manuscripts submission to the IJReSES must be original with a clear definition of the objective(s), material used (data), methods applied, results, and should not have been published or offered for publication or submitted elsewhere. The manuscript should be written in English, using single line spacing on single-sided A4 size paper with 2.5 cm left and right margins, 2.5 cm upper and lower margins . The author(s) is (are) also required to submit original version of figures embedded in the paper along with their captions. All figures should be in tiff or jpeg format with high resolution (300 or 600 dpi). Submit your paper in Word to IJReSES secretariat via email: pukasi.lapan@gmail.com.

Manuscript Preparation

- Title should be concise and informative and not exceeding 15 words.
- The author name(s) and affiliation(s) should be written in the footnotes at the bottom of the title page.
- Abstract should contain a summary of the paper including brief introduction, the objective(s), method, and principal conclusions. Abstract should not exceed 250 words. Keywords are between 3 to 5 words and must be relevant to the subject. Do not use any sub-headings.
- Materials and methods used should clearly and concisely describe the experiment with sufficient details for independent repetition.
- Results should be presented with optimum clarity and without unnecessary detail. Results should also be presented in figures or tables but not duplicated in both format. Tables should be typed with same font size as the text and given consecutive Arabic number.
- Discussion should explain the significant findings and other important aspects of the research. Do not repeat material and methodology.
- Citation should be written in the text by the author's last name and year in one or two forms: Field *et al*. (1996) or (Field *et al*., 1996). For references with more than two authors, list the first author plus *et al*.
- Conclusion should be concise and answer the objective(s).
- Acknowledgment, if any, should be kept at minimum (less than 40 words)
- References should be in alphabetical order. It should be written as follows:
  Field, C.B., M.J. Behrenfeld, J.T. Randerson, and P. Falkowski, 1998, Primary production of the biosphere: integrating terrestrial and oceanic components. *Science*, 281(5374):237-240.
- Acronym or uncommon abbreviations must be given in full at the first text mentioned. New abbreviation should be coined only for unwieldy names and should not be used at all unless the names occur frequently.
- Latin name and family of the species should be given besides its common name at the first mention in the manuscript , and the common name only for subsequent mentions.
- International Standard unit system (kg, m, s, etc) should be used for all manuscripts.

International Journal of
Remote Sensing and Earth Sciences

December 2017

Published by:

National Institute of Aeronautics and Space of Indonesia (LAPAN)

Secretariat:
National Institute of Aeronautics and Space of Indonesia (LAPAN)
Jl. Pemuda Persil No.1, Rawamangun, Jakarta 13220 INDONESIA
Phone. (021) 4892802 ext. 144 – 145 (Hunting) Fax. (021) 47882726
Pukasi.lapan@gmail.com

INTERNATIONAL JOURNAL OF
REMOTE SENSING AND EARTH SCIENCES
Vol. 14 No. 2 December 2017
P-ISSN 0216-6739; E- ISSN 2549-516X
No. 774/AU3/P2MI-LIPI/08/2017

Contents

Published by:
National Institute of Aeronautics and Space of Indonesia (LAPAN)